Max-Planck-Institut für Metallforschung
Stuttgart

Covalent and Heterosupramolecular Interaction of Ceramic Particles

Gregor Stieger

Dissertation
an der
Universität Stuttgart

Bericht Nr. 129
Dezember 2002

Covalent and Heterosupramolecular Interaction of Ceramic Particles

Von der Fakultät Chemie der Universität Stuttgart zur Erlangung der Würde eines Doktors der Naturwissenschaften (Dr. rer. nat.) genehmigte Abhandlung

Vorgelegt von

Gregor Stieger

aus Wiesbaden

Hauptberichter:	Prof. Dr. Aldinger
Mitberichter:	Prof. Dr. Schleid
Tag der mündlichen Prüfung:	6. Dezember 2002

Max-Planck-Institut für Metallforschung und
Institut für Nichtmetallische Anorganische Materialien,
Pulvermetallurgisches Laboratorium,
Heisenbergstraße 3, D-70569 Stuttgart, Deutschland

2002

Meinen lieben Eltern

Table of Contents

1. Abbreviations 6
2. Index of Tables 8
3. Index of Figures 9
4. Index of Structure Formulas 12
5. Introduction 14
6. Cyclodextrins 16
   6.1. Nomenclature, Constitution, Synthesis and Properties of Cyclodextrins 16
   6.2. Molecular Structure of Cyclodextrins 19
   6.3. Supramolecular Inclusion Chemistry of Cyclodextrins and their Derivatisation 21
7. DLVO-Theory 23
8. Characterization Methods for Ceramic Powders 26
   8.1. ζ-Potential Measurements and Dynamic Light Scattering 26
   8.2. Rheology 30
   8.3. DRIFT-Spectroscopy 33
   8.4. Atomic Force Microscopy 34
9. Heterosupramolecular Reaction Principles 35
10. Native Powders 38
   10.1. Characterization of the Si_3N_4 Ceramic Powder 38
      10.1.1. Surface Chemistry of the Si_3N_4 Powder 43
   10.2. Characterization of the Al_2O_3 Ceramic Powder 45
      10.2.1. Purity and Purification of the Al_2O_3 Powder 45
      10.2.2. The ζ-Potential of the Al_2O_3 Surface 48
      10.2.3. Surface Chemistry of the Al_2O_3 Powder 50
      10.2.4. Particle Size Distribution of Al_2O_3 51
      10.2.5. Shape and Topology of the Al_2O_3 Particles 55
11. Functionalization of the Powders 58
   11.1. Attachment of MCT-β-cyclodextrin to Si_3N_4 58
   11.2. Synthesis of Mono-6-amino-β-cyclodextrin 62
   11.3. Epoxidation of Si_3N_4 65

11.4. Immobilization of Mono-6-amino-β-cyclodextrin on Epoxy-functionalized Si_3N_4 68
11.4.1. Ad- and Desorption of Mono-6-amino-β-cyclodextrin on Unmodified Si_3N_4 72
11.5. Immobilization of Heptakis-6-amino-β-cyclodextrin on Si_3N_4 74
11.6. Ad- and Desorption of Poly-β-CD on α-Al_2O_3 Powder Ceramics 79
11.6.1. Synthesis of Poly-β-CD and Attachment to the α-Al_2O_3-Powder-Surface 79
11.6.2. Adsorbed Amount of Copoly-maleic-acid-alt-isobutene 84
11.7. Synthesis of Iso-cyanatofunctionalized Si_3N_4 90
11.8. Synthesis of Aminofunctionalized Si_3N_4 93
12. Interaction of Ceramic Particles 95
12.1. Covalent Interaction of Si_3N_4-Powder-Particles 95
12.2. Heterosupramolecular Interaction of Si_3N_4 Particles 106
12.3. Improved Dispersibility of Al_2O_3 with Cyclodextrin 108
13. Discussion 110
14. Future Prospectus 114
15. Abstract 119
16. Zusammenfassung 121
17. References 126
18. Acknowledgment 141

1. Abbreviations

abs. u.	absorbance units
AFM	atomic force microscopy
alt	alternating
bipur.	bipurified
CD	cyclodextrin
CIP	cold isostatic pressing
d_{10}	10 Vol% of the particles have a diameter less than d_{10}
d_{50}	50 Vol% of the particles have a diameter less than d_{50}
d_{90}	90 Vol% of the particles have a diameter less than d_{90}
DC	Dünnschichtchromatographie (=TLC)
DLS	dynamic light scattering
DMAc	dimethyl-acetamide
DMF	dimethyl-formamide
DRIFT	diffuse reflectance infra red fourier transformation spectroscopy
EA	elemental analysis
η	viscosity
$[\eta]$	Staudinger index
η_{rel}	relative viscosity
G'	storage modulus, elastic modulus
G''	loss modulus
γ	strain
$\dot{\gamma}$	strain rate
GC	gas chromatography
HIP	hot isostatic pressing
IR	infra red spectroscopy
k	number of glucose units
LOM	light optical microscopy
LPD	liquid phase deposition
LS	laser scattering
m	mass of a monolayer
M	molecular weight of the cyclodextrin **3** (1134 g/mol)

MCT	mono-chlor-triazinyl
M_W	molecular weight
n	number of cyclodextrin molecules adsorbed on 1 g
N_A	Avogadro constant ($6.023*10^{23}$ mol^{-1})
NMR	nuclear magnetic resonance
PCS	photon-correlation-spectroscopy
ϕ	volume fraction, solid loading
ϕ_{crit}	critical volume fraction for gelation
ϕ_{max}	maximum solid loading
pH_{iep}	isoelectric point (for coated particles)
pH_{pzc}	point of zero charge (for uncoated particles)
pur.	purified
PZST	lead-zirconate-stannate-titanate
PZT	lead-zirconate-titanate
R_f	retention factor
SEM	scanning electron microscopy
τ	stress
TLC	thin layer chromatography

2. Index of Tables

Table 1: Characteristic properties of cyclodextrins. 17
Table 2: Elemental analysis of impurities in Si_3N_4 powder (data from H. C. Starck). 38
Table 3: Powder characteristic of Si_3N_4. 38
Table 4: Section analysis of the AFM image shown in Figure 13. 40
Table 5: Section analysis of the image shown in Figure 15. 41
Table 6: Powder characteristic of Al_2O_3 by the manufacturer (except pH_{pzc}). 45
Table 7: Elemental analysis of impurities in Al_2O_3 by the manufacturer. 45
Table 8: Elemental analysis of Al_2O_3 as received, Al_2O_3 pur. and Al_2O_3 bipur.. 46
Table 9: Al_2O_3 particle size measurements by DLS. 54
Table 10: Ad- and desorbed mass of **3** on **5**. 72
Table 11: Sedimentation behavior of **10**. 78
Table 12: Ad- and desorbed masses of **14** on Al_2O_3. 81
Table 13: Ad- and desorbed masses of **29** on Al_2O_3. 89

3. Index of Figures

Figure 1: Scheme of cyclodextrin torus. 17

Figure 2: Numbering of the carbon atoms in the cyclodextrin molecule. 18

Figure 3: α-Cyclodextrin, view on the secondary side[88]. 19

Figure 4: Molecular structures of α-, β-, γ- and δ-cyclodextrin. 19

Figure 5: Scheme of host guest inclusion complex. 21

Figure 6: Total potential V_t, van-der-Waals-potential V_a and electric double layer potential V_r versus surface separation distance d. Positive sign means repulsive, negative attractive potential. 25

Figure 7: Steric stabilization a) scheme of polymer induced stabilization and b) polymer induced potential V_s curve, van-der-Waals potential V_a and total potential V_t. 25

Figure 8: Deformation of a sample by a) tension and b) shearing. 30

Figure 9: Principle of AFM measurement. 34

Figure 10: Scheme of heterosupramolecular interaction between guest **16** and cyclodextrinfunctionalized Si_3N_4 **6**. 35

Figure 11: Scheme of covalent interaction between Si_3N_4-particles. 36

Figure 12: Scheme of heterosupramolecular interaction between guest **16** and cyclodextrinfunctionalized Al_2O_3 **15**. 37

Figure 13: AFM image of Si_3N_4; 750 nm scan. 40

Figure 14: Section analysis of the AFM image shown in Figure 13. 40

Figure 15: AFM image of Si_3N_4, 300 nm scan of the same position. 41

Figure 16: Section analysis of the image shown in Figure 15. 41

Figure 17: AFM image of Si_3N_4, survey scan (6 μm). 42

Figure 18: AFM image of Si_3N_4 , survey scan (2 μm). 42

Figure 19: Hydrolysis of the Si_3N_4 surface. 43

Figure 20: N_B/N_A versus pH_{pzc} for Si_3N_4[153]. 44

Figure 21: DRIFT-spectra of Al_2O_3 as received and purified. 47

Figure 22: ζ-Potential measurement of Al_2O_3 as received and purified. 48

Figure 23: ζ-Potential measurement of Al_2O_3 / **29** and Al_2O_3 / poly-acrylic-acid. 49

Figure 24: Surface of α-Al_2O_3. 50

Figure 25: Particle size distribution of Al_2O_3 as received after injection of the sample and after 5 min. 51
Figure 26: Particle size distribution of Al_2O_3 as received after 15 min, 27 min and ultrasonical treatment. 52
Figure 27: Particle size distribution of Al_2O_3 bipur.. 53
Figure 28: Comparison of different theoretical models. 54
Figure 29: SEM image of Al_2O_3 pur., survey scan. 56
Figure 30: SEM image of Al_2O_3 pur.. 56
Figure 31: SEM image of Al_2O_3 pur., high resolution. 57
Figure 32: Single Al_2O_3 pur. particles (SEM image). 57
Figure 33: DRIFT-spectra of **32**. 60
Figure 34: Zoomed DRIFT-spectra of **32**. 60
Figure 35: ζ-Potential of **32**. 61
Figure 36: ζ-Potential of **32** compared to reference systems. 61
Figure 37: DRIFT-spectra of 6-NH_2-β-CD **3**, 6-$(NH_2)_7$-β-CD **9**. 64
Figure 38: DRIFT-spectrum of epoxyfunctionalized Si_3N_4 prepared in heptane. 66
Figure 39: Hydrolysis of **5**. 67
Figure 40: Required space for a cyclodextrin of a close packing. 68
Figure 41: DRIFT-spectra of mono-6-amino-β-cyclodextrin **3** on Si_3N_4. 70
Figure 42: Influence of solvents to **6** and comparison of **6** with **5**. 71
Figure 43: DRIFT-spectra of **5** and **10** 76
Figure 44: ζ-Potential of **10** in dependence on pH. 77
Figure 45: ζ-Potential of **10** and reference systems. 77
Figure 46: DRIFT-spectra of **15** and Al_2O_3 / **29**. 82
Figure 47: DRIFT-spectra of **15** and **29** on Al_2O_3 compared to Al_2O_3. 83
Figure 48: Titration of 0, 30 and 61 mg for calibration. 85
Figure 49: First derivative of the titration curves for calibration. 85
Figure 50: Calibration curve for **29** for acid base titrations. 86
Figure 51: Titration curves after adsorption of **29** on Al_2O_3 and washing. 86
Figure 52: First derivative of the titration curve for the supernatant solution after adsorption of **29**. 87
Figure 53: First derivative of the titration curve after the first washing water of **29**. 87
Figure 54: First derivative of the second washing water of **29**. 88
Figure 55: First derivative of the third washing water of **29**. 88

Figure 56: DRIFT-spectra of **18** and **20**. 91
Figure 57: DRIFT-spectra of **20** and **18**, same as Figure 56,
but with labeled signals. 94
Figure 58: ζ-Potential of **18**, **20** and Si_3N_4 in water. 95
Figure 59: G'(τ) and G''(τ) in dependence of time for a 28 vol% gel of **18** + **20**. 97
Figure 61: G'(τ) and G''(τ) in dependence of the volume fraction for gels of **18** + **20**.98
Figure 63: G'(τ) and G''(τ) for suspensions of **18**, of **20** and for gels of **18** + **20**
from 20 to 28 vol%. 98
Figure 65: G'(τ) and G''(τ) for suspensions of **18**, of **20** and for gels of **18** + **20**
from 35 to 37.6 vol%. 99
Figure 67: η versus $\dot{\gamma}$ of gels and **18**. 100
Figure 64: η versus $\dot{\gamma}$ of gels and **20**. 101
Figure 70: Relative viscosity η_{rel} versus volume fraction ϕ for the gel formed by
mixing, **18** and **20**. 101
Figure 66: LOM-image of agglomerates of **18** + **20**. 104
Figure 67: LOM-image of agglomerates of **18** + **20**. 104
Figure 68: LOM-image of agglomerates of **18** + **20**. 105
Figure 70: LOM-image of agglomerates of **18** + **20**. 105
Figure 70: Temperature dependent reversible crosslinking of particles. 115
Figure 71: Construction of ceramic mulitlayer systems. 117
Figure 72: Nanostructured deposition of ceramics. 117

4. Index of Structure Formulas

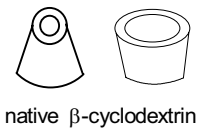

native β-cyclodextrin

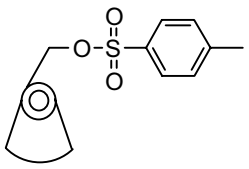

1

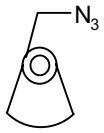

2

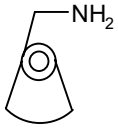

3

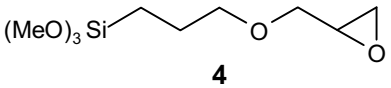

4

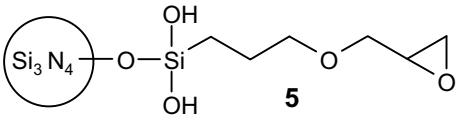

5

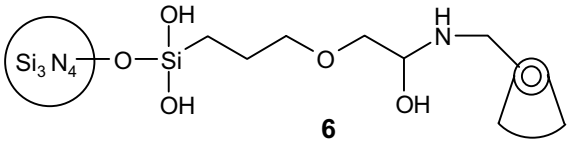

6

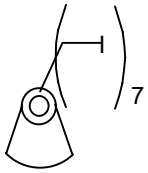

7

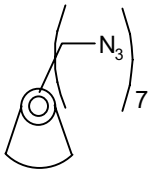

8

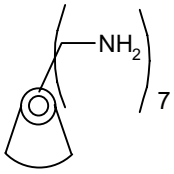

9

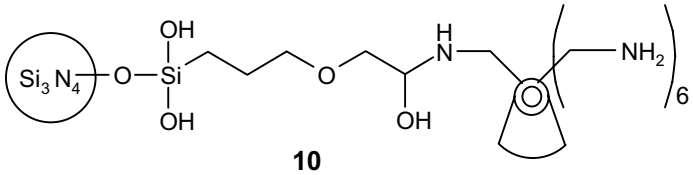

10

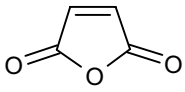

11

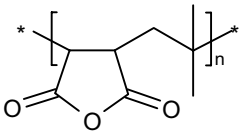

12

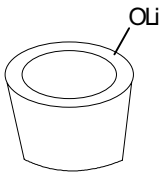

13

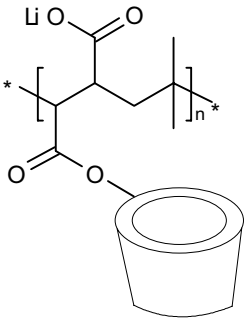

14

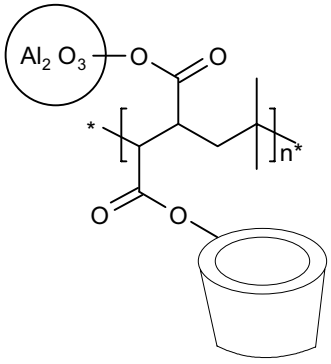

15

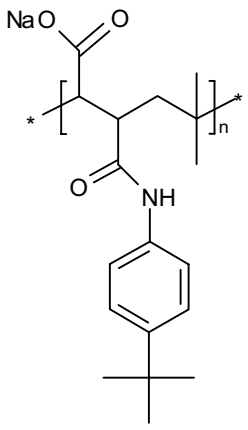

16

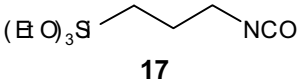

17

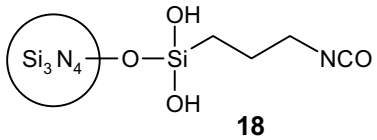

18

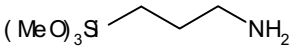

19

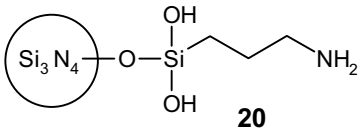

20

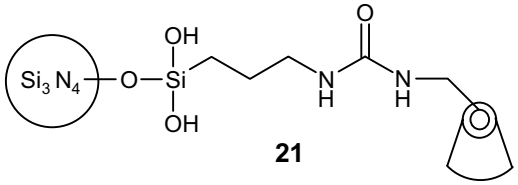

21

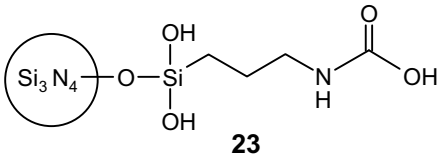

23

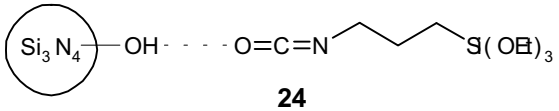

24

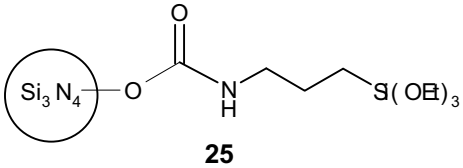

25

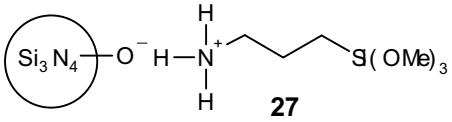

27

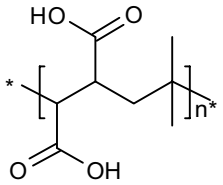

29

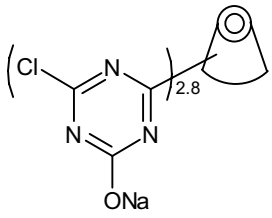

31

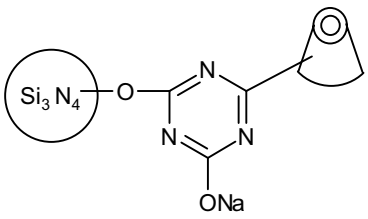

32

5. Introduction

For the industrial production of ceramic parts several methods are used for the conversion of a ceramic powder into a monolith. The most important ones can be grouped into dry pressing and plastic forming[1-7]. For dry pressing the powder is either compacted in a die under uniaxial forces or encapsulated in a flexible form and put into a hydraulic oil where the pressure is applied. Dry pressing is an established method for the industrial mass production of not too complex shaped ceramic parts since many years. Due to the missing dispersion and density gradients inhomogeneities can be present in the part. Machining is sometimes required as a post-treatment to yield high precision parts. Plastic forming involves extrusion, injection molding[8], slip casting and pressure casting[9, 10]. In extrusion the ceramic powder is mixed with a wax or polymer and pressed as a stiff paste into the mold whereas in injection molding the ceramic powder is suspended in a solvent with a dispersant and a binder. The suspension[11-15] provides a homogeneous distribution of the particles. The binder is removed by heating causing shrinkage up to 50 % due to the high binder content. Heating has to be done slowly to prevent cracks and voids, parts with a large cross section need several days for binder burn out. Injection molding is an attractive method for the production of complex shaped parts with high surface precision. In pressure casting or pressure filtration[16-18] the suspension is poured into a porous mold or filter and the solvent is separated from the ceramic using an external pressure while in slip casting capillary forces remove the solvent. Pressure casting and pressure filtration offer a higher productivity compared to slip casting. The consolidation is achieved by removal of the solvent. The liquid flow affects the microstructure of the suspension and causes an orientation of non-spherical particles. To avoid these problems the suspension can be consolidated by chemical means without removal of the solvent. Consolidation can be achieved e. g. by a temperature induced gelation (TIG) as described by L. Bergström et al.[19], a temperature induced irreversible bridging flocculation of Al_2O_3[20] or by using a change in the ζ-potential by a pH-shift causing a strong increase of the viscosity of the suspension[21]. Many publications[22-30] describe how acrylic acid or methacrylic acid is used for polymerization induced gelation based on the solidification of the matrix in which the particles are trapped without

selective and directed linkage of particles. B.-H. Kim[31] describes the crosslinking of particles by molecules adsorbed on the surface. A. Kulak[32] fixed zeolite crystals on glass and mica wafers by reaction of the epoxy- and the amino-functionalized surfaces.

In this study a new processing method will be developed by bridging suspended particles covalently and heterosupramolecularly using silanation and host guest chemistry[33-39] of cyclodextrins. The consolidation step will be done by keeping the solvent avoiding the liquid flow problems. The amount of organic additives is low compared to other techniques, so the binder-burn-out-step is not necessary and the accompanying heating problems do not occur.

6. Cyclodextrins

6.1. Nomenclature, Constitution, Synthesis and Properties of Cyclodextrins

Cyclodextrins[40-50] are cyclic oligosaccharides of D-glucose. k α-D-glucose molecules form a cone-shaped macrocyclic ring. These glucose units are (1→4‘)-glycosidicly linked by etherbridges. Both O-atoms at the 1- and 4-position have down-conformation[51]. Correct names for cyclodextrins informing about the molecular structure are cyclo-[(1→4‘)-α-D-glucopyranose]$_k$ or cyclo-heptakis-[(1→4‘)-α-D-glucopyranose] for β-cyclodextrin. Other names are also used in literature such as cycloamylose, which is reasonable because amylose consists of equivalently linked D-glucose units. Additionally cyclodextrins are named as cyclomaltoses, which is misleading because maltose is a disaccharide and not the repeating unit of the cyclodextrins. Sometimes – especially in the older literature - they are named after the researcher who developed the cyclodextrin chemistry further as Schardinger dextrins. Natural cyclodextrins exist with 6 to 12 glucose units[52]. α-cyclodextrin consists of 6 glucose units, β-cyclodextrin of 7 and so on. The α-, β- and γ-cyclodextrins are the mostly used and investigated ones. A five membered cyclodextrin can be chemically synthesized being tense, a reason for the inavailability by enzymatic synthesis. Many cyclodextrin analogues[53-56] consisting of non-glucose units are synthesized. The structures and properties of the lower and higher analogues that are not available by synthesis can be calculated with molecular mechanics[57].

Cyclodextrins are produced by enzymatic degradation[58-63] of starch. Starch consists of two polysaccharides - amylose and amylopectine. Both species are built up with α-D-glucose. The difference between both species is the connection of the glucose units: A 1→4‘ linkage leads to amylose, a 1→6‘ linkage is present in amylopectine. The glucose chain of amylose forms a left-handed helix with six glucose units per routine. Cyclodextrin-glycosyltransferase enzymes cut the amylose chain and merge both ends together so that a ring shaped molecule is produced. The

cut length is not selective yielding many cyclodextrins. The cyclodextrin-glycosyl-transferases are produced by bacillus macerans[59, 64], bacillus megaterium[65, 66], krebsiella pneumoniae M 5 al[67] and bacillus stereothermophilus[68].

Table 1 depicts some characteristic properties of cyclodextrins[40, 69].

Table 1: Characteristic properties of cyclodextrins.

	α-cyclodextrin	β-cyclodextrin	γ-cyclodextrin
number of glucose units	6	7	8
molecular mass	972 g/mol	1135 g/mol	1297 g/mol
solubility in water at RT in g/100 ml	14.5	1.85	23.2
specific angle of rotation $[\alpha]_D^{25}$	150.5±0.5°	162.5±0.5°	177.4±0.5°
height	790-800 pm	790-800 pm	790-800 pm
diameter of cavity at C-5 atom	470 pm	600 pm	750 pm
diameter of cavity at C-3 atom	520 pm	640 pm	830 pm
outer diameter	1.46±0.04 nm	1.54±0.04 nm	1.75±0.04 nm
pK_a (25 °C)	12.33	12.20	12.08

The cone-shaped macrocyclic ring is schematically drawn in Figure 1. The distances in Figure 1 are measured at atomic models. The top side in Figure 1 represents the narrow side of the cyclodextrin, the bottom side is the wide side.

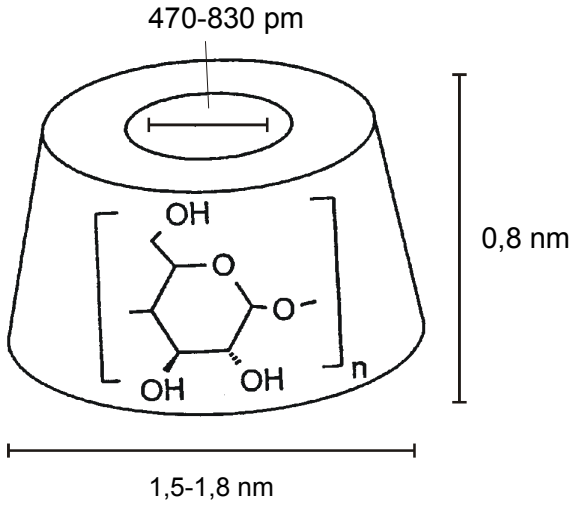

Figure 1: Scheme of cyclodextrin torus.

The numbering of the carbon atoms in the glucose molecule and in the cyclodextrin molecule is demonstrated by the diagram shown in Figure 2. The 2- and 3-positions are the secondary sites. This is the wide side of the cyclodextrin. The primary carbon atom is at 6-position which is located at the narrow side of the cyclodextrin torus.

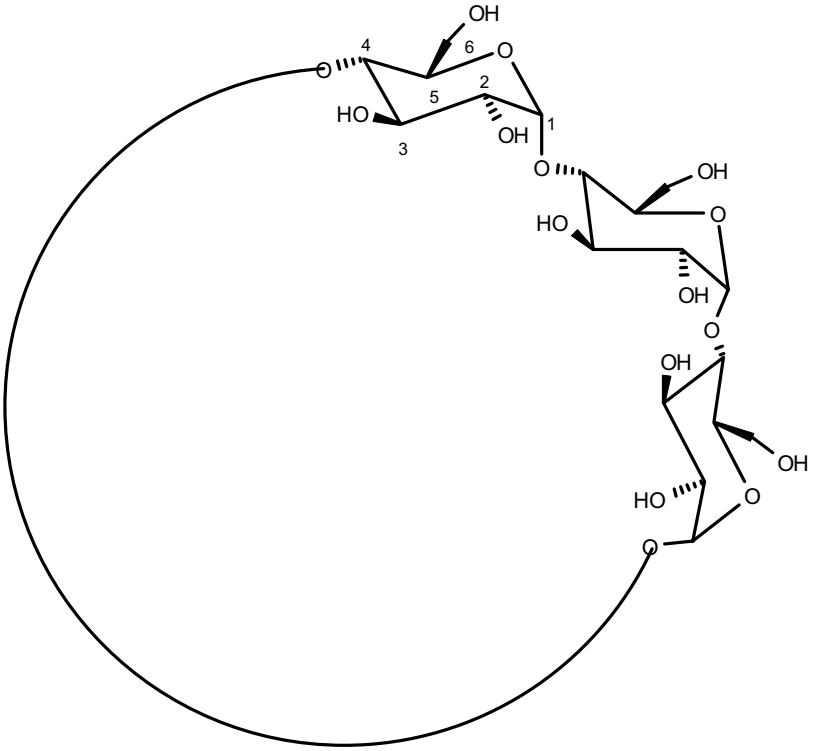

Figure 2: Numbering of the carbon atoms in the cyclodextrin molecule.

6.2. Molecular Structure of Cyclodextrins

The results of the molecular mechanics calculations[70-87] are presented in the graphics below (Figure 3 and 4). The crystal structures are described in[88-96].

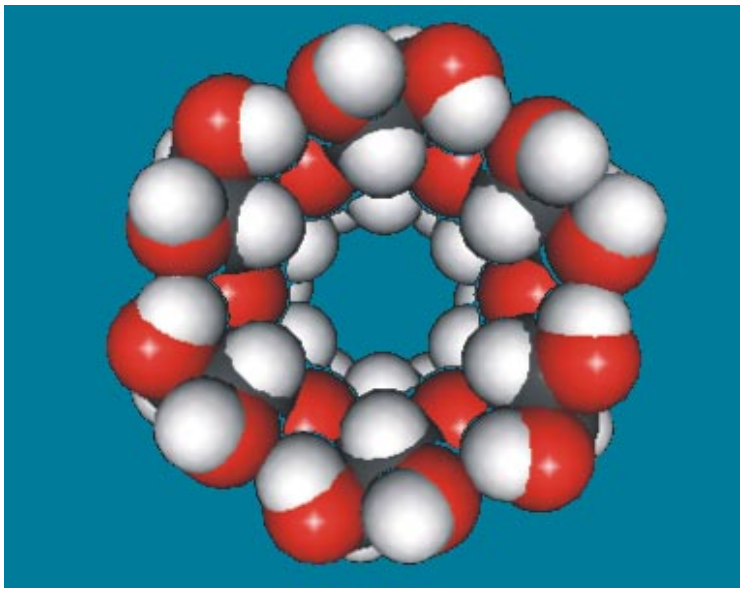

Figure 3: α-Cyclodextrin, view on the secondary side[97].

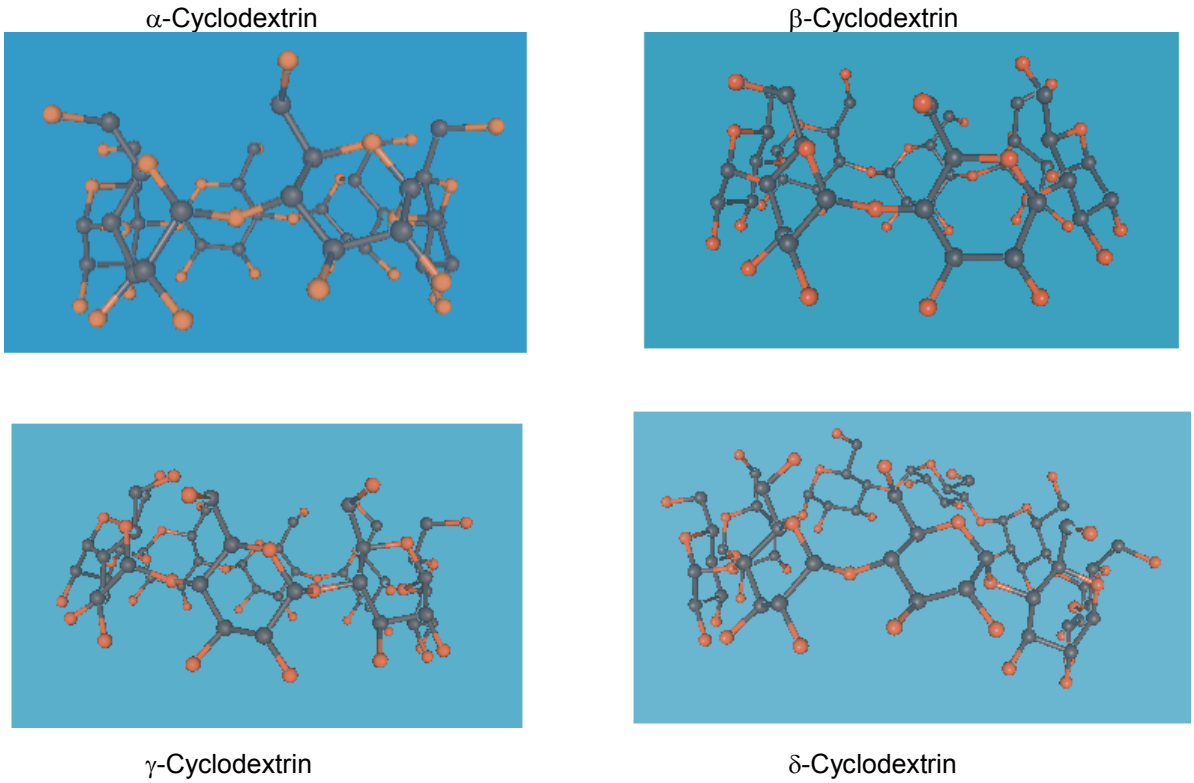

Figure 4: Molecular structures of α-, β-, γ- and δ-cyclodextrin.

In Figure 4 the hydrogen atoms are omitted in order to improve the viewing clarity of the structure. The black balls represent the carbon atoms, the red ones the oxygen atoms. The graphics clearly show the molecular structure of the cyclodextrins. The cavity, the primary and secondary sides and the cone-shaped structure are obvious. The O-6 atoms (upper side of the cyclodextrins in Figure 4) are directed to the outside of the torus and depicted in gauche-conformation, the conformation with the highest population. In some complexes the O-6 atom group can be regarded versus the inner side to form H-bridges with the guest molecule. The gain of energy by the formation of the H-bridging bond compensates the higher energy of the conformation. In accordance with the tilt angle of the glucose units the ring tension decreases from α-cyclodextrin to δ-cyclodextrin. In γ-cyclodextrin one glucose unit is slightly distorted, increased in δ-cyclodextrin, two glucose units being subjected. The δ-cyclodextrin torus has a certain flexibility meaning it has not a rigid cone structure. If the δ-cyclodextrin is viewed from the side, the curved wave-like structure of the cyclodextrin torus can be seen, the two distorted glucose units being the inflection points.

6.3. Supramolecular Inclusion Chemistry of Cyclodextrins and their Derivatisation

The cyclodextrins bear an interesting host guest chemistry[98] where the cyclodextrin acts as the host molecule and a preferably hydrophobic specimen as the guest, which is intercalated into the cavity of the cyclodextrin. Figure 5 illustrates a supramolecular[98] host-guest inclusion complex[99-101] formed by a cyclodextrin with a guest molecule. Guest molecules can be long chain polymers, too. The formed complexes are called polyrotaxanes[102-105]. In this case cyclodextrin rings thread onto the chain of the polymer like pearls onto a cord.

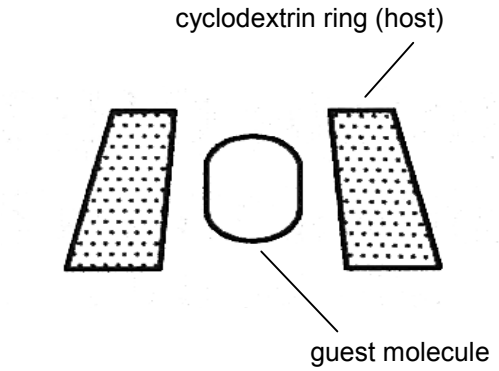

Figure 5: Scheme of host guest inclusion complex.

The Van-der-Waals interaction between the guest and cyclodextrin is one reason for the formation of the inclusion complexes. H-Bridges between the OH-groups of the cyclodextrin and polar groups of the guest molecule support the inclusion process. Energy needed to break the bonds of the water to the cyclodextrin is retained when the included water is dissolved by bulk water. From the entropic point of view the intercalation process induces order and decreases the entropy but the ejected water molecules raise the entropy when they enter the bulk solvent. There are complexes that have three different interaction entropies: a gain of entropy in total, $\Delta S=0$ and a loss of entropy. The enthalpy ΔH can also have negative, zero or positive values. The Gibbs energy $\Delta G=\Delta H - T \Delta S$ has to be considered as an important criterion for the formation of complexes.

The synthetic organic chemistry of cyclodextrins focuses on the 6-position (Figure 2) because this is a primary alcohol group where S_{N1} and S_{N2} reactions can be carried out[106-108]. The C-2 and C-3 atoms are fixed in the glucose rings limiting their possibilities of reactions[109, 110]. LiH deprotonates the only one OH-2 group of the cyclodextrin selectively. With I_2 / Ph_3P the OH-6 groups are substituted by iodine. This labels and discriminates the 6-position from the other OH groups and provides access to a multifunctionalization. By substitution of the iodine to the desired group the derivatisation can be performed. For a mono functionalization at the 6-position a tosylation with tosylchloride is reasonable inducing a regioselectivity and activation of the cyclodextrin as with the multifunctionalization.

7. DLVO-Theory

The DLVO-theory[111] named to its developers Derjaguin, Landau, Verwey and Overbeek describes the interparticle potential of suspensions being useful for the prediction of the stability of a colloidal suspension. Since a strong repulsive interparticle potential is characteristic for a stable suspension and an attractive potential induces flocculation of the particles, the knowledge of the potential is helpful for the understanding of colloidal powder processing phenomena like the liquid-solid-transition of a ceramic powder suspension in plastic forming. In general the interparticle potential can be separated into three parts: the van-der-Waals potential, the double-layer-potential and the polymer induced (steric) potential.

The van-der-Waals-potential is an ubiquitous potential. It is of electrodynamic nature and derives from the interaction of dipoles which can be approximated for two spheres by

$$V_a(d) = -\frac{Ar}{12d}, \text{ providing that } d \ll r. \qquad (1)$$

A Hamaker constant
r particle radius
d surface separation distance

For two spheres of the same material $V_a(d)$ is always attractive, in the case of different materials it can be attractive or repulsive. The magnitude of the interaction can be represented by the Hamaker constant.

In protic liquid media particles can develop a charge on the surface depending on the pH. Individual particles are surrounded by a cloud of counter ions because of this surface charge; the higher the ionic strength in solution the smaller the cloud. These charges induce an electric double layer potential:

$$V_r(d) = 2\pi r\, \varepsilon\varepsilon_0 \varphi_0^2 \exp(-\kappa d) \qquad (2)$$

r particle radius

d surface separation distance

φ_0 surface potential

κ reciprocal Debye length

The Debye length is $1/\kappa$ and defined as

$$\frac{1}{\kappa} = \left(\frac{\varepsilon\varepsilon_0 kT}{e^2 \sum_i n_i z_i^2} \right)^{1/2} \qquad (3)$$

ε dielectric constant of the liquid

ε_0 permittivity of vacuum

k Boltzmann constant

T absolute temperature

e electronic charge

n_i concentration of ions with charge z_i

Equation (2) is a simplified expression for the interaction of two spheres. Curves for $V_a(d)$, $V_r(d)$ and their sum $V_t(d)$ are plotted in Figure 6.

In some cases it is not possible to create a stable suspension by electric double layer forces because the maximum surface charge is not sufficient. In other cases electrostatic stabilization is inadequate for the technical needs of colloidal powder processing. In such cases the polymeric or steric stabilization can be used, where at the particle surface adsorbed polymers hinder the particles to come too close thus shielding the attractive van-der-Waals-forces (Figure 7a). If particles approach each other, the polymer layers interpenetrate resulting in a repulsion (Figure 7b). The magnitude and range of the repulsive interaction can be calculated by the de Gennes´ scaling theory[112-115] for a medium dissolving the polymer. In this theory the adsorbed polymer conformation is assumed to be either a low-surface-coverage

mushroom, in which the volume of the individual polymer is unconstrained by neighbors, or a high-surface-coverage brush, where the proximity of neighboring polymer chains constrains the chain volume and causes extension of the polymer into the solvent.

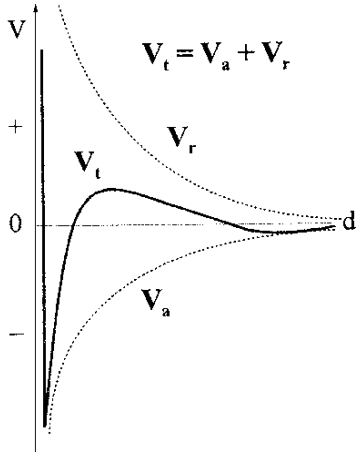

Figure 6: Total potential V_t, van-der-Waals-potential V_a and electric double layer potential V_r versus surface separation distance d. Positive sign means repulsive, negative attractive potential.

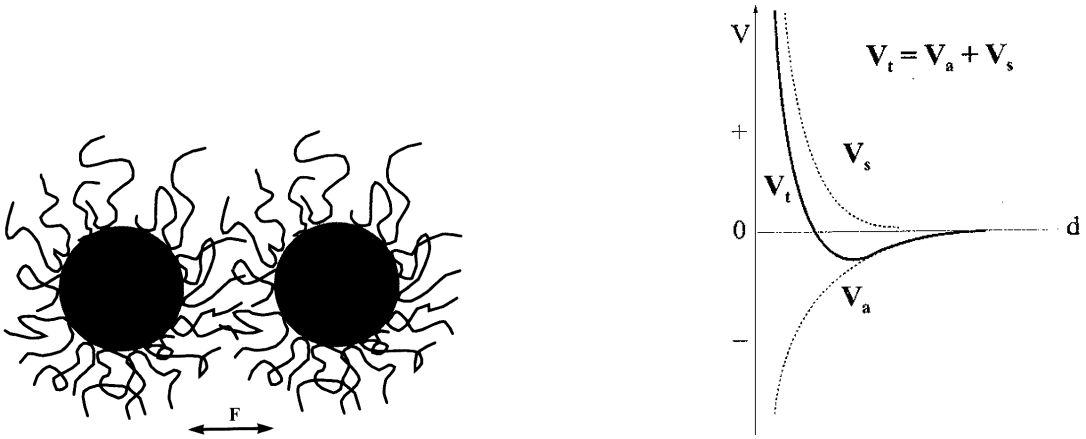

a) b)

Figure 7: Steric stabilization a) scheme of polymer induced stabilization and b) polymer induced potential V_s curve, van-der-Waals potential V_a and total potential V_t.

8. Characterization Methods for Ceramic Powders

8.1. ζ-Potential Measurements and Dynamic Light Scattering

The surface charge density of the particles in solution is a useful parameter for characterizing the surface chemistry of particles. Measurements of the ζ-potential[116-120] in dependence on the pH provide this information. A charged particle adsorbs counter ions tightly. This layer called Stern layer is surrounded by a layer of additional counter ions exceeding the ion concentration of the medium. These ions are not fixed to the particle nor do they have a defined position. This layer is refered to as diffuse layer. It moves with the particle through the medium. Its diameter is much larger than the Stern layer and depends on the concentration of ions in solution. If the particle moves, a shear gradient is formed because of the laminar flow[121] and an additional layer sticking at the outside of the Stern layer is attached to the particle. This layer is fixed to the moving particle. The ζ-potential is the electric potential at the border of this layer. Its value is usually only a little bit lower than the potential at the outside of the Stern layer (Stern potential). For highly charged particles or low electrolyte concentrations which enlarge the shear plane the ζ-potential is significantly lower than the Stern potential. An adsorption of polymers protruding strongly into the solution (hairy layers) separates the Stern layer from the shear plane leading to a relevant difference between ζ-potential and Stern potential. The pH-value for uncoated particles at ζ=0 is named pH_{pzc}, the pH for coated particles at ζ=0 is called pH_{iep}.

The ζ-potential measurement apparatus calculates the electrophoretic mobility u using the Helmholtz-Smoluchowski-equation[121],

$$u = \frac{v}{E} = \frac{\varepsilon_0 \varepsilon_r}{\eta} \zeta \qquad (4)$$

u electrophoretic mobility

v velocity of particle

E power of electric field

ε_0 dielectric constant

ε_r relative dielectric constant

η viscosity of the medium

ζ ζ-potential

the ζ-potential can be calculated from u. This equation is valid for $\kappa a \gg 1$, where κ is the reciprocal Debye-Hückel-length and a the radius of the particles. $4.6*1/\kappa$[121] is the approximative length of the diffuse layer. For the systems investigated in this work the condition $\kappa a \gg 1$ is valid, because the particle size is about 300 nm and larger and the electrolyte concentration is in a medium range (10^{-3} mol/l).

The electrophoretic mobility u is obtained from v=u*E while the particle moves in an electric field with a rectangular shaped tension-time-curve to prevent polarisation of the electrodes. Two crossed laser beams with a time independent phase shift produce a pedestrian-crossing-like-shaped interference pattern in the sample. The time dependence of the intensity of the scattered light is measured by a digital autocorrelator after amplification with a photomultiplier. The data is analyzed to get the autocorrelation function G; G in general is the coefficient of the value of a function at a certain time t and the value at the point $t+\delta t$, where δ is a short time period. Division of the value at the time t by the value at $t+2\delta t$ provides the next value of G and so on. The G-function is a plot of the correlation coefficients versus time expressing how similar the values are with proceeding time compared to the value at the time t. The sine-shaped intensity-time-curve with exponentially decreasing amplitudes is calculated from the autocorrelation function G and then converted via fourier transformation to the intensity-frequency-function. The particles move in an interference pattern with a sine-shaped intensity profile causing a sinodal intensity of the scattered light. Due to the Brownian motion the movement of the particle has an irregular statistic part inducing the exponential decay of the amplitudes, because the scattered light of the observed single particle is absorbed with increasing movement by other particles. The frequency plot represents the frequency of the sine curve of

the intensity-time-signal, the intensity in the intensity-frequency plot meaning the number of particles of a certain frequency. The frequency plot is transformed into the mobility plot using the Doppler effect, whereas the ζ-potential-spectrum is obtained with the mobility data and the above mentioned Helmholtz-Smoluchowski-equation

$$u = \frac{v}{E} = \frac{\varepsilon_0 \varepsilon_r}{\eta} \zeta .$$

For determination of the sign of the ζ-potential one laser beam is modulated with an oscillating mirror so that the interference pattern moves with a defined and known velocity. The direction of the mirror changes with the sign of the electric field, so that the particles and the interference pattern move e.g. towards each other and with changing sign of the electric field in opposite direction leading to two frequency signals. With the increased and decreased frequency the direction of movement of the particles can be retrieved.

The experimental procedure for the ζ-potential measurement is as follows: an aqueous 10^{-3} molar solution of KNO_3 is prepared. 50.6 mg KNO_3 (anhydrous, 101.11 g/mol) are dissolved in 500 ml bidistilled water. A spatula tip of the ceramic powder (≈2 mg Si_3N_4, ≈5 mg Al_2O_3) is added, the suspension is shaken and ultrasonicated for 10 min so that it is slightly turbid called stock solution. Small sealable beakers are filled with the stock solution and the pH is adjusted with HCl- and NaOH-solutions. Samples are prepared in the pH range from 1 to 12 with a step size of 1 and measured five times.

The particle size measurement with dynamic light scattering (DLS)[122-128] which is also called photon-correlation-spectroscopy (PCS) is based on the same principle as the ζ-potential measurements, but without the electric field, the modulation of the laser beam and without the second laser beam, so the interference pattern is missing. The time dependence of the intensity of the scattered light is collected and the autocorrelation function G is analyzed. If the powder is monosize and monodispers, G becomes

$$G(t) = c \exp(-D q^2 t). \qquad (5)$$

c G(t=0)-value

D diffusion coefficient

t time

$$q = (4\pi m_l / \lambda_0) \sin \Theta/2 \quad (6)$$

m_l refractive index of the solution

λ_0 the wavelength of the laser

Θ the scattered angle

The semilogarithmic plot of the experimental G(t) data provides a linear curve which can be fitted with

$$\ln G(t) = \ln c - D q^2 t. \quad (7)$$

The Stokes-Einstein-equation

$$d = kT / (3\pi \eta D) \quad (8)$$

d hydrodynamic diameter

k Boltzmann constant

T absolute temperature

η viscosity

transforms the diffusion coefficient D into the desired hydrodynamic diameter d.

For sample preparation 10 ml of a 0.1% aqueous ceramic suspension is ultrasonicated for 10 min in an ultrasonic bath, after dilution to clear, transparent suspension it is fixed in the compartment.

8.2. Rheology

Rheology deals with the flow behavior and deformation of materials subjected to mechanical forces. The properties of ceramic suspensions[1, 8, 129] vary from elastic solid like behavior to that of low viscous liquids. A Hook spring is used as a model for the elastic properties, a Newtonion fluid as a model for the viscous properties. A force F is applied onto the area A of a rectangular shaped solid body resulting in a deformation dl/l with l as the original length and dl as the variation of the length (Figure 8a). The Young modulus is defined as

$$E = \frac{\sigma}{\varepsilon} = \frac{F/A}{dl/l} \tag{9}$$

with the tension σ and the deformation ε. A body is sheared by the force τ (stress) providing a shear deformation γ (strain) and a shear modulus G

$$G = \frac{\tau}{\gamma} = \frac{F/A}{\tan\alpha} \tag{10}$$

where tan α = α can be set for small deformations (Figure 8b).

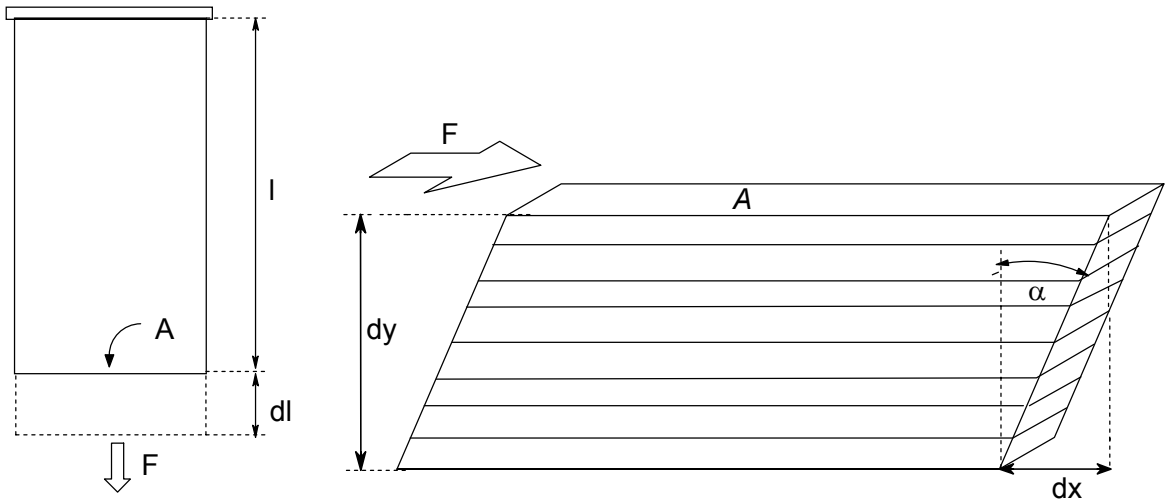

a) b)

Figure 8: Deformation of a sample by a) tension and b) shearing.

The viscosity describes the flow of fluids and is mostly measured as shear viscosity in capillary-, Couette- or cone-plate-geometry. Shearing of a fluid yields a velocity v in x-direction and a gradient of velocity dv in y-direction. The ratio of the shear stress τ and shear rate $\dot{\gamma}$ is called viscosity η

$$\eta = \frac{\sigma}{\dot{\gamma}} = \frac{F/A}{dv/dy} \text{ with } dv = \frac{dx}{dt} \text{ and t as the time.} \quad (11)$$

Liquids with a viscosity independent of the shear rate are called Newtonion liquids. The relative viscosity η_{rel} is defined by the ratio of the viscosity η and the viscosity of the solvent η_{solv}

$$\eta_{rel} = \frac{\eta}{\eta_{solv}}, \quad (12)$$

so that η_{rel} is independent of the solvent.

The viscoelastic properties can be charcterized in dynamic, oscillating measurements. The oscillating force is chosen with a small amplitude so that the deformations of the sample are low maintaining the microstructure of the sample. The complex oscillating stress is provided by

$$\tau^* = \tau_0 e^{i\omega t}. \quad (13)$$

τ^* complex stress
τ_0 stress amplitude
ω oscillation frequency
t time

The response of the sample – the complex strain – is equal to

$$\gamma^* = \gamma_0 e^{(i\omega t - \delta)}. \quad (14)$$

γ^* complex strain

γ_0 strain amplitude

δ phase shift between stress and strain

The phase shift δ is characteristic for the viscoelastic behavior: Elastic samples have a δ of 0°, viscous ones a δ of 90°. The complex dynamic modulus is defined as

$$G^* = \frac{\tau^*}{\gamma^*} = G' + iG'' \tag{15}$$

G' is called dynamic storage modulus, it describes the capability of elastic energy absorption and is a measure of the solid like properties. G'' – the loss modulus – describes the capability of plastic, irreversible energy absorption, it measures the liquid like properties. G' and G'' can also be expressed as

$$G' = \frac{\sigma_0}{\gamma_0} \cdot \cos\delta \quad \text{and} \quad G'' = \frac{\sigma_0}{\gamma_0} \cdot \sin\delta . \tag{16}$$

The ratio $\tan\delta = \frac{G''}{G'}$ is called loss tangent.

8.3. DRIFT-Spectroscopy

The studied spectroscopic range is the middle infra red (MIR) from 4000 to 500 cm^{-1}. The higher frequencies of this range are absorbed by chemical bonds like O-H or C-H. The atoms start to vibrate along the bond or in another direction. The absorption bands[130, 131] are typical for certain chemical groups. At lower frequencies (energies) the entire molecule begins to vibrate and rotate. These bands cannot be assigned to specific functional groups, they identify the molecule itself which names this spectral region finger print region.

For measurements the fine, powdery sample is placed in a container of 1 mm diameter and 1 mm depth in the experimental setup for DRIFT-spectroscopy; the reflected IR-light of the sample is directed by several spherical mirrors to the detector.

The difference between DRIFT[132] and IR-spectroscopy[98, 133] in transmission is that DRIFT is more surface sensitive than IR and that DRIFT is a semi-quantitative method while the absorption in IR is dependent on the weighed amount. In IR the analyzed substance is mixed with a carrier like KBr and pressed to a tablet. The absorption increases with the increasing mass of compound. If needed, this can be optimized by using the same masses of compound and KBr. The DRIFT investigations done in this work are carried out without KBr dilution, because the reflectivity of the probes is low. The DRIFT spectra are influenced by the grain size and package of the particles. The grinding and preparation of the DRIFT samples are performed just so in a reproducible way. SEM and particle size distribution measurements control that the original grain size is obtained after chemical modification of the powders. The reflected light is detected in DRIFT spectroscopy. Thus a raised amount of substance does not increase the absorption. Fine grinding is important, because it removes large agglomerates and particles, their surfaces causing undesired specular reflection. As the penetration depth is not so high and the scattering very low, leading to a weak absorption, inverted bands are produced in the spectrum and cover underlying signals. The occurrence and shape of the large particles is often irregular inducing inverted bands. The detected signal consists mainly of diffusely reflected light generated by multiple absorption and scattering in the sample.

8.4. Atomic Force Microscopy

The principle of the AFM measurement[134] is illustrated in Figure 9: a square-pyramidally shaped Si or Si_3N_4 tip is close to the surface of the sample; a force between the surface and the tip bending the cantilever being present because of the electrodynamic and electrostatic interactions. The magnitude of the bending is measured by laser light reflected from the cantilever via a mirror on a position sensitive detector (PSD, four field detector), the distance between the tip and the surface being controlled by a piezo element with the fixed sample. A scanning unit that moves the sample laterally in the x- and y-directions is integrated into the piezo element. The sample is moved under the tip and the piezo adjusts the distance to ensure a constant bending of the cantilever. The driven way of the piezo is the measured signal, its plot providing a topographic image of the surface. On a closer view an equipotential area is measured – an area with a constant force between the tip and the surface. That means that not a topology is plotted, but a constant force area that can be interpreted as a topological image if the type of atoms, the bonds and the charges do not vary.

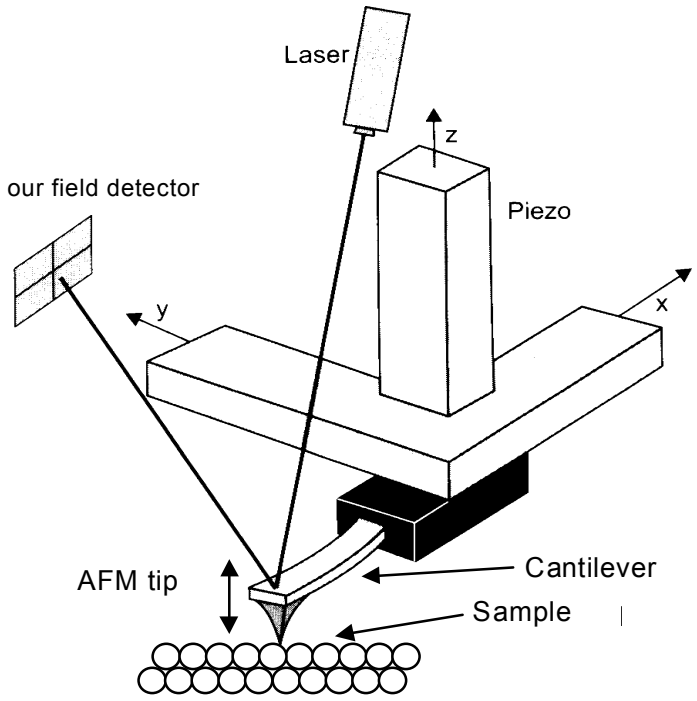

Figure 9: Principle of AFM measurement.

9. Heterosupramolecular Reaction Principles

For the crosslinking of particles two new methods are presented in the following paragraphs.

In the first approach Si_3N_4 particles functionalized with β-cyclodextrin are crosslinked by a polymer (Figure 10). The polymer molecule has tert-butyl-anilide units in its side chains which are proper guests for β-cyclodextrin. The polymer is well soluble in water. The cyclodextrins are covalently bonded to the Si_3N_4 particle via a spacer molecule. The spacer is a bifunctional silane that has a proper anchoring group for the Si_3N_4 surface on the one side (tri-methoxy-silyl-group) and a side (epoxy group) that selectively reacts with the amino group of the cyclodextrin. It is represented by the blue line between the powder particles and the cyclodextrin torus in Figure 10. In reality the Si_3N_4 particles are much bigger than the cyclodextrin molecule units. Their average diameter is 680 nm (d_{50}-value). The cyclodextrin torus has a width of about 1 nm and a height of about 0.8 nm. The spacer molecule provides a certain flexibility and distance from the surface. The cyclodextrin bears into the solution and is able to move in a small range. It can react with the tert-butyl-anilide units of the guest polymer. The cyclodextrin intercalates the tert-butyl-anilide into its cavity[135, 136]; another tert-butyl-anilide unit can be intercalated into a cyclodextrin that is bonded to another particle, so two or more particles are crosslinked by the polymer molecule.

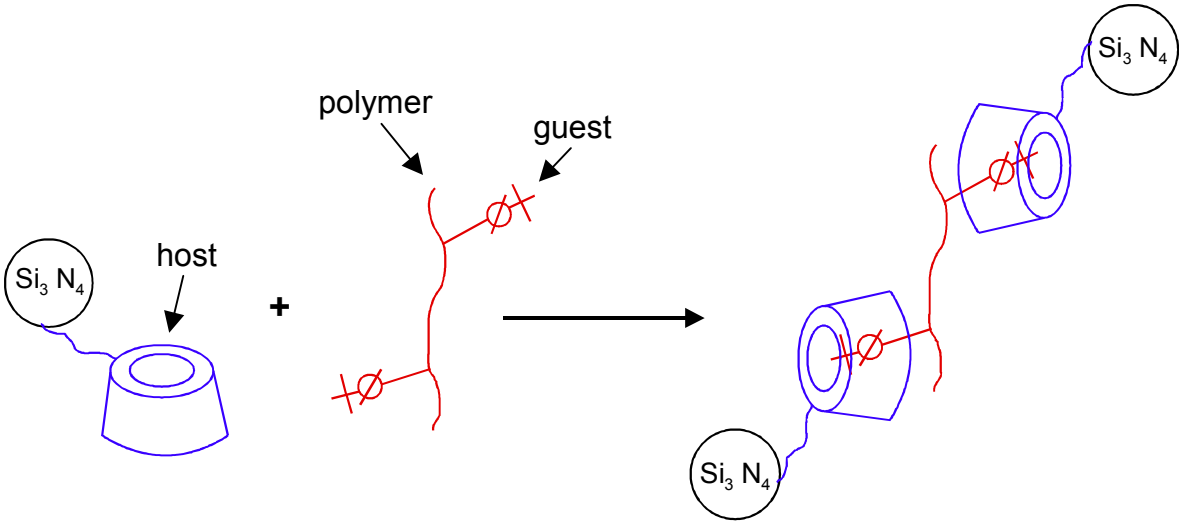

Figure 10: Scheme of heterosupramolecular interaction between guest **16** and cyclodextrinfunctionalized Si_3N_4 **6**.

The bridged particles show an enhanced sedimentation.

In a second approach Si_3N_4 particles are covalently connected (Figure 11). Two different Si_3N_4 powders are prepared. One is functionalized with a bifunctional silane bearing an iso-cyanato group on the one end and a tri-ethoxy-silyl group on the other end. The silyl group works as an anchor to the Si_3N_4 surface. So the iso-cyanato terminus protrudes into the solution and is available for reactions. For the other Si_3N_4 powder a silane with a silyl group and an amino group is selected. The resulting Si_3N_4 is amino functionalized. Both Si_3N_4 powders are suspended and can react under formation of an urea bridge. The particles are crosslinked via a molecular bridge. They form agglomerates large enough to be visible with the naked eye. The suspension of both Si_3N_4 powders shows strong sedimentation behavior.

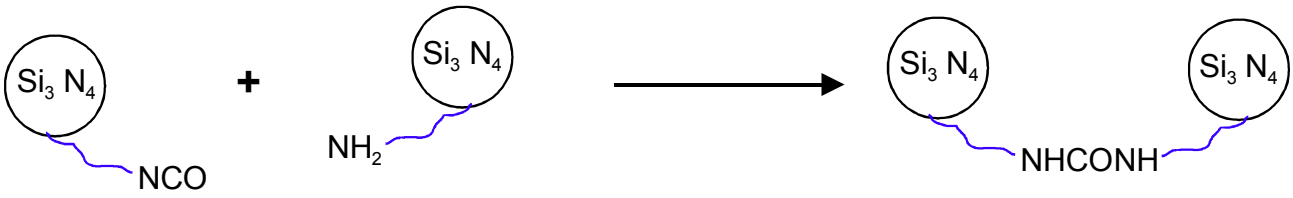

Figure 11: Scheme of covalent interaction between Si_3N_4-particles.

The heterosupramolecular chemistry of cyclodextrins can also be used to improve the dispersibility of Al_2O_3 powder ceramics.

In this approach a cyclodextrin functionalized polymer is attached to Al_2O_3 particles (Figure 12). The cyclodextrin polymer consists of the same backbone as the polymer used above but has β-cyclodextrins in its side chains. The blue loops in the diagram represent the polymer backbone. The layer of the cyclodextrin polymer at the surface of the powder particles increases the steric barrier and improves the dispersibility of the Al_2O_3 powder. The β-cyclodextrins that are fixed to the Al_2O_3 surface react with the tert-butyl-anilide units of the polymer guest molecules in the same way as described above. Thus the guest is adsorbed as a second layer on the cyclodextrin polymer in a host-guest-reaction. The guest polymer layer increases the steric barrier and further improves the dispersibility. The amount of the cyclodextrins linked to the

surface of the powder particles is much higher in this case than in the approach above (Figure 10). Preference is given to a reaction between cyclodextrins that belong to the same particle and tert-butyl-anilide units that are bonded to the same guest polymer in comparison to a reaction of the guest and cyclodextrins on different ceramic particles, the last reaction causes an enhanced sedimentation in contrast to an improved dispersibility.

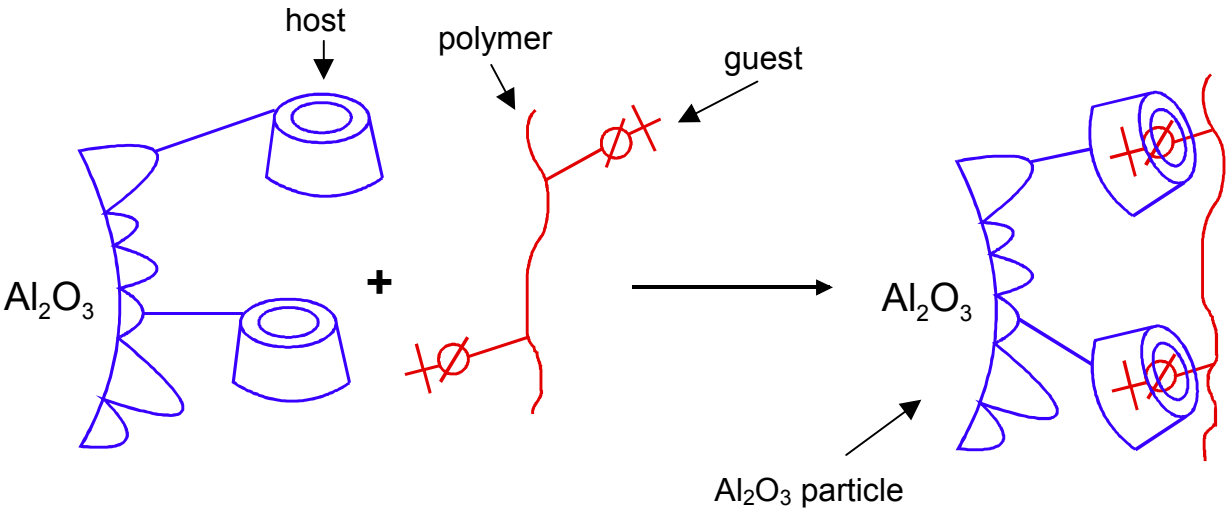

Figure 12: Scheme of heterosupramolecular interaction between guest **16** and cyclodextrinfunctionalized Al_2O_3 **15**.

Inclusion chemistry of dissolved[137, 138] and immobilized[139-148] hosts with dissolved guests is well investigated. Highly enantioselective stationary phases in gas chromatography (GC) are on silica fixed cyclodextrins[108, 149]. Therefore, this approach promises new means of systems where two hosts are bonded to a solid substrate and the guest is dissolved.

10. Native Powders

10.1. Characterization of the Si_3N_4 Ceramic Powder

The Si_3N_4 ceramic powder (type M 11) used in this work is supplied by H. C. Starck, Goslar, Germany. Compared to other powders it is a relatively pure submicron powder. The elemental analysis by L. Wang[150] and H. C. Starck[151] is shown in Table 2. Beside the indicated impurities

Table 2: Elemental analysis of impurities in Si_3N_4 powder (data from H. C. Starck).

element	amount / mg/g
Fe	0.024
Ca	0.036
Al	0.539
C	2
O	10

the powder contains 3.76% SiO_2 as a surface layer being essential for the fixation of silanes. The powder characteristics provided by L. Wang[150] and H. C. Starck[151] are given in Table 3.

Table 3: Powder characteristic of Si_3N_4.

	value		
α-Si_3N_4	94.5%		
specific surface area (BET)	12.7 m^2/g		
pH_{pzc}	4-5		
SiO_2 content	3.76%		
particle size distribution	d_{10}=300 nm	d_{50}=680 nm	d_{90}=1390 nm

The topology of the surface of the Si_3N_4 particles has been characterized by AFM. The AFM investigations are done in tapping mode (Digital Instruments, Nanoscope, Mannheim, Germany) using a conventional Si_3N_4 tip and a circle-shaped, thin platelet out of fused silica with approximatively 1 cm diameter as substrate for the Si_3N_4 powder. The platelet is covered with a two component glue (UHU Endfest 300) smoothed with a paper. After 10 min the glue has a sufficiently high viscosity and the

ground, fine Si_3N_4 is spread on the platelet. The loose particles are removed by tipping the platelet on the desk. Hardening the glue overnight fixes the particles. Large agglomerates obscured by the cantilever cannot be seen on the monitor during surface approach. So the cantilever has to be moved very carefully to the surface to avoid damage.

The topology exhibited by the AFM measurements is shown in Figure 13-18 as a line plot (four of eight measurements are presented). Figure 14 and 16 show each a cross section (left picture) taken along the black line in the right picture (top view). Bright colors mean high, dark colors low areas. The red triangles mark characteristic points of the fractal particle surface. Table 4 and 5 quantify the corresponding distances: the step size of 18 nm (Figure 14, Table 4) is 18-fold higher than the dimensions of a cyclodextrin molecule with 1 nm in length, width and height. The vertical distance between the triangles in Figure 16 is with 21 nm manyfold higher than the cyclodextrin, too. These data reveal that the magnitude of the features of the surface structure is one decade higher compared to a cyclodextrin molecule enabled to be deposited on the surface in a layer-like structure and not to be trapped. The surface roughness of 1 nm estimated from the cross section diagram confirms this. So it can be concluded that the particles should be able to interact with each other to form bridges and to be crosslinked.

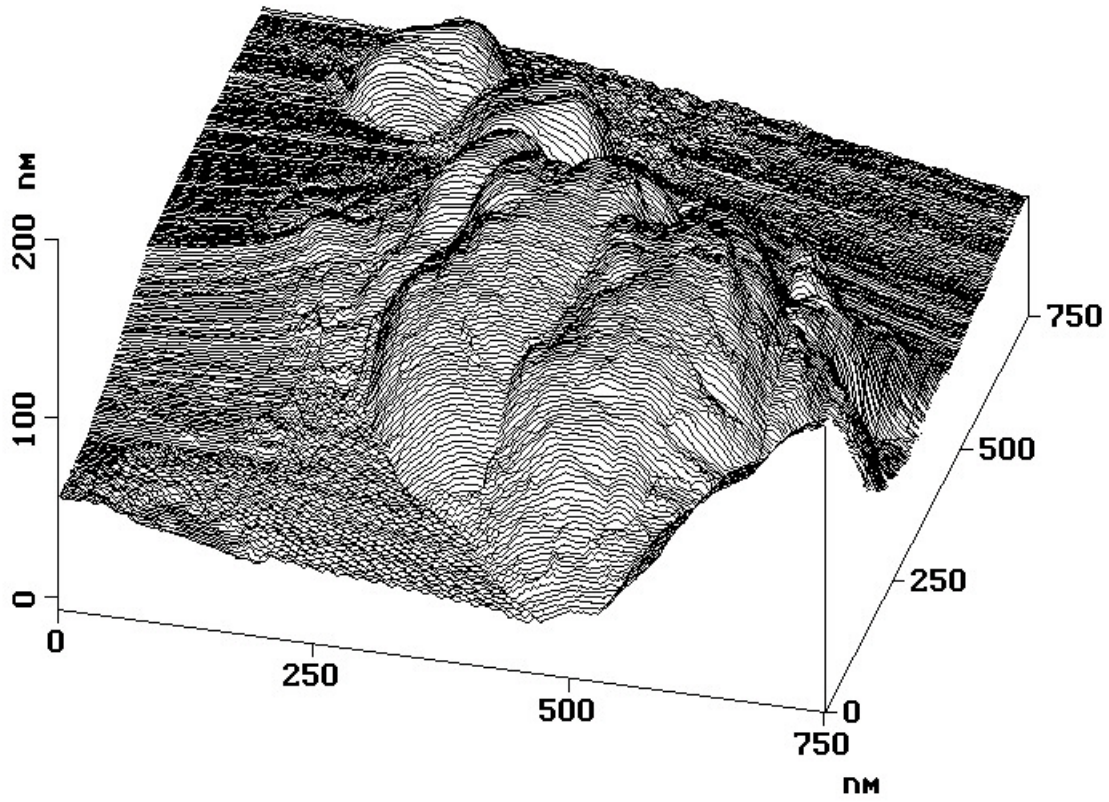

Figure 13: AFM image of Si_3N_4; 750 nm scan.

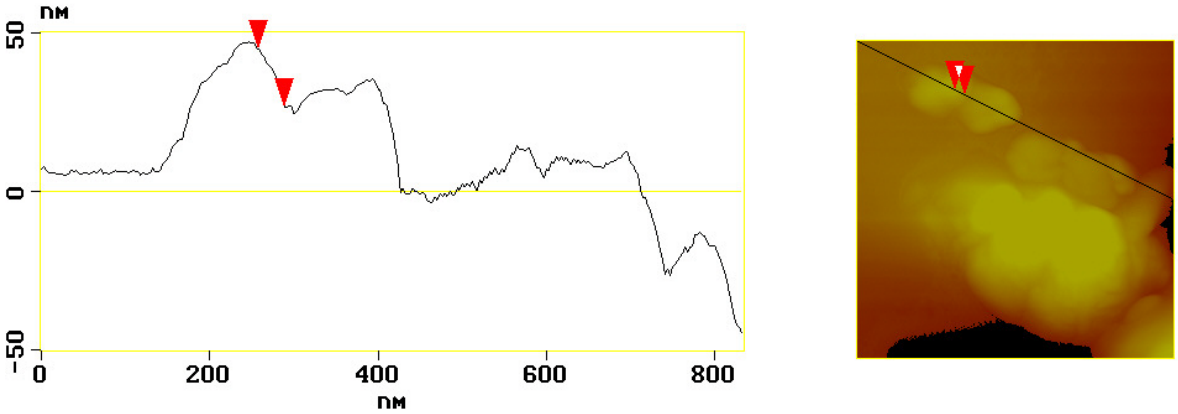

Figure 14: Section analysis of the AFM image shown in Figure 13.

Table 4: Section analysis of the AFM image shown in Figure 13.

distances between the red triangles	
surface distance	35 nm
horizontal distance	29 nm
vertical distance	18 nm
surface roughness	≈1 nm

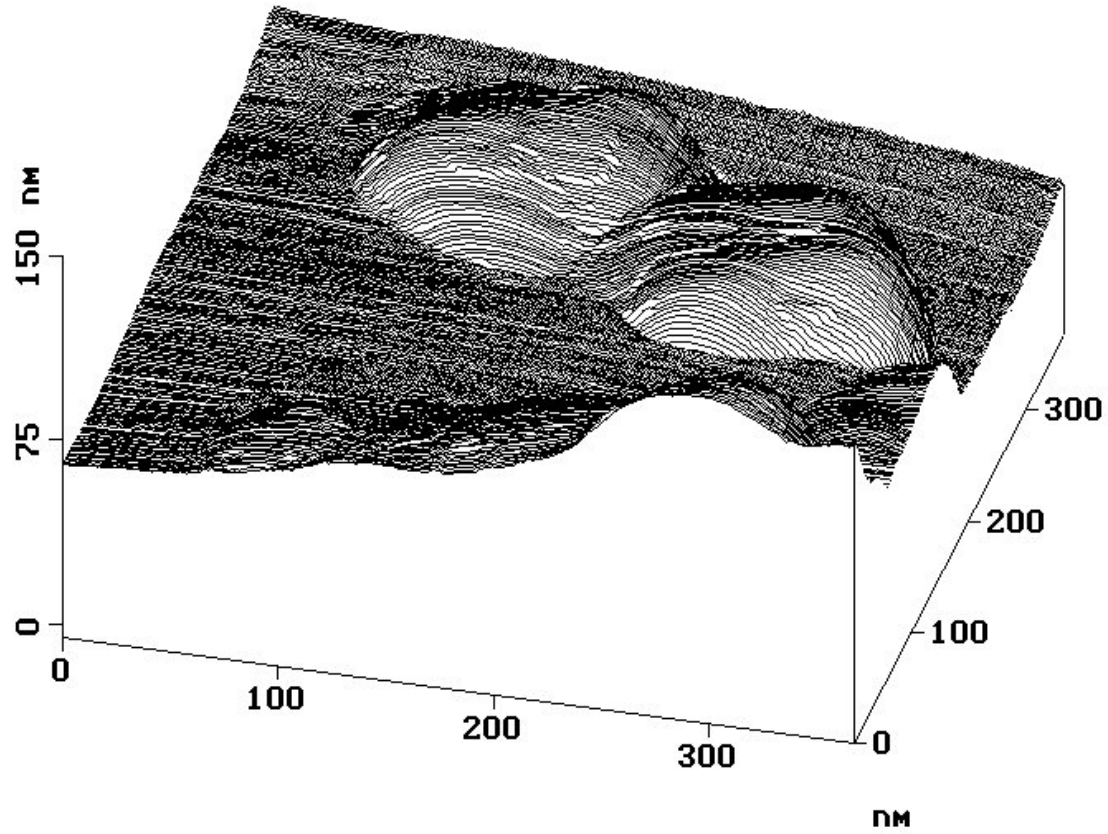

Figure 15: AFM image of Si_3N_4, 300 nm scan of the same position.

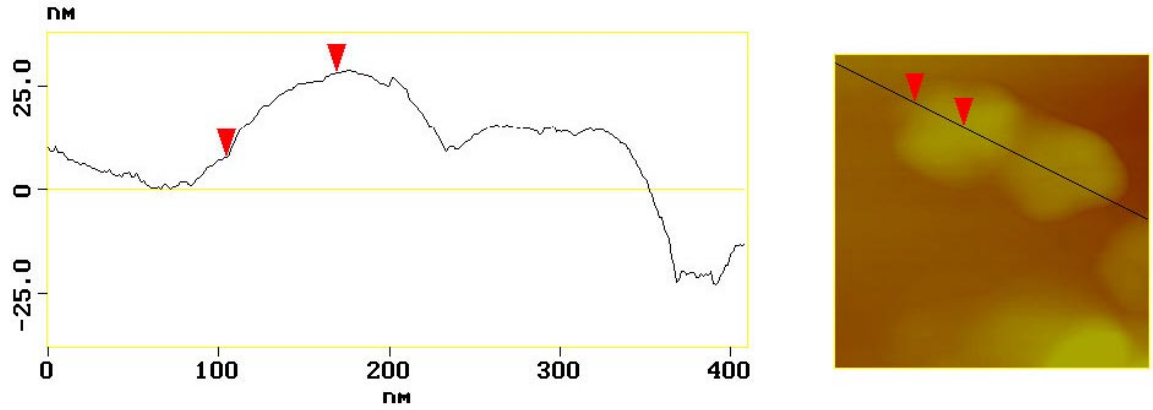

Figure 16: Section analysis of the image shown in Figure 15.

Table 5: Section analysis of the image shown in Figure 15.

distances between the red triangles	
surface distance	70 nm
horizontal distance	65 nm
vertical distance	21 nm
surface roughness	≈1 nm

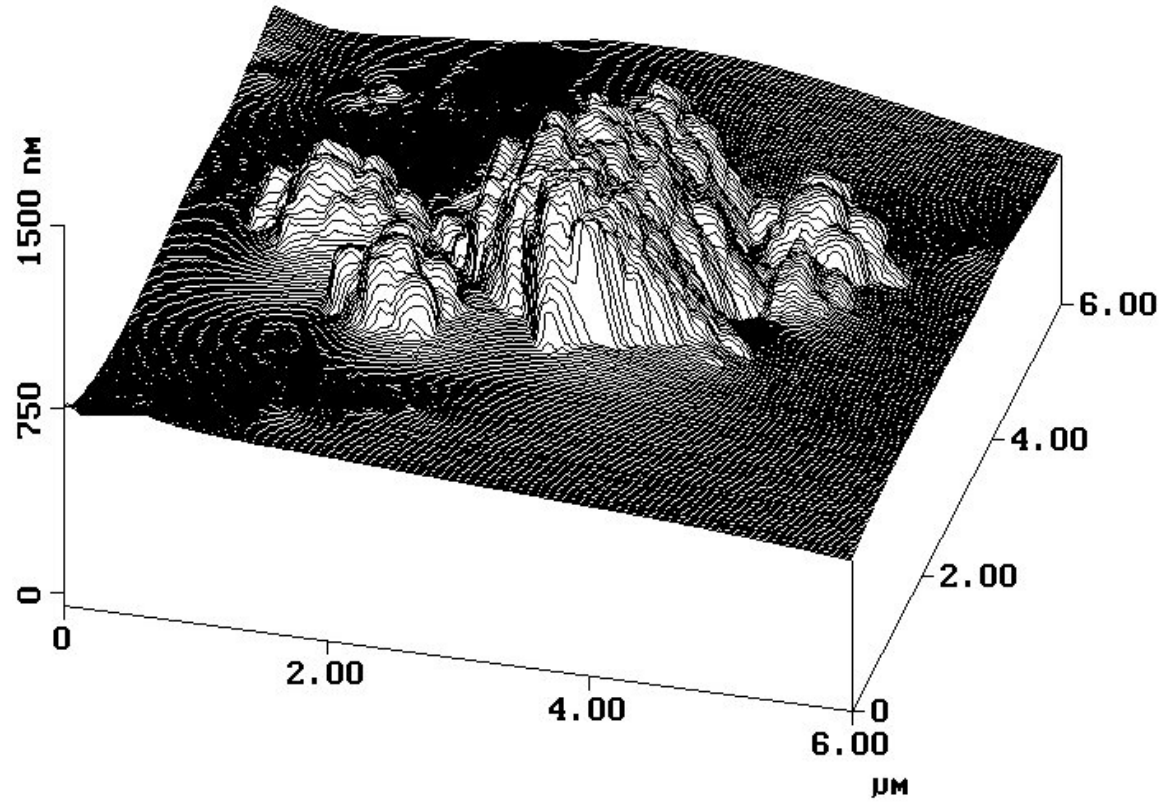

Figure 17: AFM image of Si_3N_4, survey scan (6 μm).

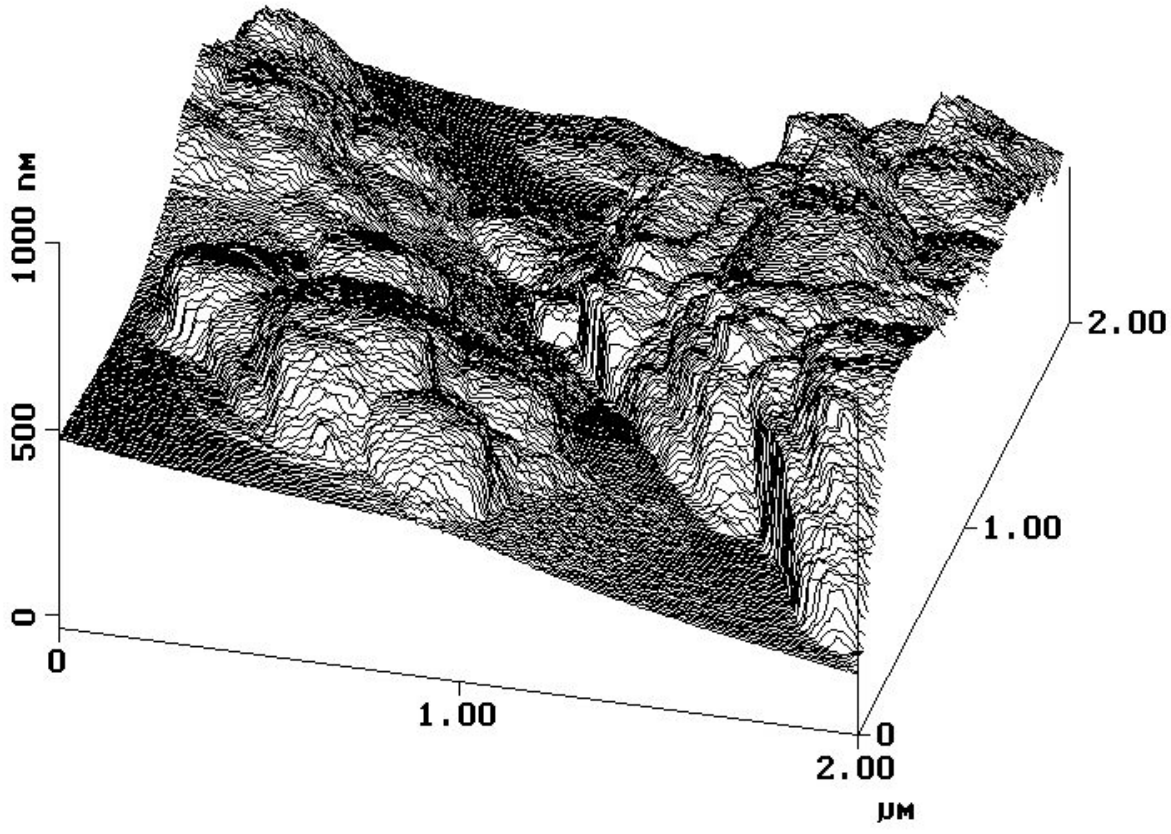

Figure 18: AFM image of Si_3N_4 , survey scan (2 μm).

10.1.1. Surface Chemistry of the Si_3N_4 Powder

The used α-Si_3N_4 is synthesized via a direct nitridation:

$$3\,Si + 2\,N_2 \xrightarrow{1200-1450\,^{\circ}C} Si_3N_4\,.$$

The powder is subjected to wet milling and treatment with HF and HCl to remove elemental Si and SiO_2[152]. Instable, basic imino groups (Si_2=NH) and stable, acidic silanol groups (Si-OH) are the first step in the hydrolysis ot the Si_3N_4 surface[153-158]. The imino groups react with water to form amino groups (Si-NH_2) and silanol groups; recently ammonia is set free (see DRIFT-spectrum in Figure 33). Amorphous[153] SiO_2[159], covering the Si_3N_4 particles, is formed with proceeding time protecting the bulk from further hydrolysis. A long time treatment with HF or highly concentrated alkaline solutions under heat removes the silicon dioxide layer and retains the bare Si_3N_4. Figure 19 depicts the hydrolysis of the Si_3N_4 surface.

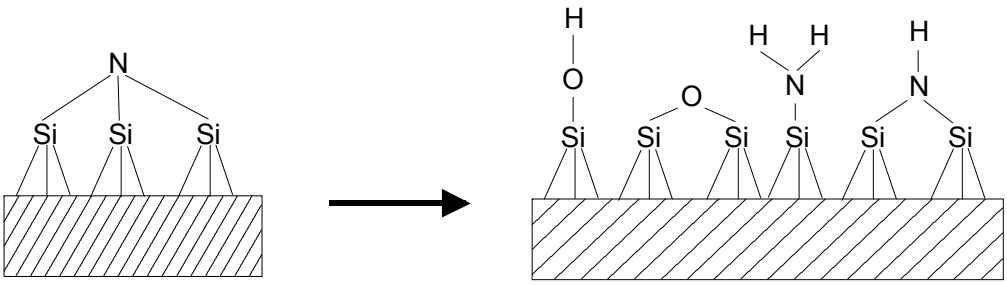

Figure 19: Hydrolysis of the Si_3N_4 surface.

The pH-dependent reactions of the surface groups are:

$$Si-OH_2^+ \xleftarrow{H^+} Si-OH \xrightarrow{OH^-} Si-O^- + H_2O$$

$$Si-NH_3^+ \xleftarrow{H^+} Si-NH_2 \xrightarrow{OH^-} Si-NH^- + H_2O$$

The silanol groups shift the basic Si_3N_4 surface thus the pH_{pzc} to the acid indicating the progress of the hydrolysis. The ratio N_B/N_A of

N_A = [Si-OH]+[Si-OH_2^+]+[Si-O^-] and
N_B = [Si-NH_3^+]+[Si-NH_2]+[Si-NH^-]

in dependence of the pH_{pzc} is described by L. Bergström[160] (Figure 20).

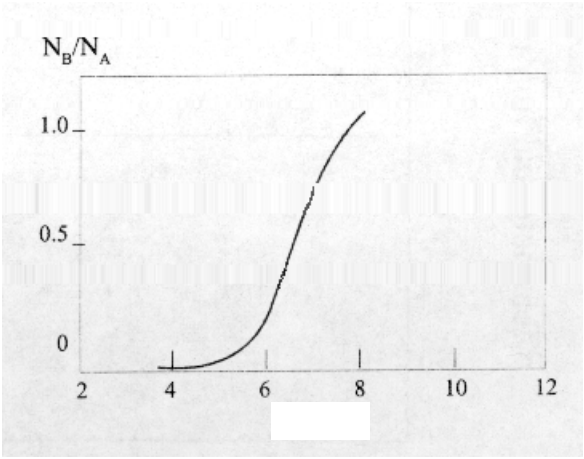

Figure 20: N_B/N_A versus pH_{pzc} for Si_3N_4[160].

According to this model the surface species of the Si_3N_4 powder used here consist of ≈95% silanol groups and ≈5% amino groups leading to an acidic surface.

In DRIFT-spectroscopy the solid body appears with intense signals at wavenumbers below 2000 cm^{-1}. Because of the strong intensity it is difficult to detect organic compounds in this spectral region. These signals are caused by Si-N- and Si-O-vibrations.

10.2. Characterization of the Al_2O_3 Ceramic Powder

10.2.1. Purity and Purification of the Al_2O_3 Powder

The α-Al_2O_3 (type AKP-53) used here is supplied by Sumitomo Chemical Company, Japan. It is a high purity, low soda, submicrometer alumina powder. Table 6 and 7 show the results of the material characterization (Table 6) and the elemental analysis (EA, Table 7).

Table 6: Powder characteristic of Al_2O_3 by the manufacturer (except pH_{pzc}).

parameter	value
crystal type	α
purity	> 99.99%
specific surface area (BET)	12.3 m^2/g
particle size	d_{50}=290 nm
pH_{pzc}	≈8-9

Table 7: Elemental analysis of impurities in Al_2O_3 by the manufacturer.

element	amount / μg/g
Fe	9
Cu	< 1
Mg	20
Na	7
Si	140

The purity of >99.99% as declared by the manufacturer is not in accordance to their EA-results: The purity of >99.99% means that the total impurity content is less than 0.01%. However 0.01% correlates to 0.1 mg/g = 100 µg/g. But even the Si content (140 µg/g) is higher than 100 µg/g.

The purified powder was obtained after washing the as-received powder once with bidistilled water (pH=5), the bipurified powder after washing twice with bidistilled water. The elemental composition of Al_2O_3 as received, Al_2O_3 pur. (purified) and Al_2O_3 bipur. (bipurified) was analyzed (Table 8).

Table 8: Elemental analysis of Al_2O_3 as received, Al_2O_3 pur. and Al_2O_3 bipur..

element	Al_2O_3 as received, mass%	Al_2O_3 pur., mass%	Al_2O_3 bipur., mass%
C	0.186	0.112	0.0922
N	0.086	0.116	0.149
H	0.082	0.056	0.053
Na	0.36	0.48	0.4
K	≤0.12	≤0.12	≤0.25

The carbon content clearly shows that there are organic compounds mixed to the Al_2O_3 powder confirmed by the DRIFT-spectroscopic investigation (Figure 21). Parallel to the DRIFT-spectroscopy the carbon content is decreased with increased washing of the powder. The organic compound is water soluble so that most of this additive can be removed and only a small amount remains. The hydrogen content is also decreased with increased purification. Before washing it is lower than the carbon content, after the purification both values reach a similar level of 0.0922 mass% C and 0.053 mass% H. The low and decreasing hydrogen content is attributed to hydrogen in the organic compounds, so that the content is decreased during the purification. But this also means that the Al_2O_3 contains only 388 µg/m^2 water and that the drying after purification is successful, because the water content does not increase much. The sodium and potassium content remain on the same level during both purification processes, either because the sodium and potassium compounds are not water soluble or the sodium and potassium are incorporated into the lattice of the Al_2O_3. It was verified that there is no sodium or potassium contamination due to the purification process.

The difference between the sodium value of the manufacturer ($7*10^{-4}$ %) and the value determined in this work (0.4%) can be explained by contamination during storage, but nevertheless both values are low. The powder can be classified as pure with a confined purity of 99.166% Al_2O_3 for Al_2O_3 as received and 99.0558% Al_2O_3 for Al_2O_3 bipur. using the data in Table 8.

Even without any surface modification this powder and the Si_3N_4-powder have some colloidal stability exhibited by a missing sedimentation of the diluted aqueous suspensions. This is important for the further investigations. The Al_2O_3 consists of methylene or methyl and carboxylic acid containing compounds (Figure 21), probably milling additives which can be removed by washing with slightly acidified bidistilled

water (pH=5). The DRIFT-spectra (Bruker, IFS 66, Karlsruhe, Germany, Figure 21) demonstrate the removing of the contaminants to get the purified powders used here.

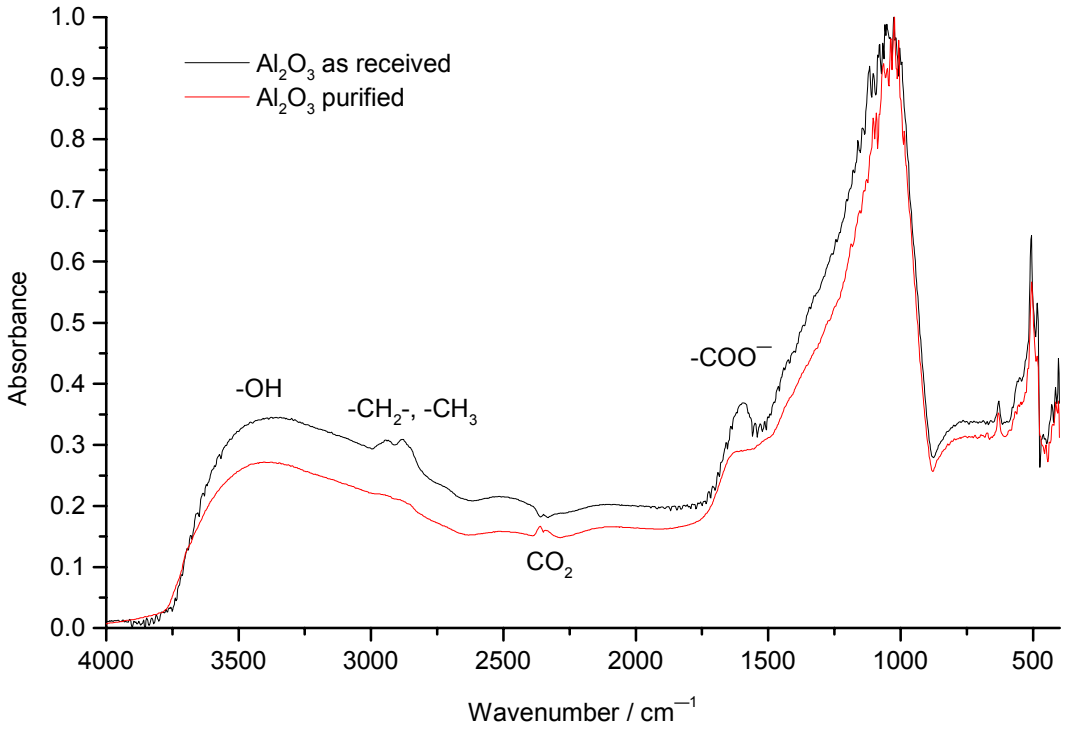

Figure 21: DRIFT-spectra of Al_2O_3 as received and purified.

10.2.2. The ζ-Potential of the Al_2O_3 Surface

According to ζ-potential measurements (Malvern Instruments, Zetamaster, Herrenberg, Germany) the Al_2O_3 powder has an alkaline surface with a pH_{pzc} of approximately 8.8 (Figure 22). The deposition of poly-acrylic-acid (M_W=50000 g/mol) and copoly-maleic-acid-alt-isobutene **29** (M_W=60000 g/mol) cause an acidic shift[13, 14] due to the carboxyl groups (Figure 23). The pH_{iep} of the Al_2O_3 / poly-acrylic-acid system is ≈3.3 and the pH_{iep} of Al_2O_3 / **29** is ≈5.4.

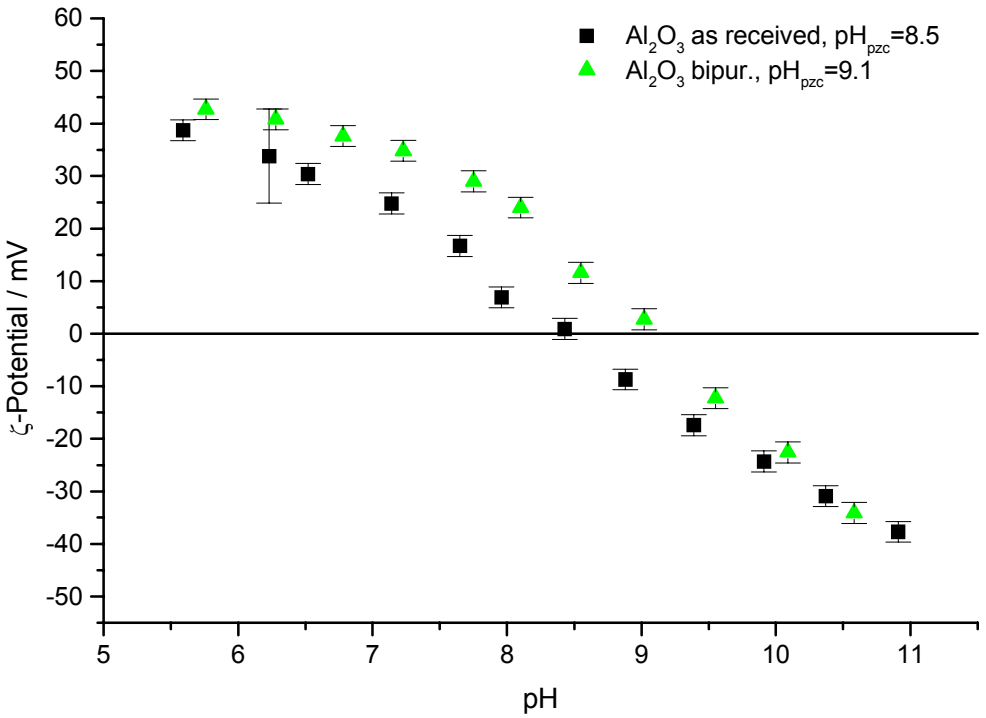

Figure 22: ζ-Potential measurement of Al_2O_3 as received and purified.

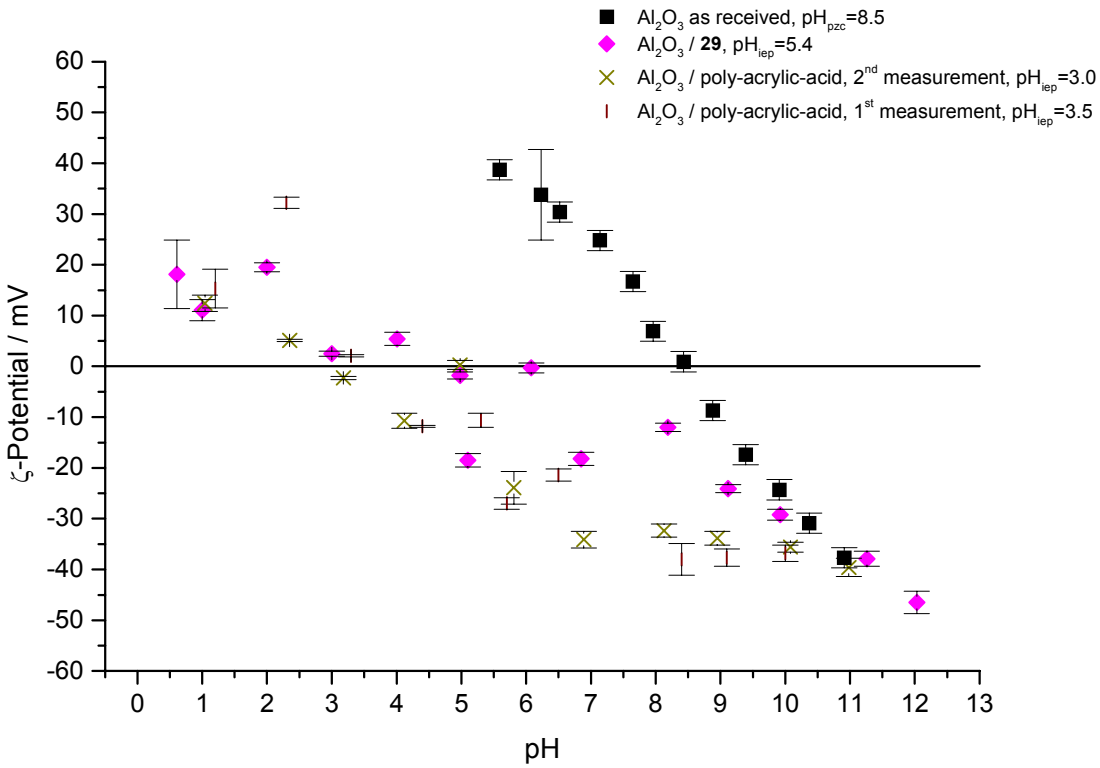

Figure 23: ζ-Potential measurement of Al_2O_3 / **29** and Al_2O_3 / poly-acrylic-acid.

10.2.3. Surface Chemistry of the Al_2O_3 Powder

The Al_2O_3 surface[12, 161-163] consists of Al, Al-OH and Al-O-Al species as illustrated in Figure 24.

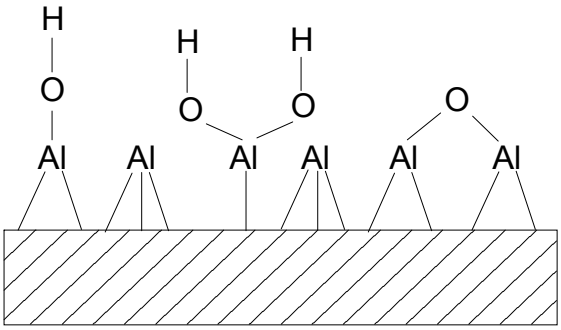

Figure 24: Surface of α-Al_2O_3.

Carboxylic acids bond to the basic groups of the α-Al_2O_3 surface. An electrostatic attraction between the negatively charged carboxylate anion and cationic centers on the Al_2O_3 surface leads to adsorption. The carboxyl group can bind as a ligand or chelat ligand to the aluminum.

10.2.4. Particle Size Distribution of Al_2O_3

The particle size[116] is investigated with laser scattering[164-167] (LS, Malvern Instruments, Mastersizer 2000 with Hydro 2000M dispersion unit, Herrenberg, Germany) during dispersion of the Al_2O_3 powder in water. A tip of a spatula of Al_2O_3 (≈5 mg) is added under stirring with 2520 min^{-1} to the liquid flow cell of the LS-apparatus (pH ≈ 8). The particle size is with d_{50}=52.9 μm and the main peak at 60 μm high at the beginning (Figure 25), because of the presence of agglomerates. Stirring, ultrasonification and increasing time destroy the agglomerates leading to a reduced particle size (d_{50}=174 nm, main peak 150 nm, Figure 26). This is in agreement with the d_{50}=290 nm value provided by the manufacturer, if different dispersion conditions are taken in account.

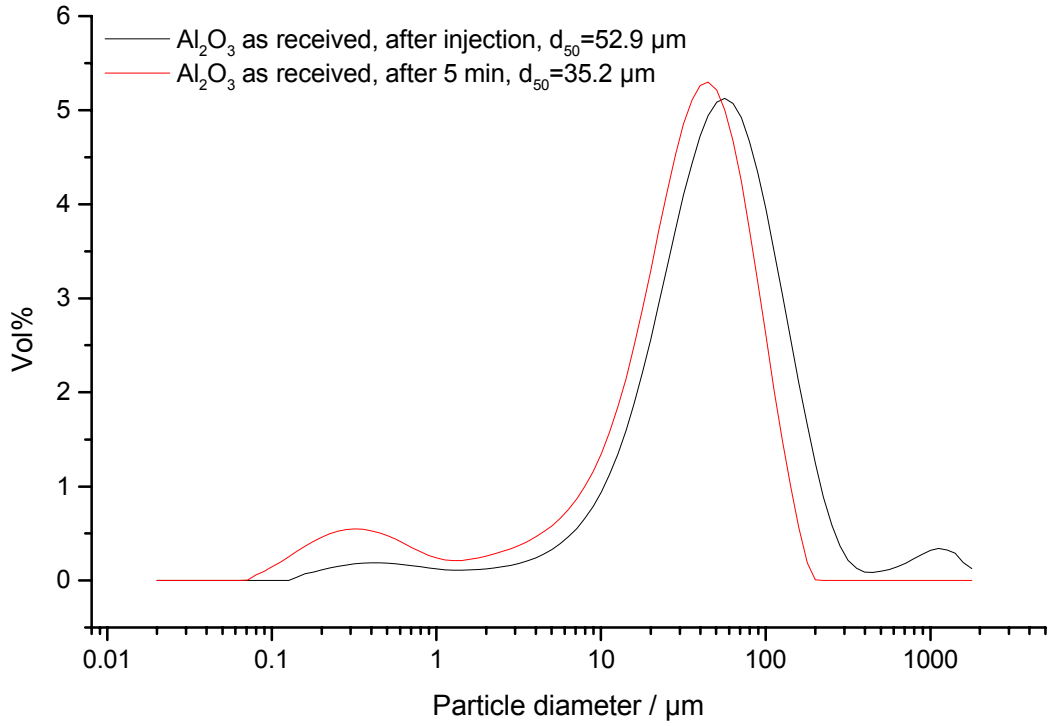

Figure 25: Particle size distribution of Al_2O_3 as received after injection of the sample and after 5 min.

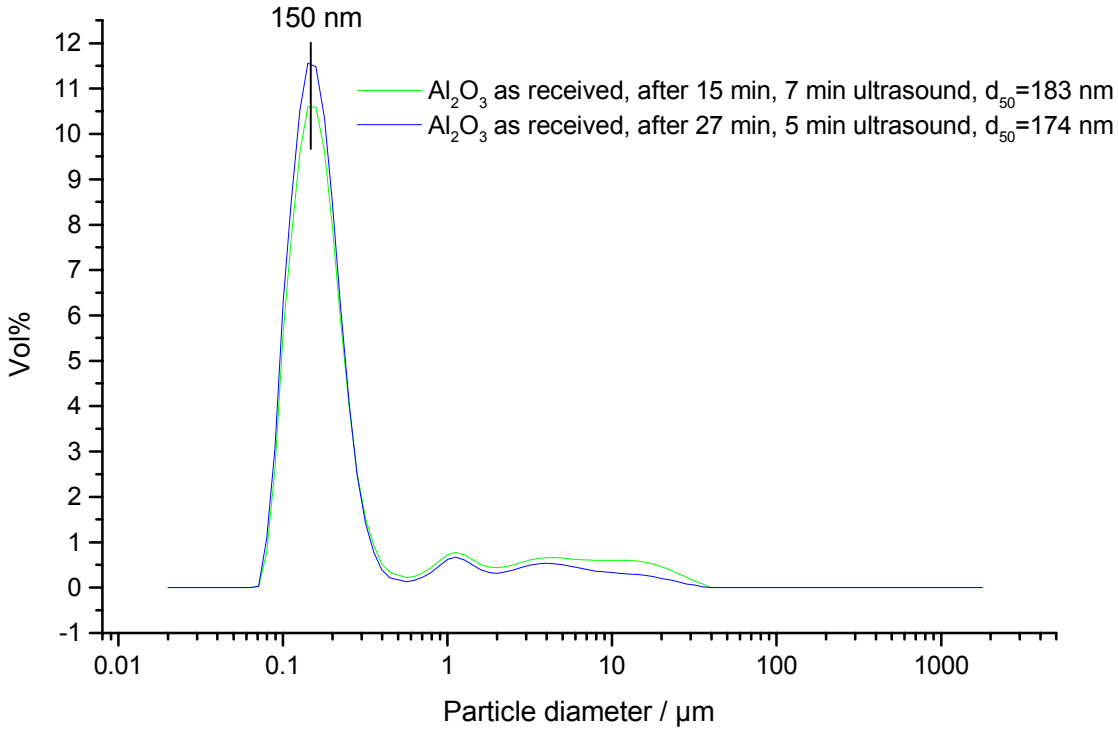

Figure 26: Particle size distribution of Al_2O_3 as received after 15 min, 27 min and ultrasonical treatment.

The bipurified Al_2O_3 is also investigated with laser scattering (LS). To purify the Al_2O_3, the powder is suspended two times in water (pH=5) and centrifuged. After decanting and drying at 60 °C in an oven the Al_2O_3 forms a monolithic cake that is ground in an agate mortar to a fine powder. The particle size distributions after the purification process (d_{50}=232 nm, main peak 178 nm, Figure 27) and before (d_{50}=174 nm, main peak 150 nm, Figure 26) are similar leading to the conclusion that the purification has no significant influence.

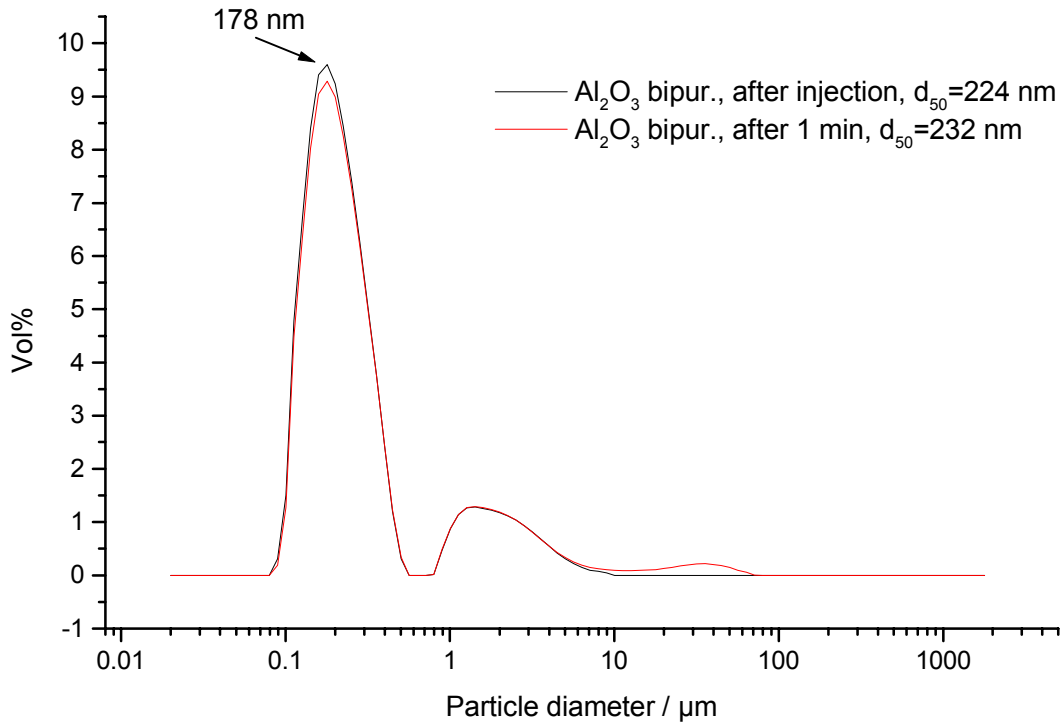

Figure 27: Particle size distribution of Al_2O_3 bipur..

Different theoretical models[165-167] can be used for the calculation of the particle size distribution such as the Mie theory for smaller particles. The calculation with this theory requires the complex refractive index of the analyzed material, that is the regular refractive index (the real part of the complex number) plus the extinction coefficient (the imaginary part), whereas for larger particles the Fraunhofer theory should be used. This theory does not require material constants of the analyzed substance. As a criterion for the size 40*λ can be used (where λ is the wavelenght of the applied light, here λ=632.8 nm, He-Ne-laser). So 40*λ ≅ 25 µm. The particle size distribution is calculated for Al_2O_3 (as received, after injection) using different theories (Figure 28) which show no remarkable divergence in the result. There are only slight differences in the range lower 5 µm particle diameter and above the curves are congruent. So the Mie theory is applied in this work, being suitable for small particles and describing larger particles as well. Changes in the optical constants do not affect the curve much. The constants for alumina are used in this study.

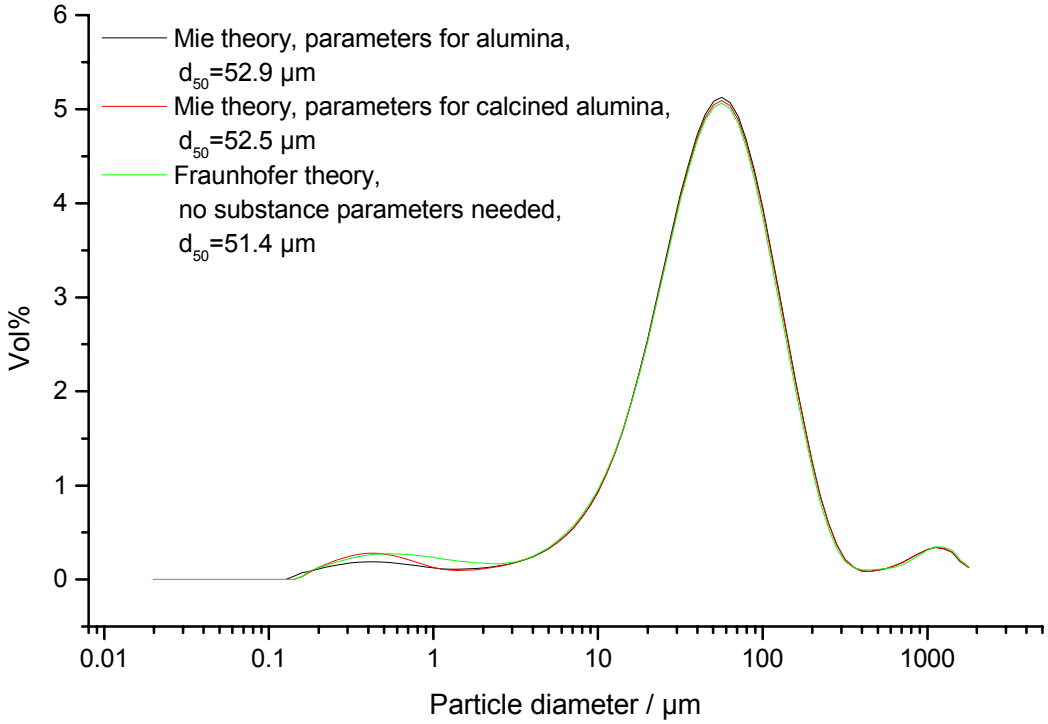

Figure 28: Comparison of different theoretical models.

The particle size was also measured with DLS[122-128] as a second method using an angle of 90°:

Table 9: Al_2O_3 particle size measurements by DLS.

measurement	hydrodynamic diameter / nm	
1	234	+ agglomerates
2	248	+ agglomerates
3	262	+ agglomerates
average	248	

The data analysis was done with the Contin theory providing a hydrodynamic particle diameter of 248 nm. The corresponding LS result is 174 nm, the producer´s value 290 nm.

10.2.5. Shape and Topology of the Al_2O_3 Particles

Figure 29-32 show four of the eleven SEM images taken from two samples of Al_2O_3 pur. (field emission SEM, Zeiss, DSM 982 Gemini). For preparation of the SEM samples the alumina powder is dispersed in iso-propanol and the suspension is ultrasonicated for 10 min (Bandelin, Sonorex Super RK 514 BH). After dropping the suspension with a Pasteur pipette on the sample holder and evaporating the iso-propanol, the SEM micrographs are taken.

In the SEM-resolution the surface of the particles is more or less flat (Figure 29, 30) only sometimes showing steps and roundly shaped elevations on the surface (Figure 31, 32). The particles lie separately on the sample holder. Congruent to the LS investigations the purification of the Al_2O_3 does not merge the particles and does not affect the particle size distribution. As provided by the SEM images the smallest particles have a diameter of 20 nm, the middle one of 200 nm and the largest one of 600 nm. Small particles are often attached to larger ones; the 20 nm particles cannot be detected with LS because of their weak scattered light intensity. Agglomerates are detectable in the particle size distribution of Al_2O_3 (Figure 25) directly after adding the powder to water. According to the SEM investigation they do not consist of one large particle so that an intense long term stirring or ultrasonical treatment destroy them.

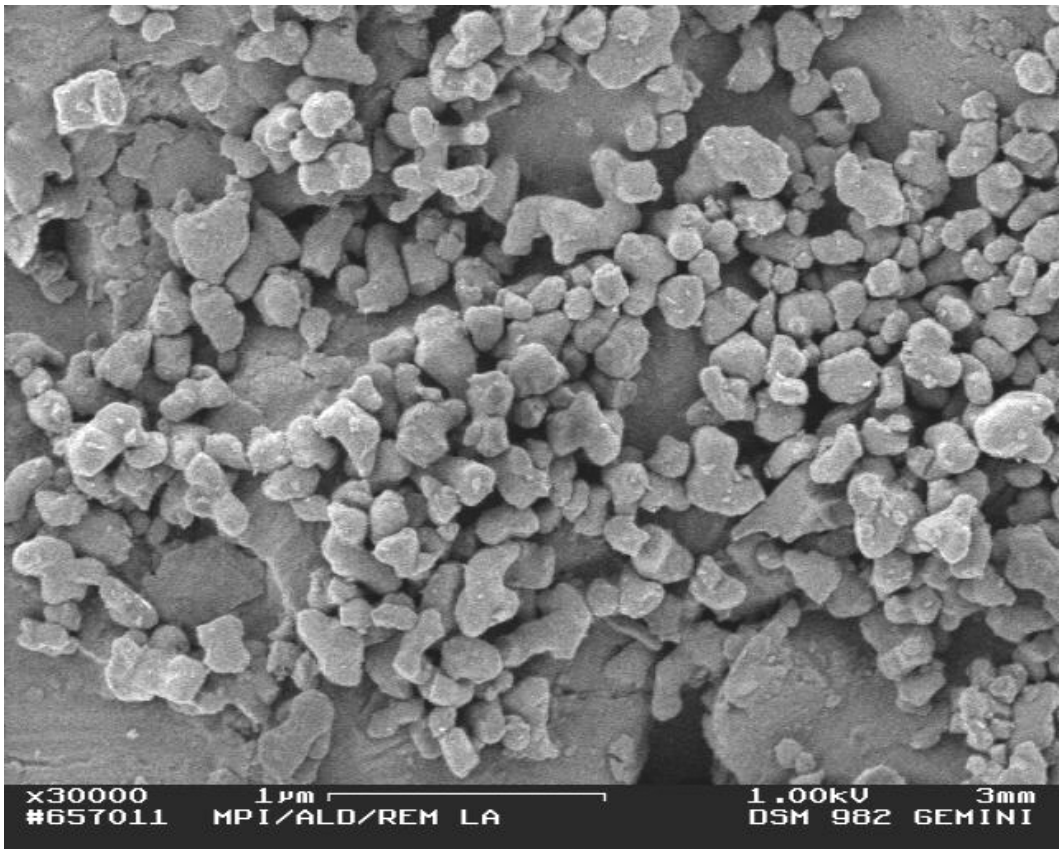

Figure 29: SEM image of Al_2O_3 pur., survey scan.

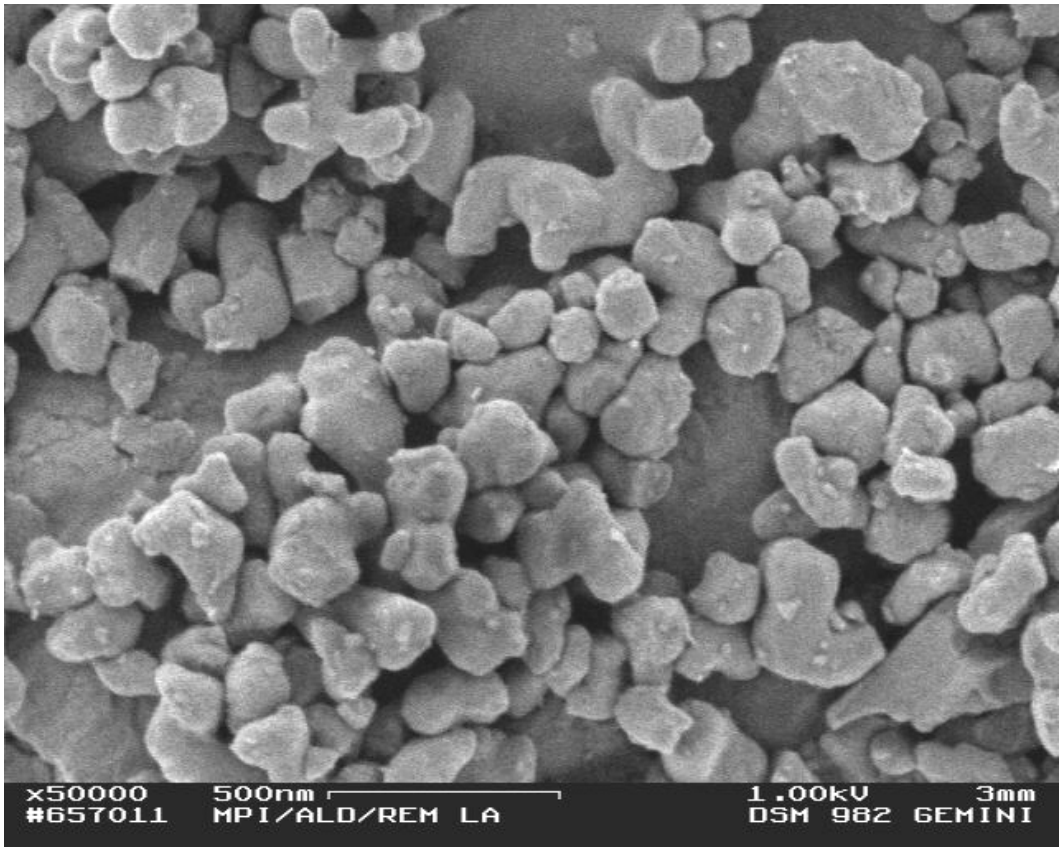

Figure 30: SEM image of Al_2O_3 pur..

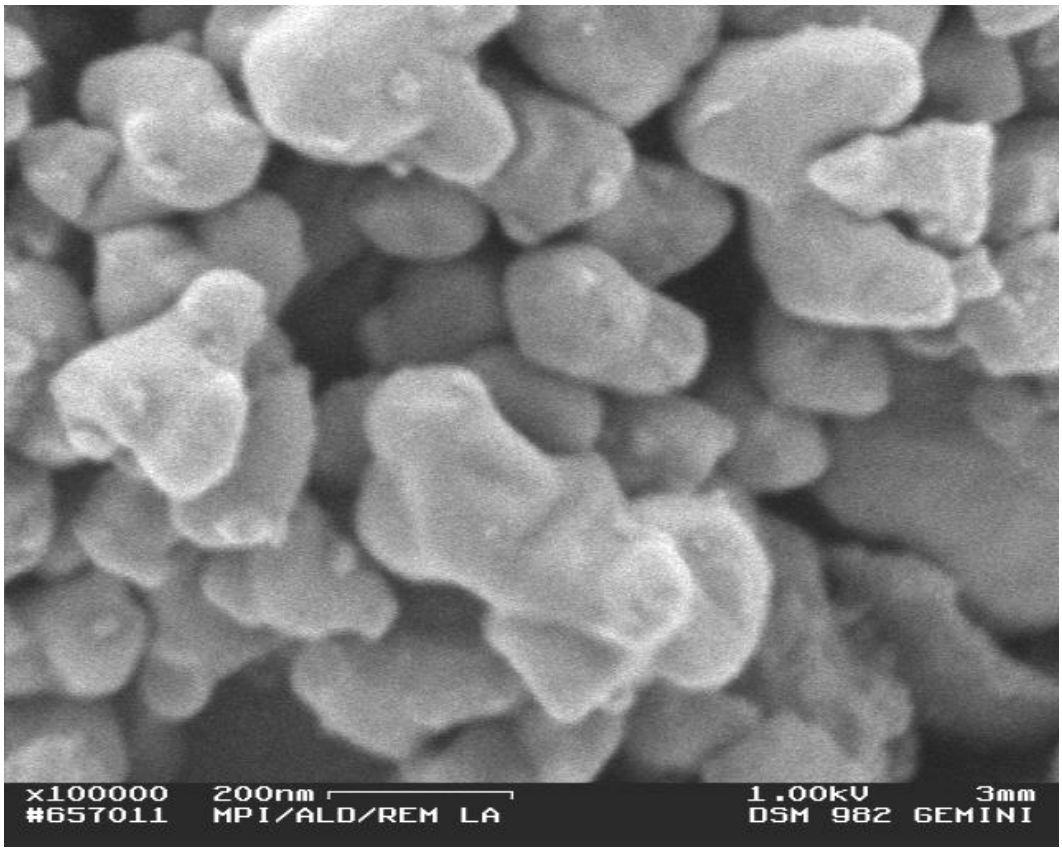

Figure 31: SEM image of Al_2O_3 pur., high resolution.

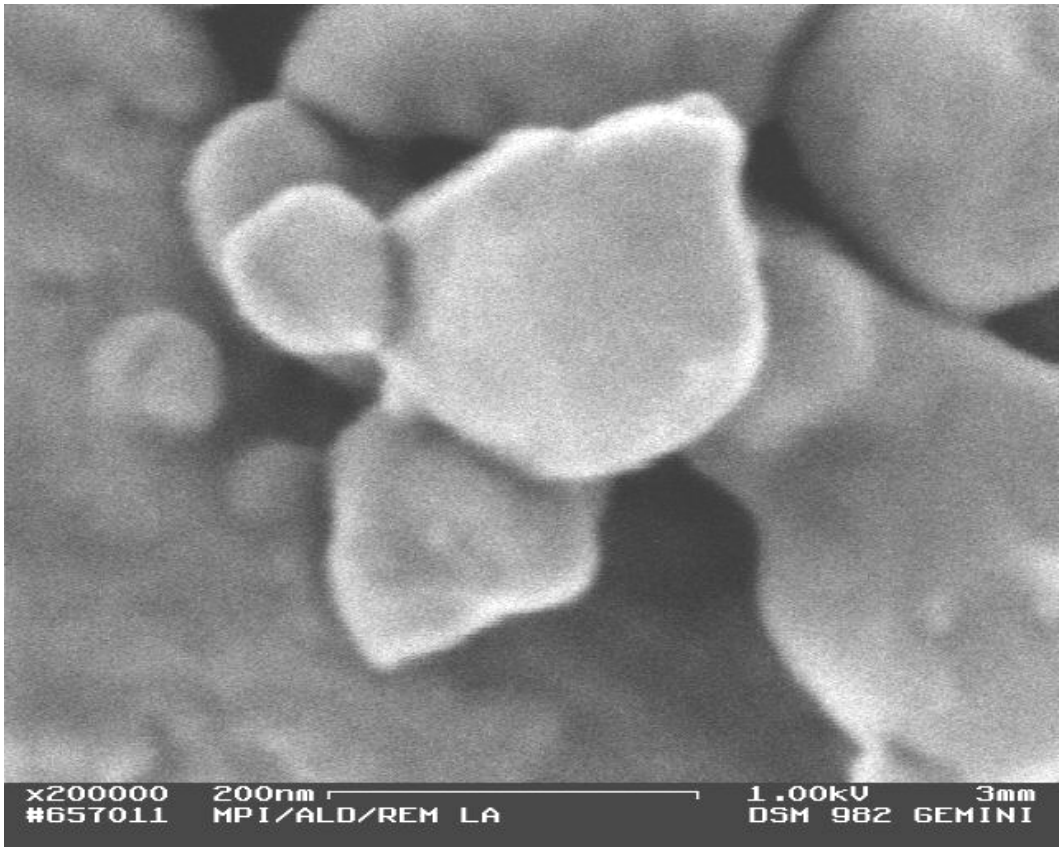

Figure 32: Single Al_2O_3 pur. particles (SEM image).

11. Functionalization of the Powders

11.1. Attachment of MCT-β-cyclodextrin to Si_3N_4

A commercially available β-cyclodextrin derivative is attached in a one-step reaction to Si_3N_4 ceramic powder making a multi-step derivatisation of the cyclodextrin unnecessary. The cyclodextrin described as MCT-β-cyclodextrin is produced and distributed by Wacker, Burghausen, Germany. It is a white and very well water soluble compound. MCT stands for mono-chlor-triazinyl, the sodium hydroxyl group and the positions are not expressed. Its full name should be 3-chlor-5-sodium-hydroxyl-triazinyl-β-cyclodextrin. The number of 3-chlor-5-sodium-hydroxyl-triazinyl-groups per β-cyclodextrin ring varies from molecule to molecule, the average value is 2.8. The positions where the triazinyl rings are attached to the cyclodextrin are not defined. The 2-, 3- and 6-positions of the cyclodextrin are used for attachment. Which and how many D-glucose units are used is also not defined. A very defined and regioselective derivatisation of β-cyclodextrin will be presented in the following chapters.

The Si_3N_4 powder was used without further surface modification and the MCT-β-cyclodextrin **31** was fixed to the Si_3N_4-surface in one step. These advantages are accompanied by the loss of regioselectivity.

The molecular structure of **31** and its attachment to the Si_3N_4-surface is as follows:

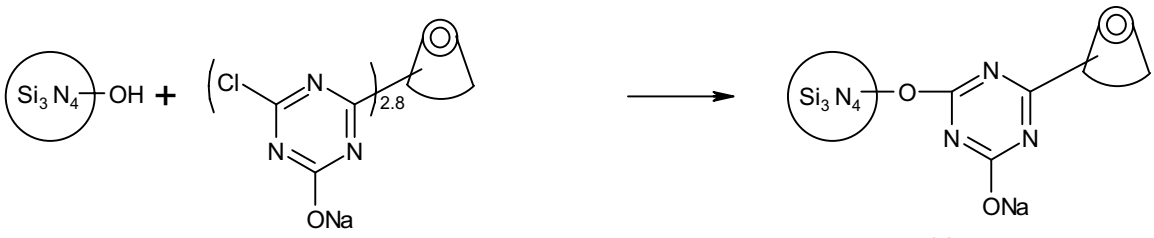

31 **32**

The reactions[168, 169] of the heteroaromatic triazine[170] ring with the Cl-C=N group, a N-heteroanalogous carboxyl chloride, are carbonyl reactions at the C-atom. While the triazinyl reacts with the silanol groups of the Si_3N_4–surface, the O- or O^--

atom of the silanol group attacks the partly positively charged carbonyl C-atom and forms a silyl ester. The carboxyl chloride can also be hydrolyzed in a side chain reaction so that the chloro group is converted to an OH-group.

The reaction for the attachment of **31** to Si_3N_4 is carried out in two different ways. The first is a reaction of **31** with Si_3N_4 in an aqueous suspension at 67 °C by isolating and drying the wet powder overnight at 40 °C in an oven. The moderate temperature and the comparatively low water content of the drying paste avoid hydrolysis whereas the long reaction time, the high concentration and the use of intense mixing of **31** support the reaction during drying. It is called "reaction at 67 °C". In the second approach a suspension containing Si_3N_4, **31** and water is prepared for intense mixing of the compounds. Most of the water is removed by evaporation at room temperature and predrying is done for 2 h at 45 °C to start the reaction. At 145 °C for 10 min the reaction is completed while the cyclodextrin resists temperatures up to 180-200 °C in the dry state. This reaction is called "solid state reaction". The reactions are carried out as follows:

2.44 g **31** are dissolved in 55 ml water (20 mmolar). 10 g Si_3N_4 as received are suspended and stirred overnight at 67 °C. The product **32** is centrifuged, washed and dried overnight at 40 °C then crushed in an agate mortar.

12.2 g **31** are dissolved in 120 ml water. 50.0 g Si_3N_4 are added. The suspension is stirred, ultrasonically treated for 10 min and centrifuged. The wet precipitate is poured into a crystallization vessel and predried at room temperature then dried for 2 h at 45 °C. Thereafter the temperature is raised for 10 min to 145 °C. For purification **32** is resuspended in water, centrifuged several times, dried at 50 °C and finally ground in an agate mortar.

The DRIFT-spectrum (Figure 33) is measured and the methylene region is zoomed in (Figure 34), so that the signals can be seen.

The ζ-potential measurements are shown in Figure 35 and 36. They prove that **31** is bonded to the Si_3N_4–surface because the curve is slightly shifted to the basic region due to the small amount adsorbed, the basic triazine ring cause the shift. The pH_{iep} of

7.2 compared to pH_{iep}=7.7 for **20** can be easily understood. One amino group causes a shift similar to that of the triazine ring. The curve has a flat shape as expected. The position of the curve is different from all the others, what is another evidence for the attachment of **31**.

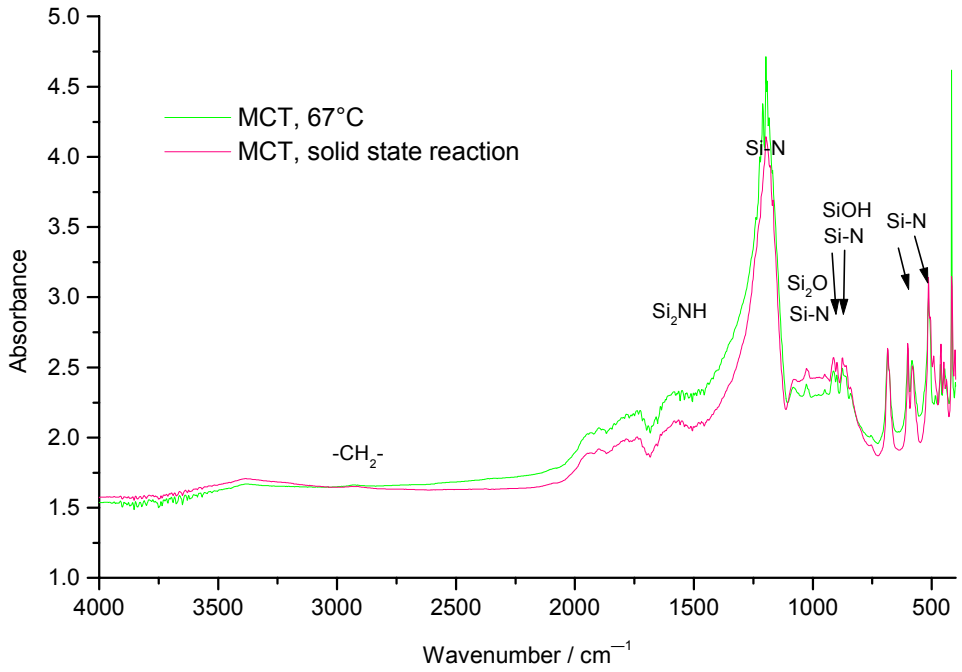

Figure 33: DRIFT-spectra of **32**.

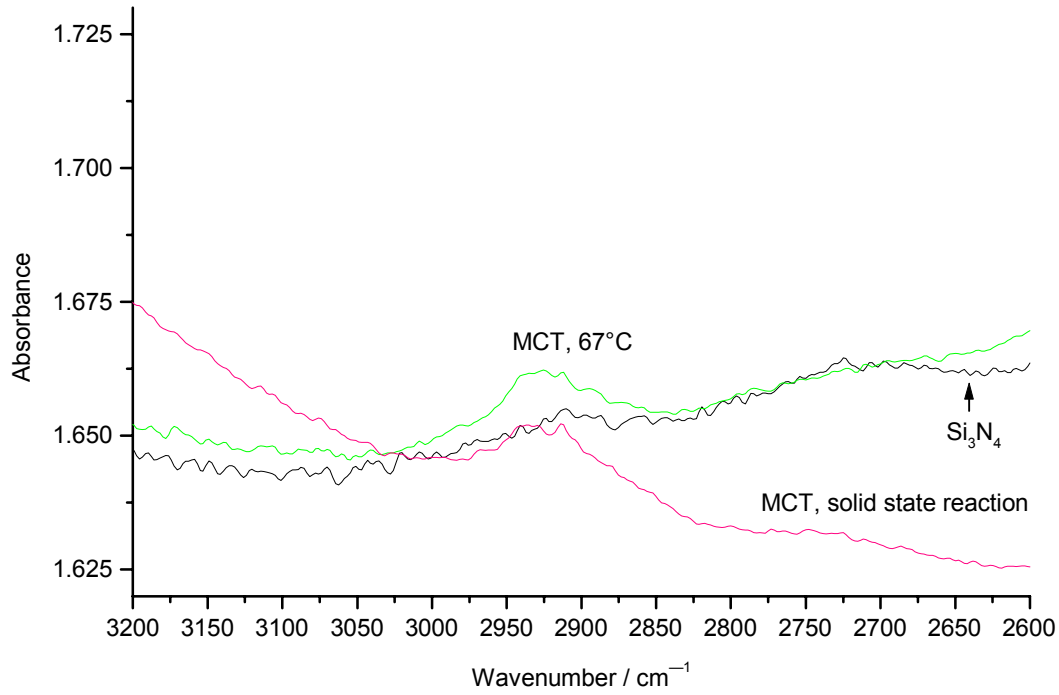

Figure 34: Zoomed DRIFT-spectra of **32**.

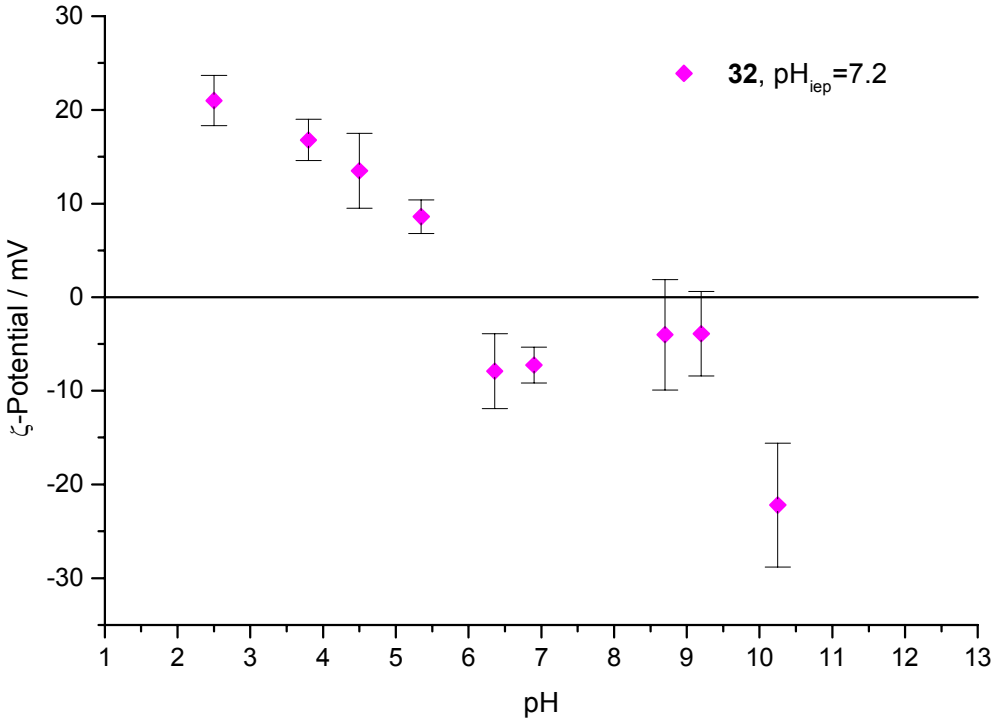

Figure 35: ζ-Potential of **32**.

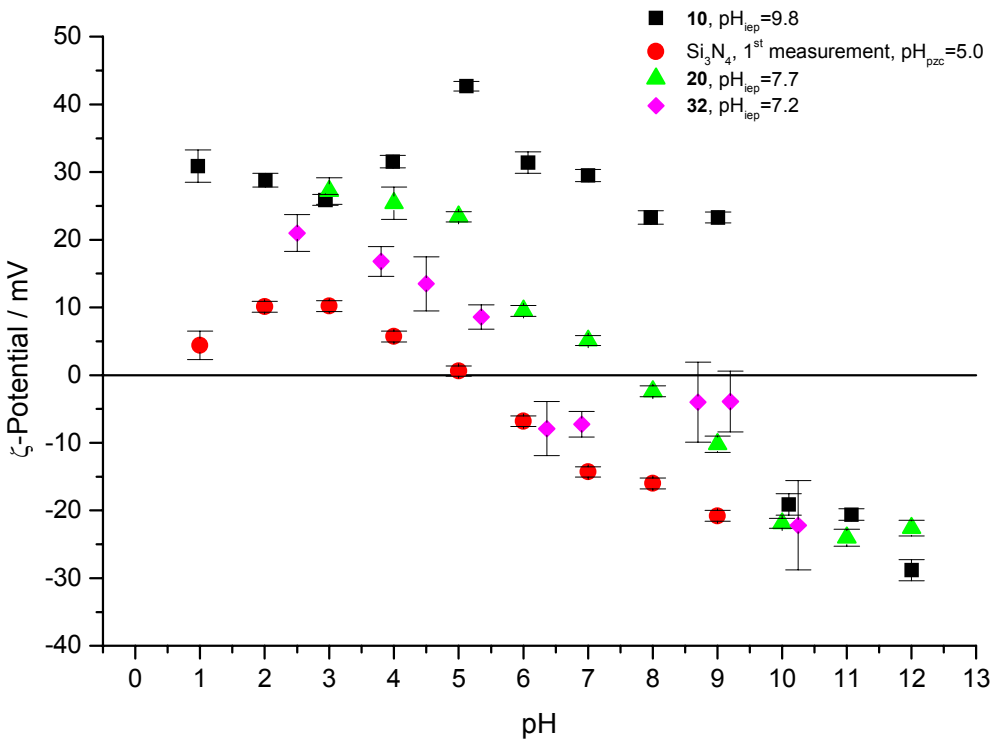

Figure 36: ζ-Potential of **32** compared to reference systems.

11.2. Synthesis of Mono-6-amino-β-cyclodextrin

The synthetic route is as follows:

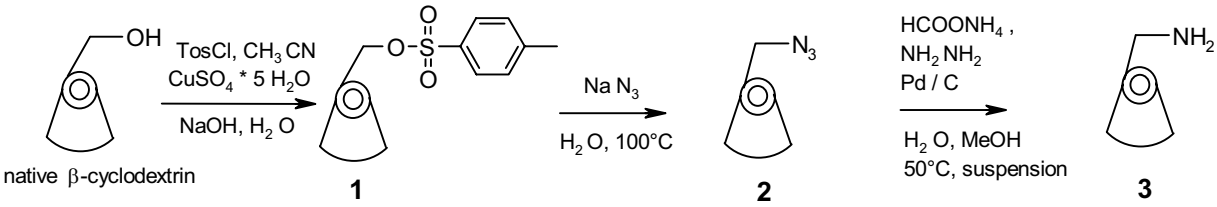

The two products **1** and **2** are prepared as described in literature[171-177]. For the conversion of **2** to **3** a direct hydrogenation with gaseous H_2 and **2** in an appropriate solvent in an autoclave under increased pressure can be used as successfully done in the group of G. Wenz[173]. Because initiation of the reaction failed sometimes, an indirect hydrogenation method is applied, where hydrogen is donated in situ by hydrazine or ammonium formate. The synthesis is based on L. Jicsinszky[178]. In the approach used in this work the isolation and purification is improved:

1 g Mono-6-azido-β-cyclodextrin **2** is suspended in 10 ml methanol under nitrogen, cooled down to –20 °C and 2 g Pd/C (≈50 % water content, 10 % Pd on C) are added. There is no remarkable heat formation, so the reaction mixture is heated to room temperature. 0.2 g of ammonium formate is added and heated to 50 °C at a stirring speed of 700 rpm without reflux. There is no indication of a reaction by gas bubbles. After three hours some drops of hydrazine hydrate are added. The reaction is carried out for 18 h while the loss of solvent is compensated by adding of water. During the entire reaction time there is no visible gas formation contrary to[178]. Probably because of the lowered amount of educts (a third of the amounts used in[178], but the solvent being more than a third) all gas is dissolved. The suspended **2** settles down at the bottom of the flask. It is scratched with a spatula from the wall to redispers it. But a complete reaction is detected by TLC with alumina sheets and an iso-propanol-ethylacetate-water-mixture (1:1:1) using mono-6-azido-β-cyclodextrin **2**, β-cyclodextrin and heptakis-6-amino-β-cyclodextrin **9** as references. **2** provides two spots. One by unreacted β-cyclodextrin at R_f = 0.39 and one by **2** at R_f = 0.57 (Kräuter[179] 0.49). The reaction mixture provides a spot by β-cyclodextrin

(R_f = 0.39) and by product **3** at R_f = 0.29 (Kräuter[179] R_f = 0.39). There is no spot from **2**. **9** stays at the baseline, because it is too polar and the interaction with the alumina too strong.

The reaction mixture is cooled to room temperature. The catalyst is filtered off with regular filter paper, washed with cold and hot water (45 °C) and filtered with a 450 nm membrane. The solvents are removed by rotary evaporation and freeze drying. The crude product is suspended in methanol to extract the ammonium formate, the methanol is filtered off and the product is dried. **3** is dissolved in water. The aqueous solution of mono-6-amino-β-cyclodextrin **3** has a pH of 6.8. When adding an activated (OH^- - form) strongly basic anionic exchanger (DOWEX 2X8), the pH of the suspension is 9.3 after some hours. After filtration (450 nm membrane) and washing the ion exchanger with water, the filtrate has a pH of 7.3. Then it is freeze dried yielding 357 mg **3** (36.5 %).

L. Jicsinszky separates the catalyst by hot filtration with a paper filter and adsorption to charcoal. The separation by filtration and membrane filtration has the advantage that no product is adsorbed to the charcoal and that it is more effective. For the isolation of **3** from ammonium formate L. Jicsinszky transfers **3** to the hydrochloride, dissolves the formate in water and precipitates the hydrochloride of **3** by addition of methanol. In this work the ammonium formate is extracted from the solid **3** with methanol. The treatment with the ion exchanger ensures that **3** is obtained in the reactive, neutral form suitable for nucleophilic substitutions (S_{N2}) and not in the inactive ammonium form.

The product is azide free (IR, Figure 37). There is a strong signal from the azido-group of **2** at 2101 cm^{-1} as described in literature[180]. Partially hydrogenated azido-groups at 2043 cm^{-1} do not appear in[180]. The azido signals disappear after conversion to the amine **3**. This is a hint for the reaction of **2** to **3**. At 1640 cm^{-1} β-CD, mono-6-azido-β-cyclodextrin **2** and mono-6-amino-β-cyclodextrin **3** show signals of OH-groups in the solid state. The NH_2-groups of heptakis-6-amino-β-cyclodextrin **9** show a signal at 1601 cm^{-1}, but not at 1640 cm^{-1} solid state OH. Partially hydrogenated azido groups or amino groups from **2** are also at 1601 cm^{-1}. A slight

shoulder at 1601 cm^{-1} in the spectrum of **3** derives from amino functions, an evidence for the formation of the amine **3**.

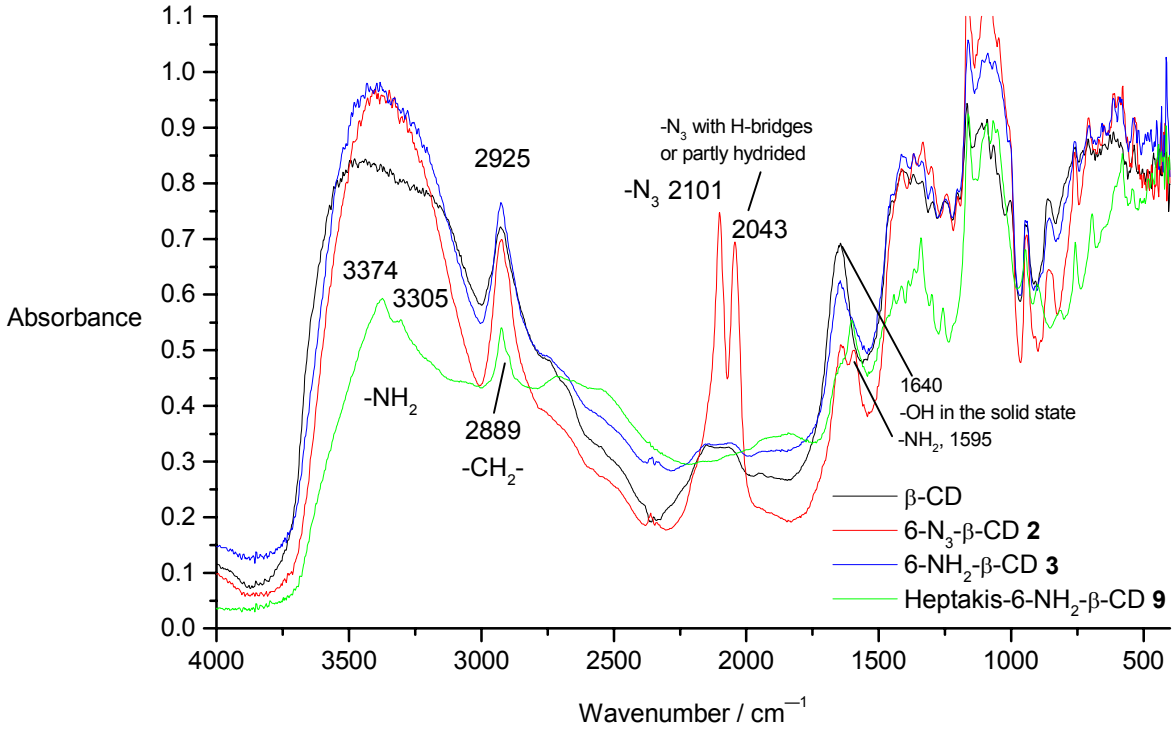

Figure 37: DRIFT-spectra of 6-NH_2-β-CD **3**, 6-$(NH_2)_7$-β-CD **9**.

11.3. Epoxidation of Si_3N_4

This chapter describes the epoxy-functionalization of Si_3N_4. Native cyclodextrins have many hydroxyl groups that react similarly but that are not very reactive. For a defined reaction the functionalization of the cyclodextrins is important, so the cyclodextrin is activated and a discrimination of the hydroxyl groups is induced. The reaction partner of the cyclodextrin should also be selective. If both conditions are satisfied, a defined reaction is achieved. Otherwise side reactions like oligomerisations are present.

The epoxy group of **5** reacts predominantly with the amino group of mono-6-amino-β-cyclodextrin **3**. The reaction with water and hydroxyl groups of β-cyclodextrin is very slow. This leads to a defined reaction between **3** and **5**. Another way is the silanisation of **3** with **4** followed by the fixation to Si_3N_4. The cyclodextrin is prepared so that it can be bonded to Si_3N_4 ceramics in one step. This sounds very promising, but it has some disadvantages. Not only the epoxy terminus reacts with the amino group, the silanol terminus of **4** formed after hydrolysis of the MeO-groups reacts with amino groups under formation of a cation-anion-pair, too. The silanol part can also react with the OH-groups of the cyclodextrin causing an oligomerisation of **3**.

Reaction pathway:

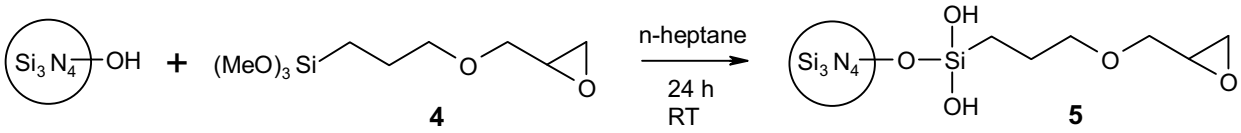

5 g Si_3N_4 are suspended in 57 ml n-heptane (Aldrich) in a 250 ml single neck flask. 390 µl (3-glycidyloxypropyl)-trimethoxysilane (2,3-epoxypropyl-propyl-ether)-trimethoxysilane, Fluka) **4** are added and stirred with a magnetic stirrer at room temperature for 24 hours. The suspension is centrifuged at 4000 min^{-1} for 12 min. The solvent is decanted and the precipitate is washed (redispersed) twice with 50 ml n-heptane and centrifuged. The supernatant solution is decanted and the product is dried for 12 h under regular pressure at room temperature and then for 2 h in a vacuum chamber at room temperature.

Figure 38 shows the DRIFT-spectrum. CH_2- valence vibrations (2936, 2869 cm^{-1}) prove that the silane is attached to the surface. Si_3N_4 itself has no organic contamination at the surface since there are no signals typical for organic compounds detectable in the DRIFT-spectrum.

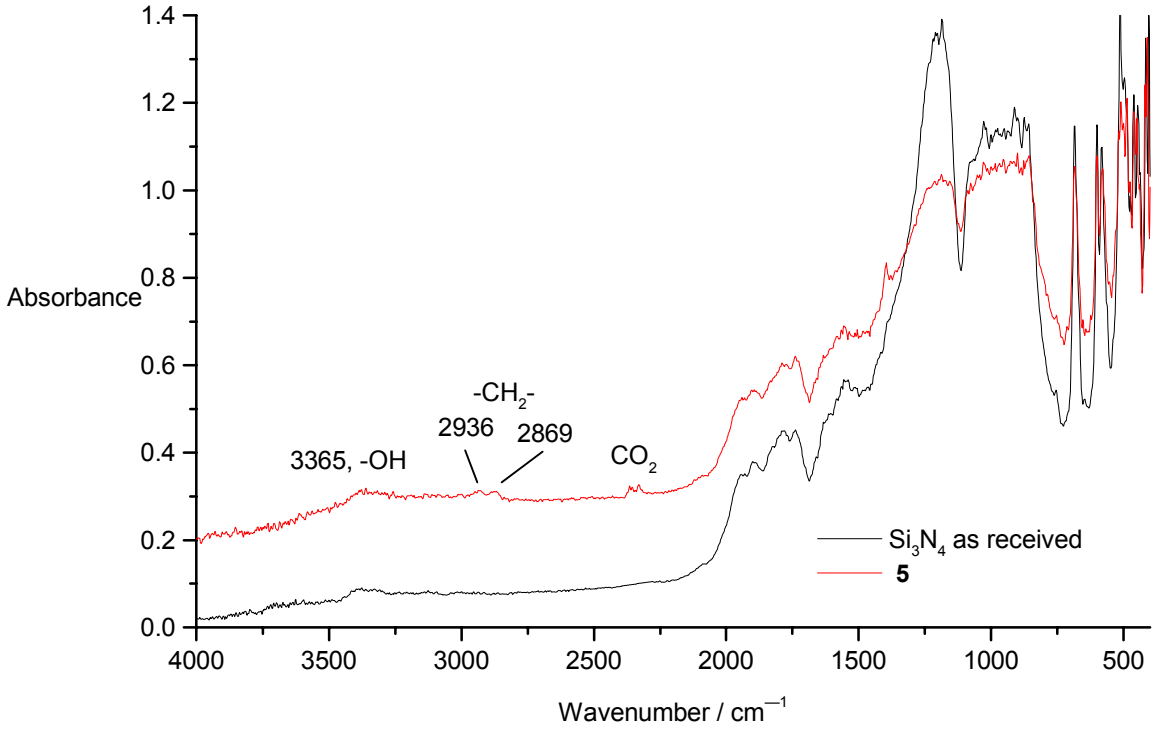

Figure 38: DRIFT-spectrum of epoxyfunctionalized Si_3N_4 prepared in heptane.

The hydrolysis of the epoxy group in **5** is slow. **5** is prepared as described above. This time n-hexane is used as a solvent and a higher concentration of **4** is applied. Two DRIFT-spectra are taken with a time distance of 14 days (Figure 39). The epoxy group can be seen at 3053 and 3002 cm^{-1} close to the methylene vibrations. It is shifted to higher frequencies because the three membered ring tightens the bonds. The two spectra are exactly the same (CO_2-signal excluded). **5** was stored and measured in air. The intensity of the epoxy signals does not decrease. This means the epoxy group does not show significant hydrolysis under these conditions.

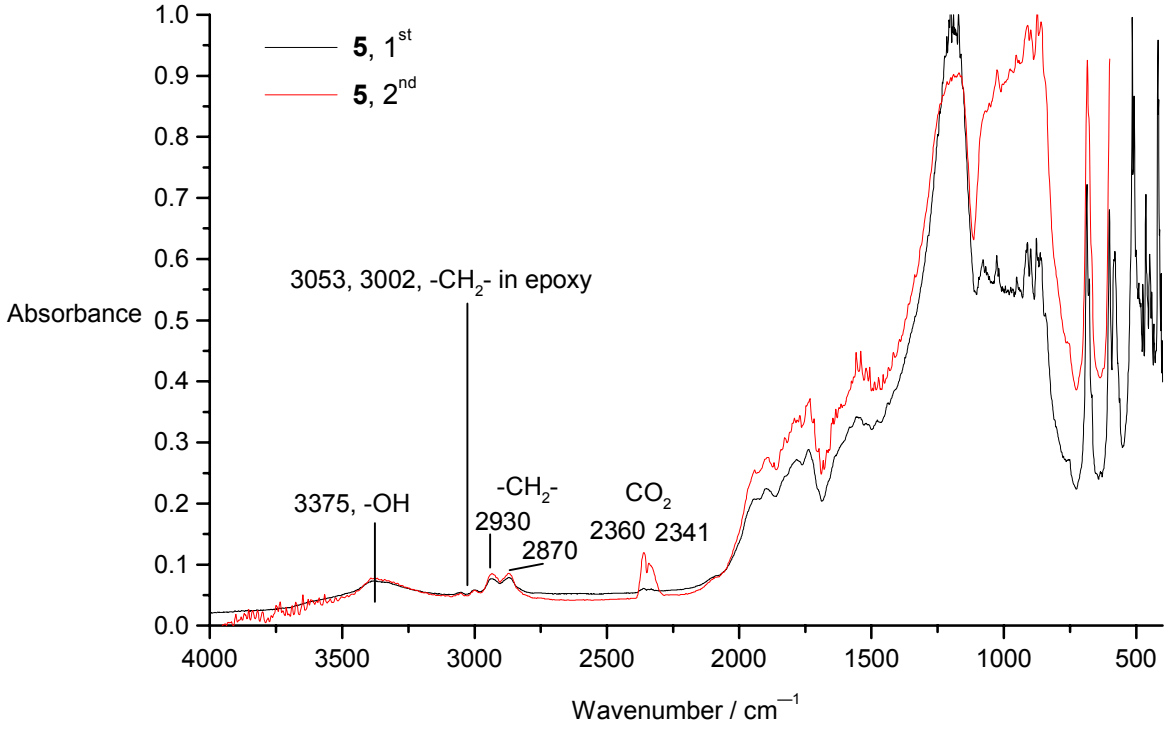

Figure 39: Hydrolysis of **5**.

11.4. Immobilization of Mono-6-amino-β-cyclodextrin on Epoxy-functionalized Si_3N_4

For the immobilization of mono-6-amino-β-cyclodextrin **3** on epoxy-functionalized Si_3N_4 **5** the following reaction is used.

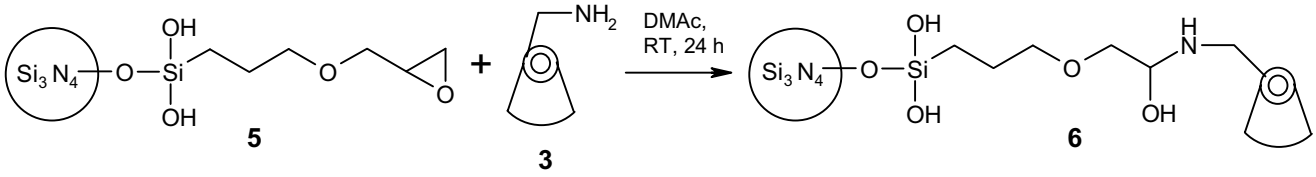

The total mass needed to cover the Si_3N_4-surface completely with a cyclodextrin monolayer is calculated on the basis that the required space for one cyclodextrin of a close packing is a square of 1 nm side length (1 nm^2 area) according to the circle shaped bottom side of the cyclodextrin (Figure 40).

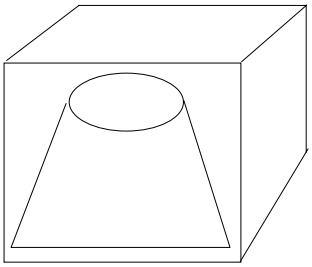

Figure 40: Required space for a cyclodextrin of a close packing.

The Si_3N_4-ceramic powder has a specific surface area of 12.7 m^2/g. On 1 g Si_3N_4 n=12.7 m^2 / 10^{-18} m^2 cyclodextrin molecules can be adsorbed. m=n/N_A*M provides the mass of a monolayer with N_A as the Avogadro constant (6.023*10^{23}) and M as the molecular weight of the cyclodextrin **3** (1134 g/mol). 23.9 mg **3** form a monolayer on 1 g Si_3N_4. In the following investigation mono-6-amino-β-cyclodextrin **3** is bound to **5** and the adsorbed amount is measured. This gives information whether **3** is bound or not, the amount in mg and as percentage of the total amount. The desorption properties are also investigated. They provide information about the power of the binding of **3** to the surface.

1.000 g **5** are given into a centrifuge tube. 15.0 mg **3** are dissolved in 3.0 ml DMAc. For complete dissolution 10 min are needed to get a colorless, transparent solution.

The solution of **3** is added to **5** and stirred at room temperature for 24 h in the centrifuge tube. The system is centrifuged at 4000 min^{-1} for 30 min. The centrifuge tube should not get any mechanical shock because **6** is easily redispersed. 1 ml of the overstanding solution is taken into a 1 ml syringe with a long canula. The volume of the overstanding solution is measured by pouring it into a cylinder. The rotation angle is measured and the mass is calculated (Table 10).

3.0 ml water are added to the precipitate **6**. The system is redispersed by stirring with a spatula for 10 min, centrifuged, 1 ml is taken into a 1 ml syringe and the remaining volume is measured. The rotation angle is measured. The powder is dried in a vacuum chamber at 40 °C and ground in an agate mortar. The results are described in Table 10.

Figure 41 shows DRIFT-spectra of **3** on Si_3N_4–powder. As indicated by the measurement of the adsorbed mass (Table 10), there are no methylene vibrations for the non-epoxyfunctionalized system (Si_3N_4 + **3**). Only 8.5% (Table 10) of **3** bind to unmodified Si_3N_4, whereas 17.3% (Table 10) of **3** bind to **5**. **6** does not have higher methylene signals than **5**. Either the adsorbed amount of **3** is too low to be detected with DRIFT, or a small amount of the epoxysilane **4** is dissolved and **3** is bound so that in the result the methylene signal is constant or decreases, if more of **4** is dissolved than **3** bound to **5**.

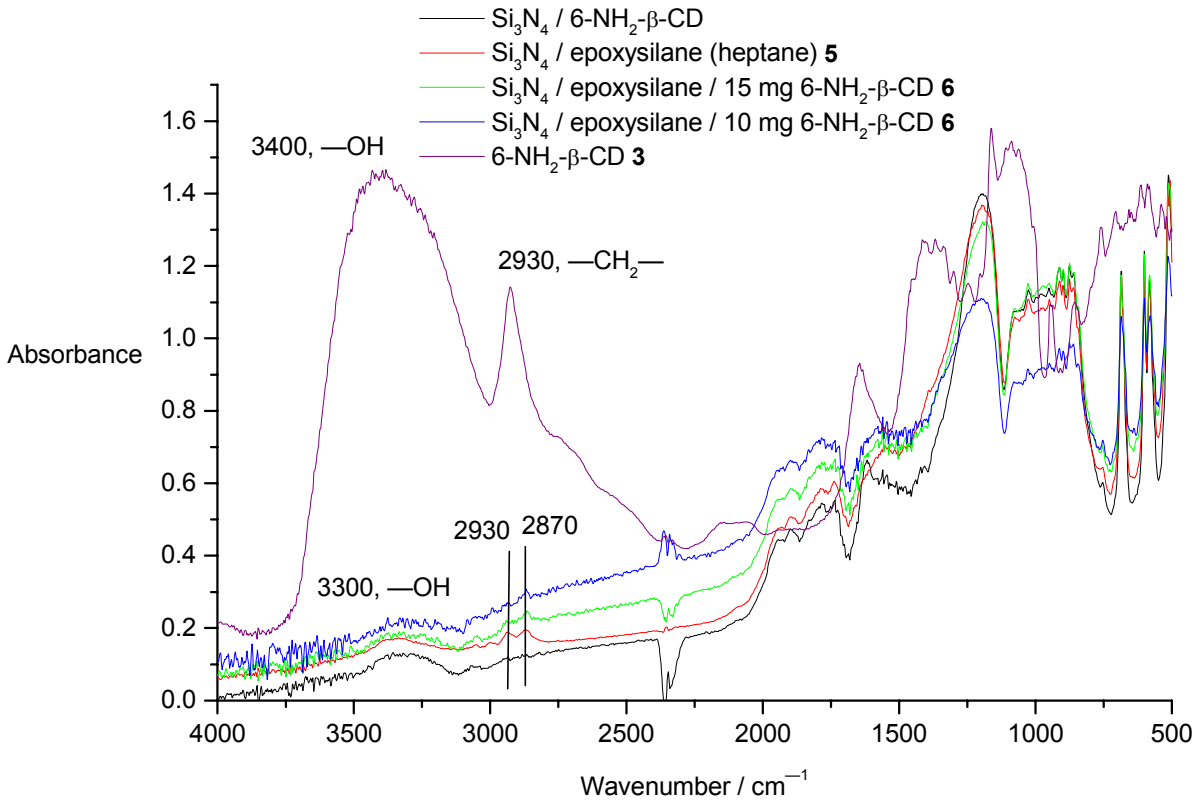

Figure 41: DRIFT-spectra of mono-6-amino-β-cyclodextrin **3** on Si_3N_4.

Figure 42 shows **5** after stirring in DMAc and washing with H_2O under the same conditions as described above for the fixation of **3** but without **3**. It is obvious that no silane is removed in contrast to a long stirring in water (Figure 43).

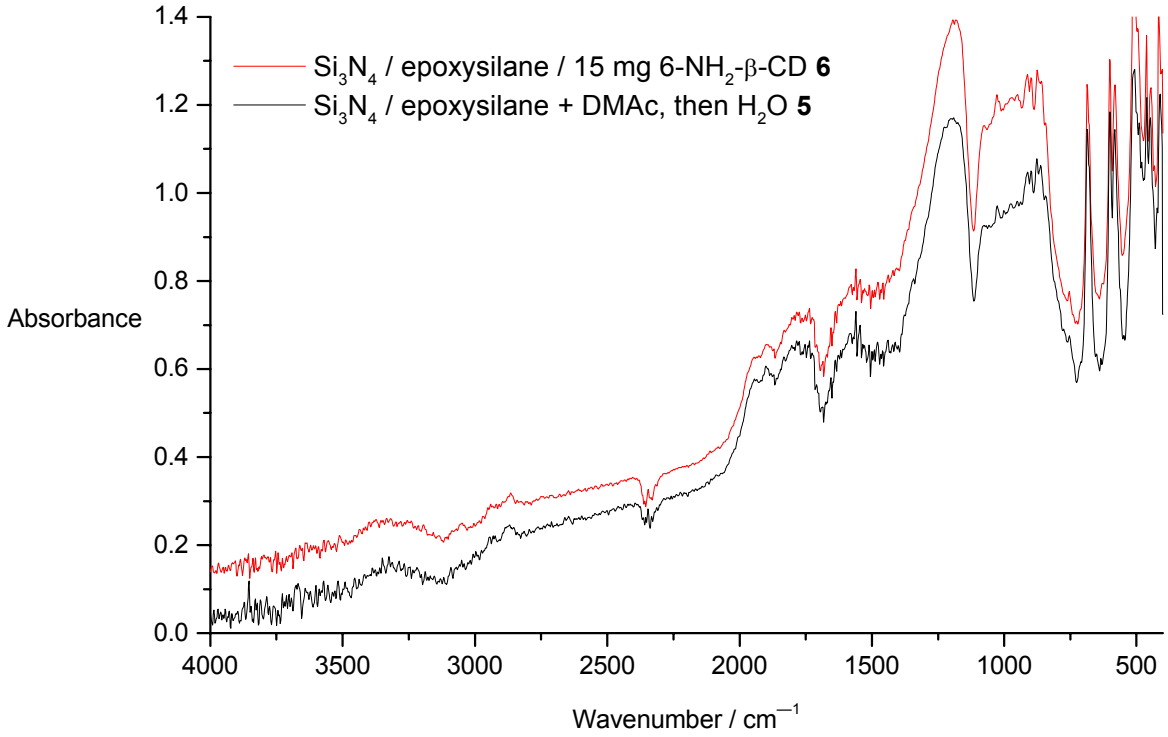

Figure 42: Influence of solvents to **6** and comparison of **6** with **5**.

11.4.1. Ad- and Desorption of Mono-6-amino-β-cyclodextrin on Unmodified Si_3N_4

As a reference experiment it is checked whether mono-6-amino-β-cyclodextrin **3** adsorbs also on unmodified Si_3N_4. The blind adsorbed mass not bound or adsorbed to epoxy groups is measured.

15.0 mg mono-6-amino-β-cyclodextrin **3** are dissolved in 3.0 ml (2.82 g) DMAc in a centrifuge tube. 10 min are needed for complete dissolution. 1.000 g Si_3N_4 are added and dispersed, then stirred with a magnetic stirrer for 12 h and centrifuged (3000 min^{-1}, 30 min). The volume and rotation angle of the solution is measured.

For the investigation of the desorption 3.0 ml water are added. The powder is dispersed, centrifuged and the rotation angle and volume are measured. Table 10 shows the results. The total amount of **3** that is included by the precipitate is called "trapped" amount. The precipitate contains solvent in which some **3** is dissolved. This amount is called "in solvent". "Bound" is called what is bound to the solid surface of Si_3N_4. The number of decimal digits does not represent the accuracy of the measurement. They are used for the calculation, the first digit after the decimal point in the result is valid.

Table 10: Ad- and desorbed mass of **3** on **5**.

6-NH_2 - β-cyclodextrin **3**	conditions	trapped	bound	in solvent
15.0 mg	3.0 ml DMAc, 1.000 g Si_3N_4 as received	3.10 mg	1.27 mg, 8.5%	1.83 mg
Desorption	3.0 ml H_2O		0.64 mg, 4.3%	2.46 mg in 3.1 ml H_2O
15.0 mg	3.0 ml DMAc, 1.000 g epoxy Si_3N_4	4.81 mg	3.68 mg, 24.5%	1.13 mg
Desorption	3.0 ml H_2O	2.66 mg	2.59 mg, 17.3%	0.07 mg

The measurement shows that **3** binds to **5**. A blind adsorption of **3** to Si_3N_4 is recognized. By redispersing in water a part of **3** is dissolved from the ceramics. About a quarter of the total amount is adsorbed by **5**. The influence of the epoxysilane **4** on

the adsorption of **3** can be clearly seen. **5** binds more (2.88-fold) **3** than Si_3N_4. **3** is only loosely adsorbed to Si_3N_4. So a large amount is desorbed by redispersing in water.

11.5. Immobilization of Heptakis-6-amino-β-cyclodextrin on Si_3N_4

β-Cyclodextrin with seven amino groups at the 6-position **9** (one at each D-glucose unit) is a proper derivative for fixation on epoxyfunctionalized Si_3N_4 **5**. Because of these seven amino groups per cyclodextrin compared to one in mono-6-amino-β-cyclodextrin **3** there should be a better reactivity with **5**. But the disadvantage of **9** is that the formation constant of complexes is much lower than for **3**. The synthetical pathway for the synthesis of **9** is as follows.

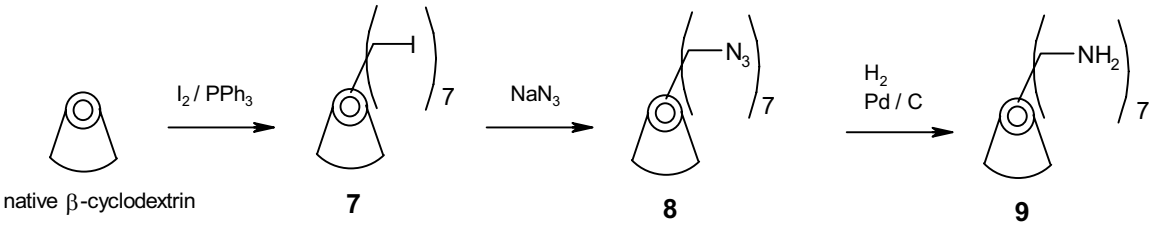

7 **8** **9**

The attachment of **9** to Si_3N_4 was described by[181-184] in the following way.

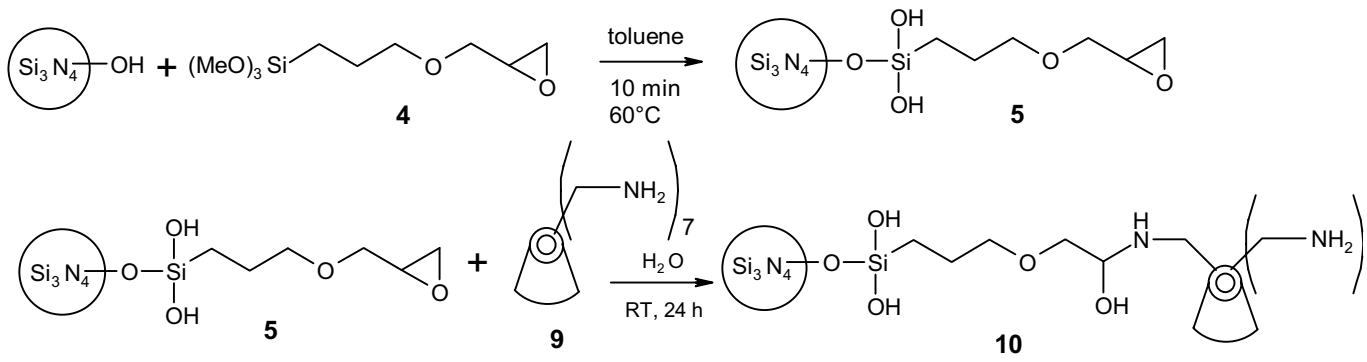

4 **5** **5** **9** **10**

De Paoli[185] prepared **10** as follows:

"0.5 ml (3-Glycidyloxypropyl)-trimethoxysilane are dissolved in 50 ml toluene. 0.8 g Si_3N_4 ceramic powder are suspended in 50 ml of this mixture and stirred for 10 minutes at 60 °C. The suspension is filtered and washed three times with fresh toluene. The ceramic powder is dried for 24 h in a vacuum chamber, then added to an aqueous 10 mass% heptakis-6-amino-β-cyclodextrin solution (pH 7) and stirred

for 24 h at room temperature. The suspension is filtered, washed three times with distilled water and dried for 24 h in a vacuum chamber at room temperature."

9 is not soluble in water, DMF and DMAc according to this work; it is probably suspended in water during reaction with **5**[185]. The DRIFT-spectrum (Figure 43) shows the reaction takes place. The mono-amino derivative **3** is very well soluble in water. The one amino group increases the polarity and makes the molecule more hydrophilic. The solubility is improved compared to the native β-cyclodextrin. At first glance **9** should have a higher solubility because of the seven amino groups. But it is just the other way round. Because of the full substitution at the 6-position the symmetry is enhanced and the polarity is decreased. The insolubility does not allow to do measurements of the adsorbed mass, because this method requires soluble cyclodextrins. The DRIFT-spectrum shows that a higher amount of **9** is bonded to **5** (0.1 absorbance units, methylene 2940 cm^{-1}, the baseline substracted) than of mono-6-amino-β-cyclodextrin **3** (0.0 absorbance units, Figure 42, corresponding to 3.7 mg **3** / g). The surface coverage of **3** is only 15% of a monolayer (23.9 mg/g), but even this amount changes the colloidal behavior into the desired direction (see chapter 12.2.). The thesis above proposes that the higher number of amino groups increases the reactivity which is verified by the adsorbed amount, but it does not mean a better crosslinkage of the particles.

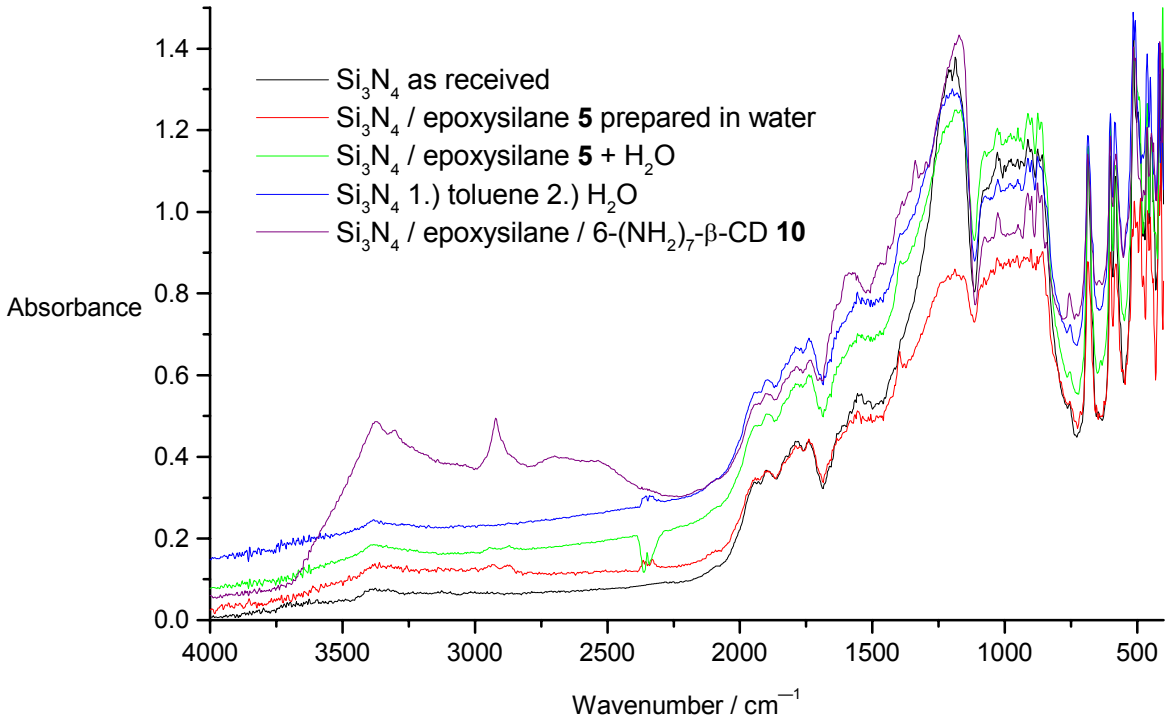

Figure 43: DRIFT-spectra of **5** and **10**

Si_3N_4 has no methylene-containing contamination (no peaks at 2930, 2890 cm^{-1}). Epoxidation in H_2O is successful. But stirring for 24 h in water dissolves silane (decreasing intensity of methylene signals). Preparation of **10** without **4** and **9** (treatment of Si_3N_4 with toluene and H_2O) yields Si_3N_4 with the same DRIFT-spectrum as for Si_3N_4 as received. Toluene and water is completely removed by drying for 12 h in a vacuum chamber at room temperature. So peaks at 2924 and 2889 cm^{-1} in spectrum of **10** derive mainly from cyclodextrin **9** and in a minor part from epoxysilane **4**. Influences of solvents are excluded.

The ζ-potential of **10** and reference systems are investigated. The following diagrams show the results (Figure 44, 45).

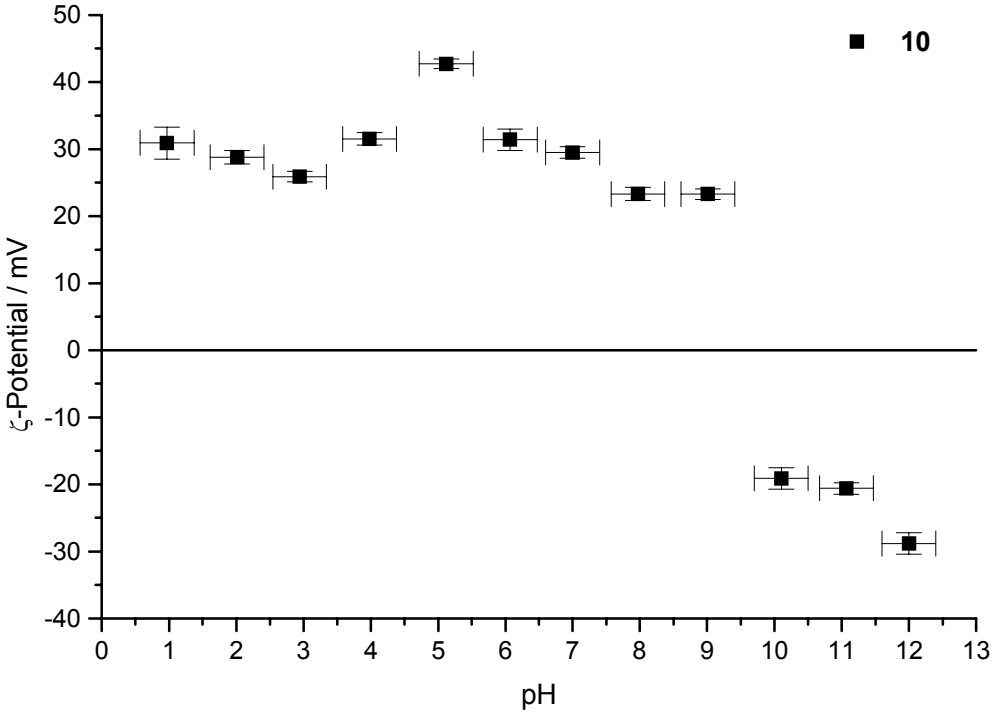

Figure 44: ζ-Potential of **10** in dependence on pH.

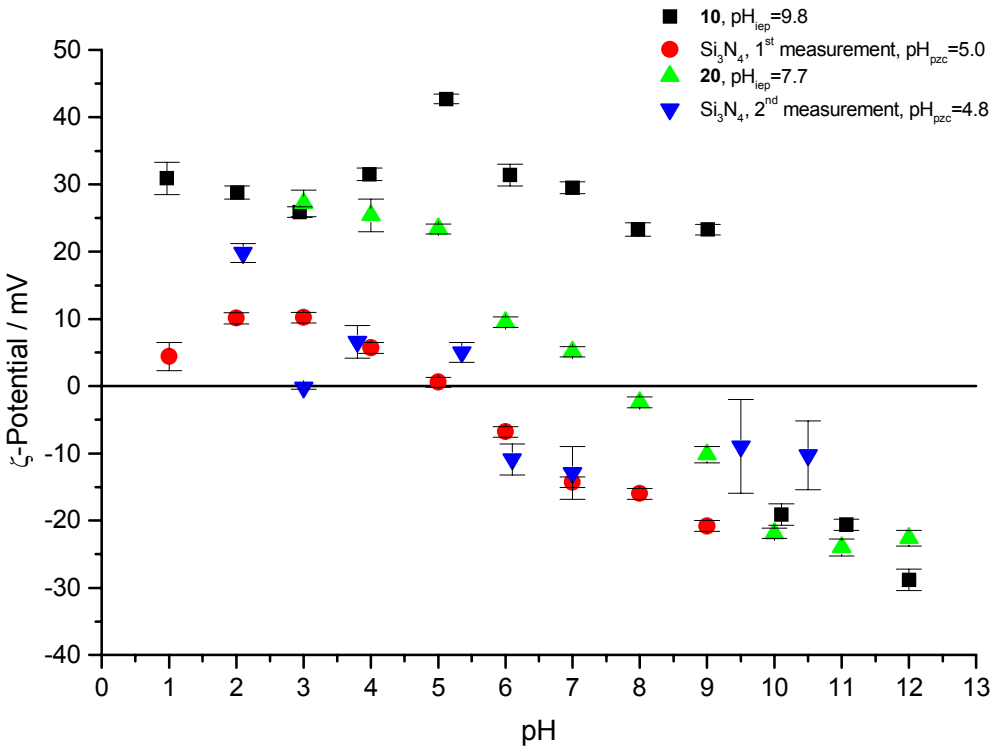

Figure 45: ζ-Potential of **10** and reference systems.

The pH_{pzc} of **10** is with 9.8 clearly basic and different from the other systems. The seven amino groups of **9** cause the strong pH shift into the basic region. This proves the stable bonding of **9** resistant to the ultrasonical treatment and to strong dilution. The aminofunctionalized Si_3N_4 **20** has a mildly basic pH_{pzc} of 7.7. The amino group causes this shift being lower than for **10** because there is only one amino group. For comparison unmodified Si_3N_4 has a pH_{pzc} of 4.9[160, 186, 187]. The two Si_3N_4 curves for the pH_{pzc} have nearly the same position. They are very flat and do not show high positive values for the pH_{pzc}. **20** has a steeper curve with higher positive values shifted to the right. **10** has a very steep curve, the high positive values lie on a horizontal line leading into a step at the pH_{pzc}. The change of the curve shape is similar to an acid base titration. The titration of a weak acid with a weak base provides a flat, rounded curve. The titration of a weak acid with a strong base provides a step-like looking curve where the inflection point can clearly be detected. The titration of a strong acid with a strong base provides a well step shaped curve. The step is located at the inflection point.

10 does not sediment during 12 h (Table 11) according to observation of the aqueous stock solutions for ζ-potential measurement (10^{-3} mol/l KNO_3, 2 mg powder in 500 ml bidistilled H_2O).

Table 11: Sedimentation behavior of **10**.

system	sedimentation	pH
Si_3N_4	no	4
10	no	8

11.6. Ad- and Desorption of Poly-β-CD on α-Al_2O_3 Powder Ceramics

11.6.1. Synthesis of Poly-β-CD and Attachment to the α-Al_2O_3-Powder-Surface

In the chapters above the immobilization of cyclodextrins on Si_3N_4 powder surfaces was demonstrated, here the bonding of cyclodextrins to Al_2O_3 powder surfaces will be investigated. The mechanism of the attachment of the cyclodextrin to the Al_2O_3 surface will be explained. After presentation of the synthesis and consitution of the cyclodextrin containing polymer the adsorption of the cyclodextrin polymer will be described.

In this approach the cyclodextrin containing polymer is ionically bound to the Al_2O_3 surface, whereas at Si_3N_4 it is covalently bonded to the surface. In this case the β-cyclodextrin is attached to a polymer backbone as a side chain. The polymer has another side chain consisting of a carboxylic acid group as the anchoring group to the Al_2O_3–surface. The surface of Al_2O_3 has basic groups to which the carboxylic acid can be bonded. Beside that an electrostatic interaction between the negatively charged carboxylic acid group and cationic centers on the Al_2O_3 can also be a reason for the adsorption. The carboxylic group binds as a ligand or chelat ligand to the aluminum and forms complexes like the hydroxo-complexes. The attachment of the cyclodextrin to the Al_2O_3 is achieved in one step. The polymer is dissolved in water and the Al_2O_3 is added, so that a surface modification of the Al_2O_3 is not necessary.

The reaction pathway is depicted below. Synthesis of poly-β-CD **14** (M_W=76000 g/mol, M_W of backbone 60000 g/mol) is developed in[188] (**14** is named as **4d**). One D-glucose ring of the β-cyclodextrin is regio and stereo selectively deprotonated at the 2-position. The molecule represents an alkanol anion. So the β-cyclodextrin is activated for further synthesis. The polymer backbone is a copolymer consisting of isobutene and maleic acid anhydride as monomers. The two monomer units alternate strictly in the copolymer. The maleic acid anhydride ring is the reactive unit in the copolymer. The anhydride is an activated carbonyl. The O^- of

the β-cyclodextrin attacks the carbonyl C-atom of the anhydride and opens the ring. The remaining molecule is an ester, the product is hydrolyzed to open unreacted anhydride rings. The retained carboxylic group works as an anchor group to Al_2O_3 ceramics as mentioned above.

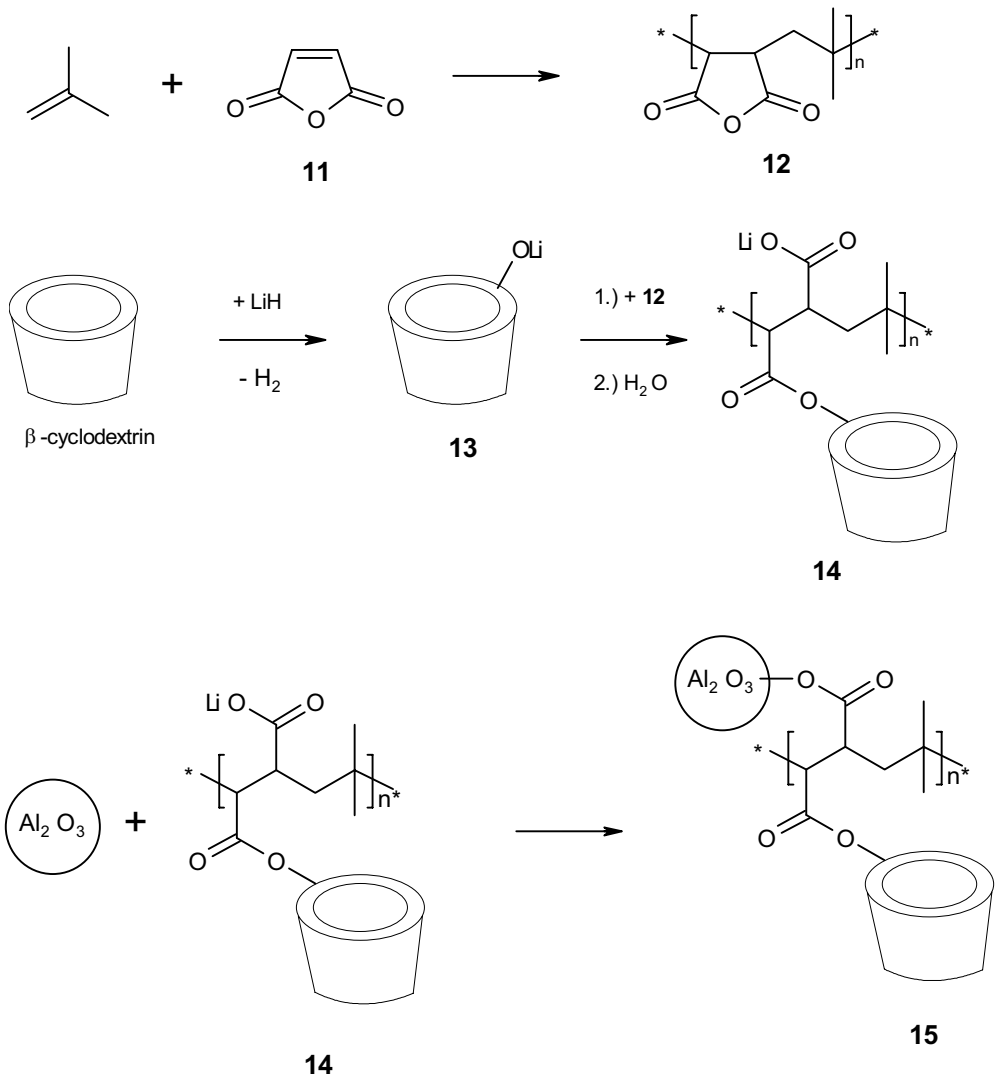

For adsorption of **14** to Al_2O_3 1.000 g α-Al_2O_3 bipur. are suspended in 4.0 ml H_2O and ultrasound is applied for 10 min yielding a pH of 5.0. 10 mg **14** are dissolved in 6 ml H_2O. The pH is adjusted from 6.3 to 4.8 by addition of 75 µl diluted HCl. A solution of **14** is added in small portions to the Al_2O_3–suspension. During 10 min of reaction pH is kept at 5 by addition of 100 µl diluted HCl. The reaction mixture is centrifuged and the overstanding solution is analyzed (Table 12). To the remaining solution 1.000 g α-Al_2O_3 bipur. are added and the adsorbed mass of **14** is measured as described in chapter 11.4.. To investigate the desorption properties of **14** 10 ml

H_2O are added to the Al_2O_3 precipitate of the first adsorption. The suspension is stirred for 5 min, centrifuged and analyzed.

The expressions "trapped", "bound" and "in solvent" ("in H_2O") are explained in the chapter 11.4.1.. The statements related to the number of decimal digits are also valid for this investigation.

Table 12: Ad- and desorbed masses of **14** on Al_2O_3.

	conditions	trapped	bound	in H_2O
1st adsorption	1 g Al_2O_3 bipur., 10.175 ml H_2O, 10 mg **14**, 0.1%, pH=5	6.6 mg	5.7 mg, 57%	0.91 mg
2nd adsorption	1 g Al_2O_3 bipur., 6 ml H_2O, 2.5 mg **14**, 0.042%, pH=5	1.9 mg	1.8 mg, 72%	0.1 mg
Desorption of 1st precipitate	10 ml H_2O	6.1 mg	5.9 mg	0.2 mg

14 adsorbs to Al_2O_3 as confirmed by the DRIFT-spectrum (Figure 46, 47). In the first adsorption with a 0.1%-solution 57% of the total (10 mg) **14** are adsorbed, in the second with a 0.042%-solution 72% of the total (2.5 mg) **14** are adsorbed. **14** has a significant affinity to the Al_2O_3-surface. In the second adsorption experiment the concentration and volume of the poly-β-CD solution is lowered to about half. The amount of Al_2O_3 is kept constant. The relative adsorbed amount in % should increase, because more Al_2O_3-surface is available in relation to **14** compared to the first adsorption. This should draw the balance of the reaction to the side of the products (right side) which is proved by the increased adsorbed amount. This phenomenon is investigated by DRIFT in the following paragraphs coming to the same results. The desorption measurement shows that nothing of **14** is desorbed by redispersing in water, a result to be looked at warily, but it shows that a small amount is desorbed concluding that **14** has a high affinity to the Al_2O_3–surface.

In an alternate preparation the concentration of poly-β-CD **14** in water is increased. The mass of Al_2O_3 is lowered as well as the total surface area to enlarge the attached amount whereas the volume of solvent is low to increase the probability of collision of **14** with the surface. 50.5 mg **14** are dissolved in 1 ml phosphate buffer (pH=7.2) in a small centrifuge tube. The dissolution process is slow and runs overnight yielding a low viscous solution (≈200 mPa s, water 1 mPa s), where

505.5 mg α-Al_2O_3 are added. During the reaction time of 40 min the suspension is shaken several times. After its centrifugation at 4000 min^{-1} for 20 min the supernatant solution is decanted and the precipitate is dried at 60 °C in an oven with circulating air. The DRIFT-spectrum is shown in Figure 46 and 47.

The high intensity of the methylene signals (0.1 absorbance units) shows that **14** is fixed to the surface and indicates a larger adsorbed amount than for copoly-maleic-acid-alt-isobutene **29** (alt=alternating, 0.01 absorbance units, 7 mg/g). The adsorbed amount increases with the concentration of the solution (5% for **14**, 0.071% for **29**). In this range the Al_2O_3 is not saturated and can take up more substance while the cyclodextrin torus does not hinder the adsorption of **14**. Some of the carboxylic groups are protonated (carboxyl, 1700 cm^{-1}), some deprotonated (anion, 1573, 1397 cm^{-1}).

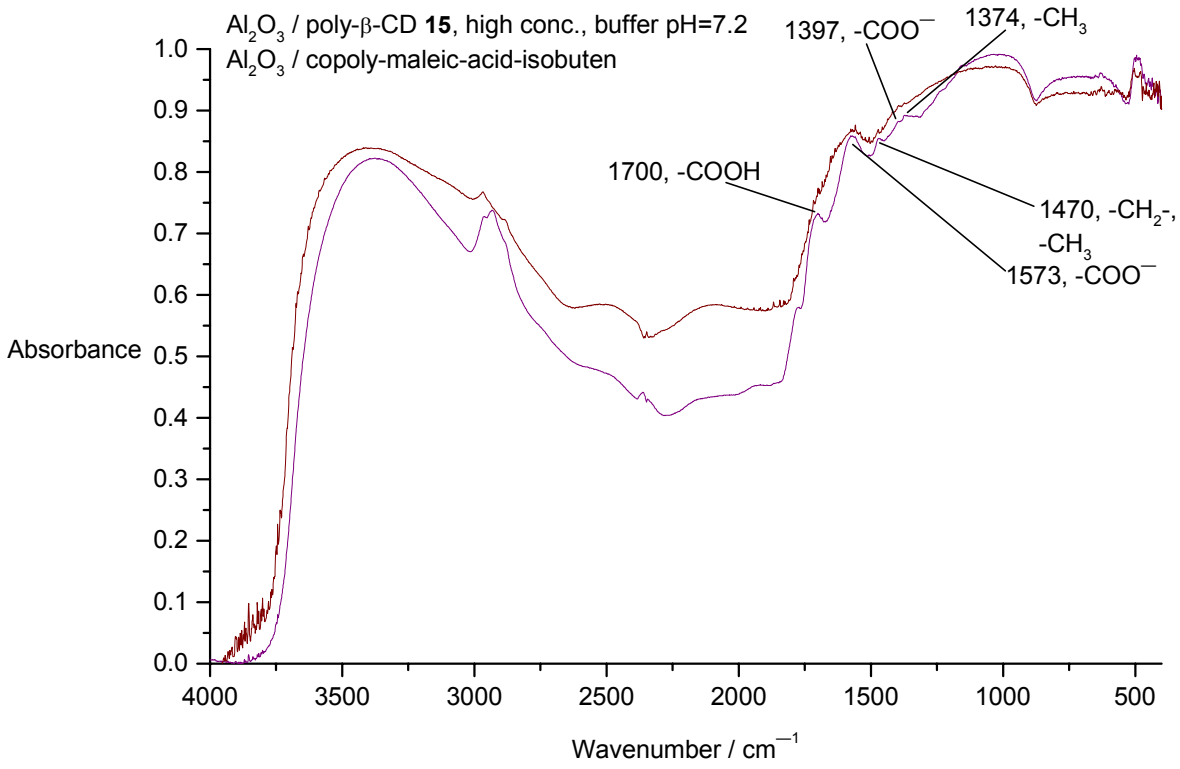

Figure 46: DRIFT-spectra of **15** and Al_2O_3 / **29**.

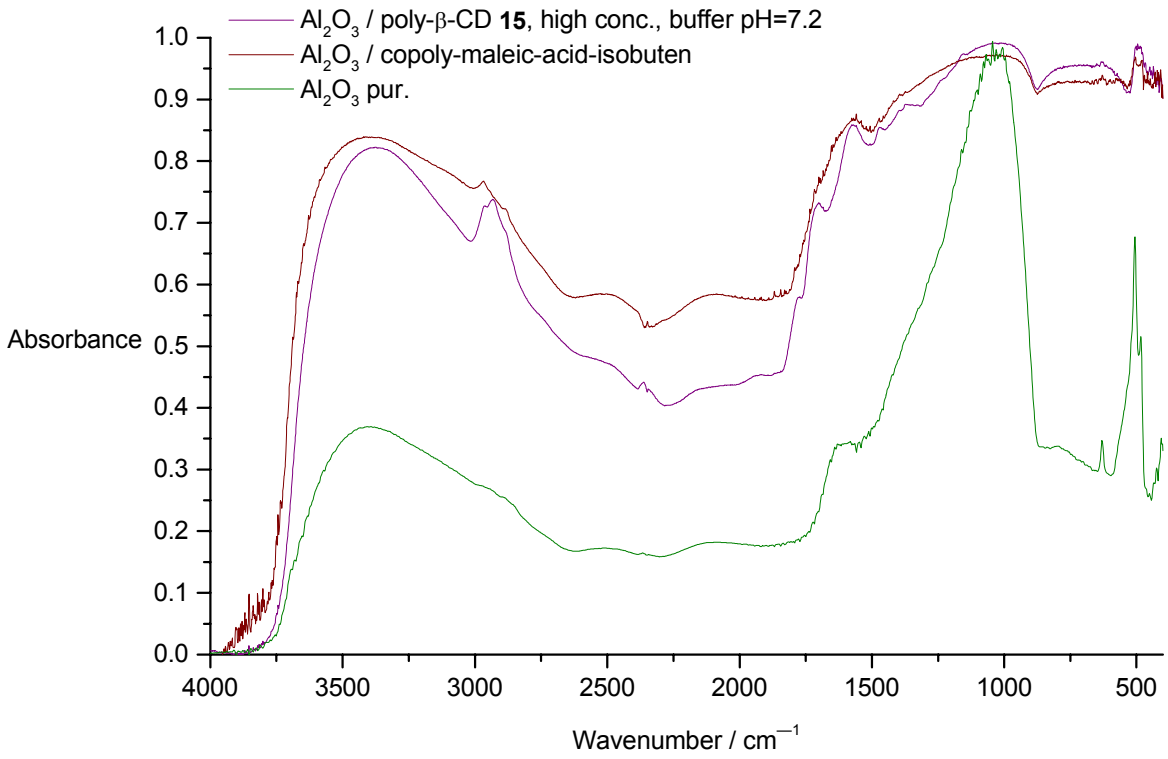

Figure 47: DRIFT-spectra of **15** and **29** on Al_2O_3 compared to Al_2O_3.

Copoly-maleic-acid-alt-isobutene **29** (M_W=60000 g/mol) is equally deposited as poly-β-CD **14** (M_W of the polymer backbone 60000 g/mol). The amounts are chosen as follows: 5.00 g Al_2O_3, 35.5 mg copoly-maleic-acid-alt-isobutene **29**, 50 ml H_2O. **29** is easily dissolved in water, the retained solution having a low viscosity (≈50 mPa s). The structure formula is depicted below.

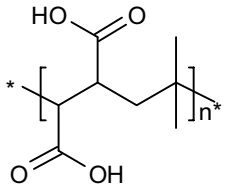

29

11.6.2. Adsorbed Amount of Copoly-maleic-acid-alt-isobutene

Copoly-maleic-acid-alt-isobutene **29** (alt=alternating) is the polymer backbone of poly-β-CD **14**. It can be used as a model substance for the adsorption of **14** on Al_2O_3 in order to investigate the influence of the cyclodextrin torus on the adsorption. As **29** is not a chiral compound the adsorbed amount cannot be measured by rotation angle measurement, but by acid base titration. The adsorption of **29** onto Al_2O_3 is carried out with a defined amount of **29**. After centrifugation the supernatant solution is taken and the remaining amount of **29** is measured, the difference to the total amount is the bound amount. The conditions like masses and concentrations used in both methods – angle of rotation measurement and acid base titration – are equivalent thus allowing a comparison of the results of both methods.

The pH of the aqueous solution that is analyzed is adjusted with HCl-solution to 2. The pH is controlled with a pH-meter (WTW, pH 535 Multical). A small amount (10-100 μl) of a 0.1 or 0.01 molar NaOH-solution is added and the pH is measured. During this procedure the pH value should be increased in small steps especially in the range of 7. In this range only small amounts (10 μl) of the 0.01 molar NaOH solution should be used because small amounts of OH^- cause a strong change in the pH. The titration is done until a pH of 12 is reached. For calibration three solutions with different amounts of the substance or a model substance are prepared and analyzed, the titration curves for the calibration are plotted (Figure 48) and the first derivative is calculated numerically (Figure 49). The derivative curve has two maxima if the weighed mass for the substance is higher than zero, their distance is the difference between the x-coordinates being proportional to the weighed mass. If the weighed mass is zero, the distance is zero, too and this means there is only one maximum. The weighed masses are plotted versus the distances. The curve (Figure 50) should be a line that runs through the origin of the coordinate system. The analytical function (line function) provides the relation between mass and distance. The titration curves for the analyzed unknown masses are also plotted (Figure 51) and derived (Figure 52-55). After reading the distance of the maxima mass is calculated with its line function.

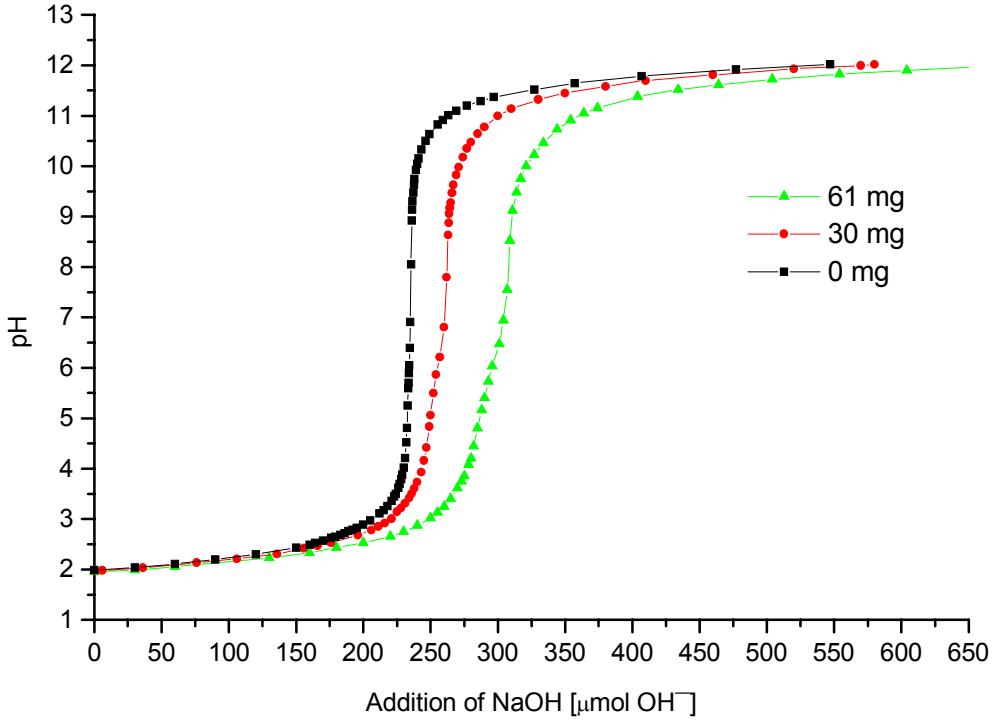

Figure 48: Titration of 0, 30 and 61 mg for calibration.

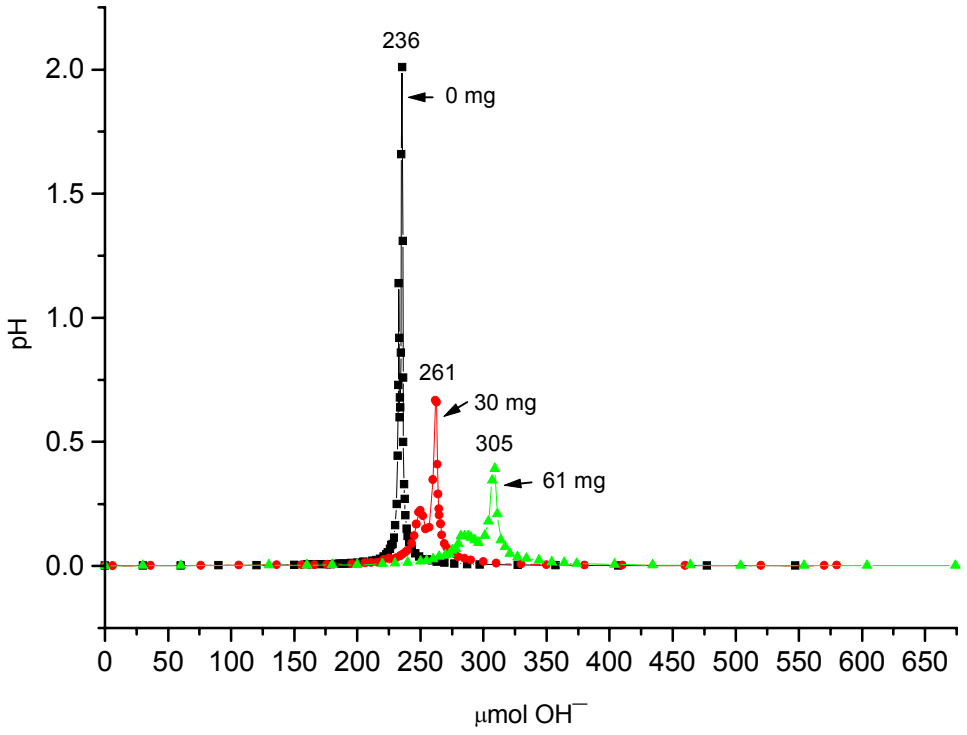

Figure 49: First derivative of the titration curves for calibration.

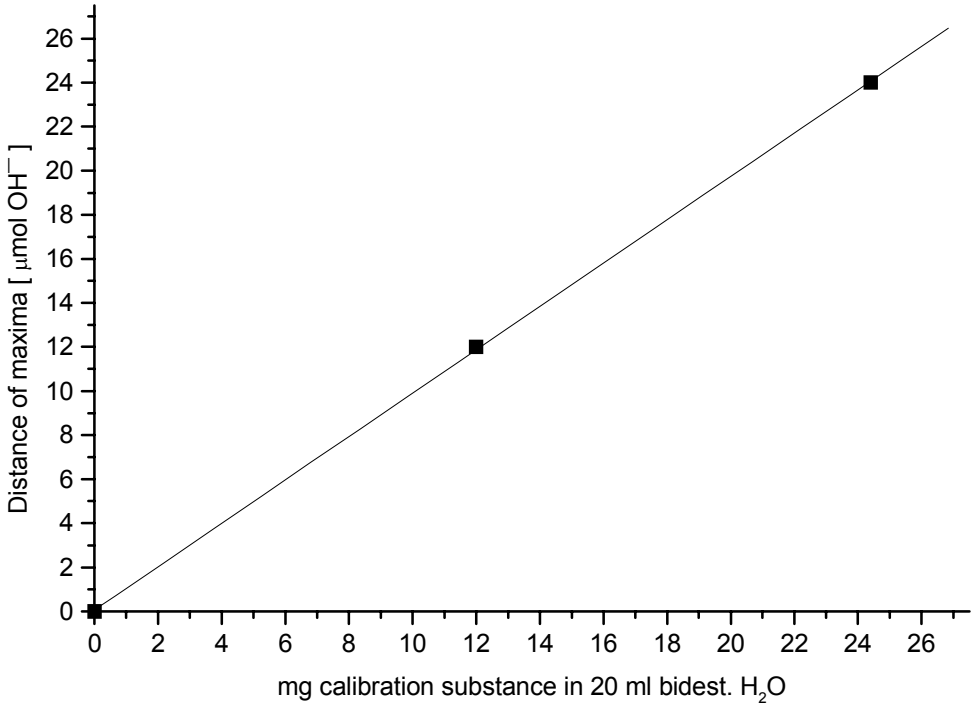

Figure 50: Calibration curve for **29** for acid base titrations.

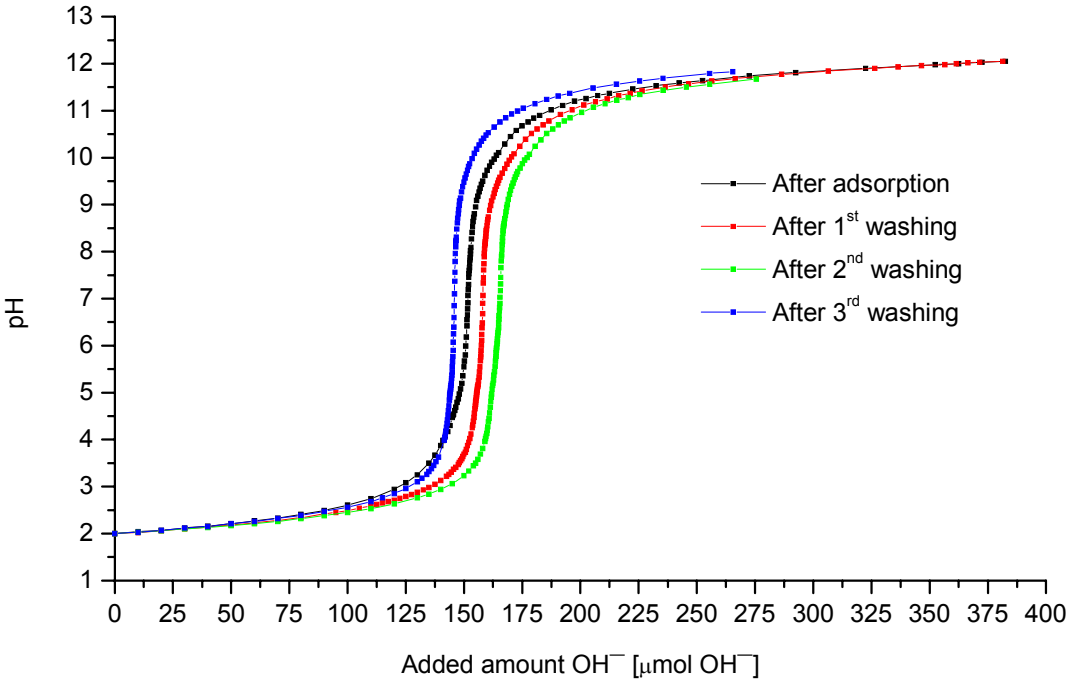

Figure 51: Titration curves after adsorption of **29** on Al_2O_3 and washing.

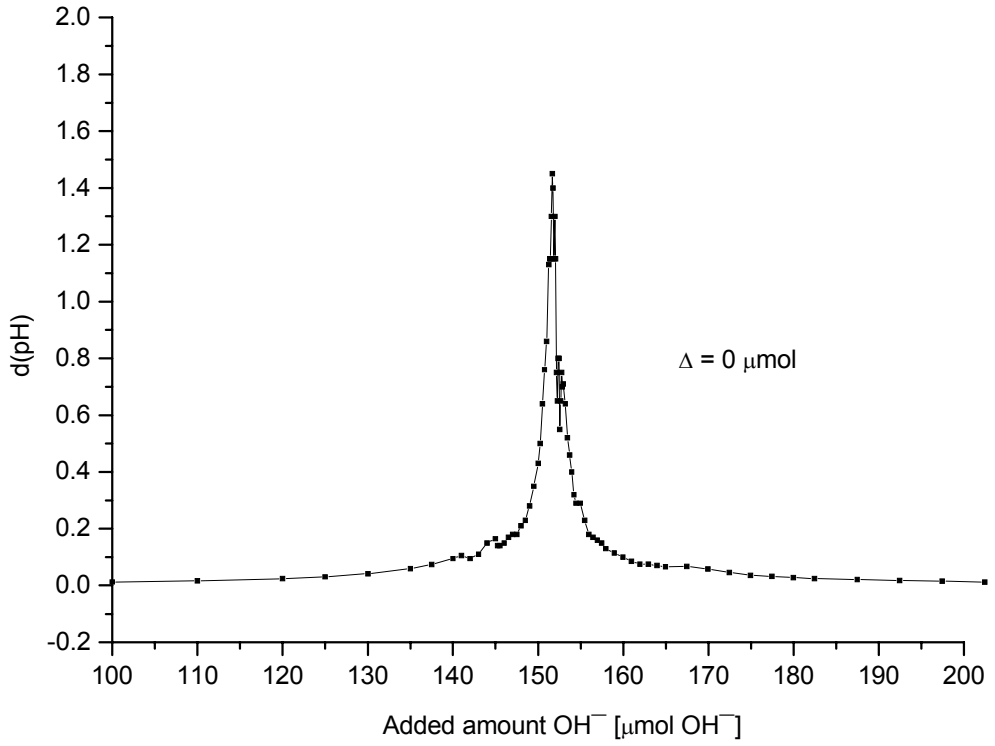

Figure 52: First derivative of the titration curve for the supernatant solution after adsorption of **29**.

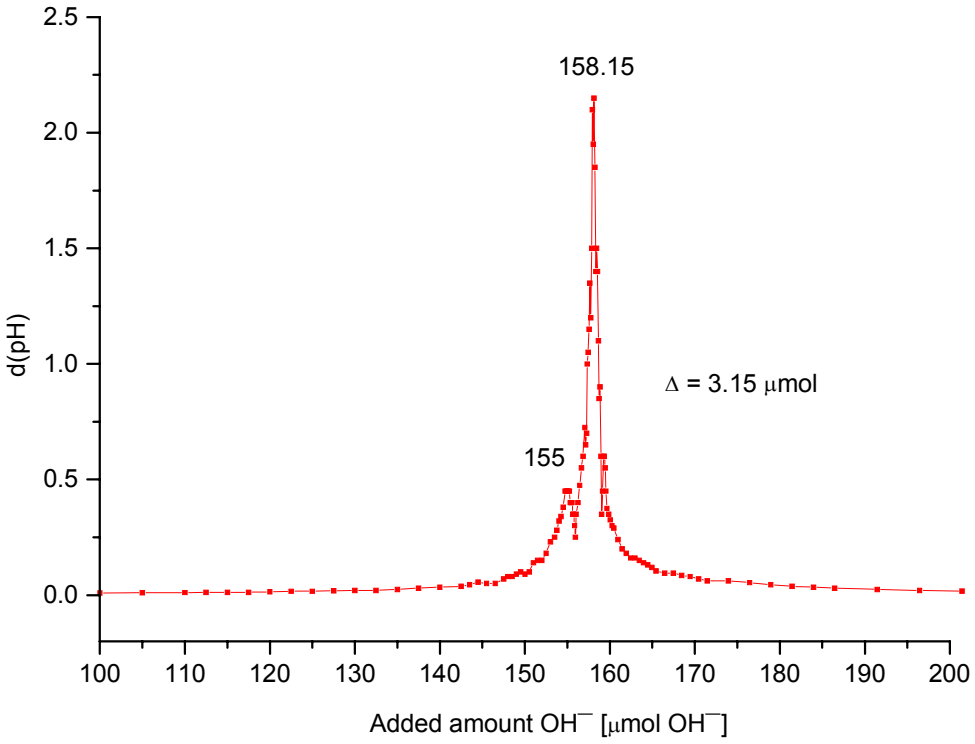

Figure 53: First derivative of the titration curve after the first washing water of **29**.

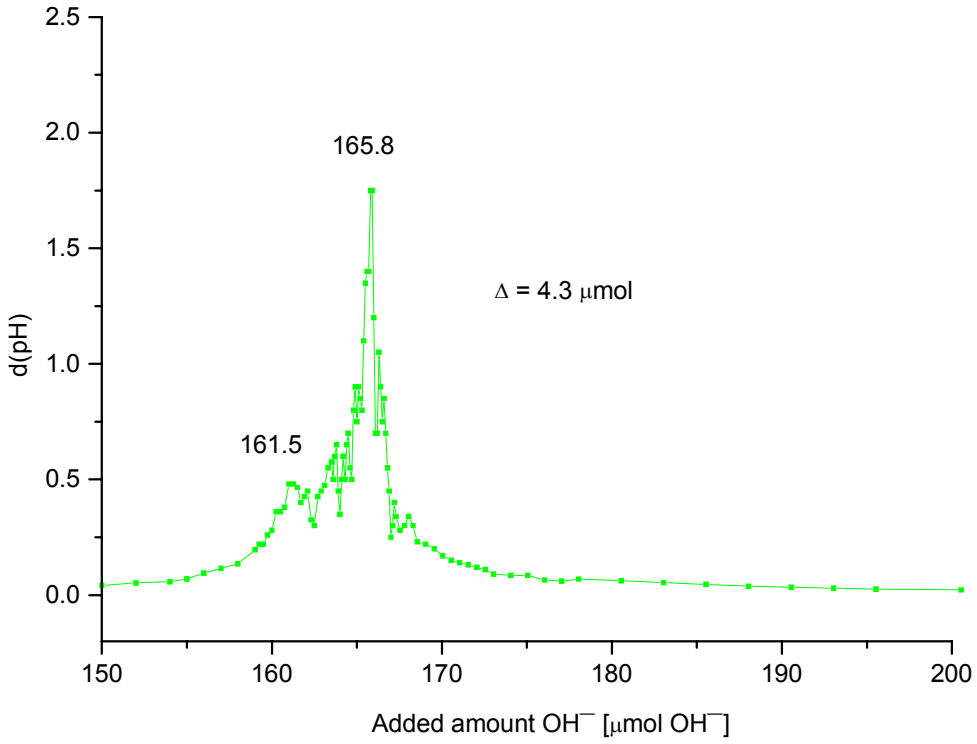

Figure 54: First derivative of the second washing water of **29**.

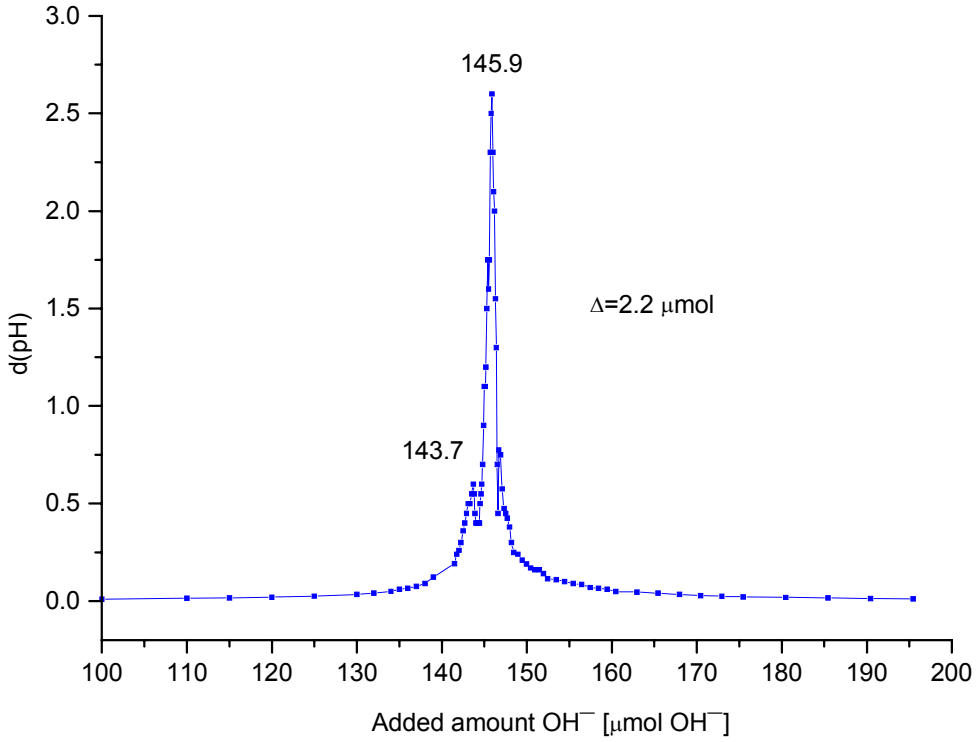

Figure 55: First derivative of the third washing water of **29**.

Table 13: Ad- and desorbed masses of **29** on Al_2O_3.

	after adsorption	1st washing	2nd washing	3rd washing
in 50 ml H_2O	0.0 mg	5.6 mg, 16%	7.69 mg, 26%	3.87 mg, 17%
bound	35.5 mg, 100%	29.9 mg	22.21 mg	18.34 mg

Table 13 shows the results of the measurement of the ad- and desorbed masses with acid base titration: The total weighed mass is 35.5 mg; **29** adsorbs on Al_2O_3 having a good affinity to it. 100% of **29** are adsorbed in the first step, but only 57% of poly-β-CD **14** are adsorbed on Al_2O_3 (see Table 12). If Al_2O_3 / **29** is washed with water, approximatively 20% of the bound amount is dissolved again. Only the parts of **29** that are directly attached to the Al_2O_3-surface are tightly bonded, the outer molecules of **29** are loosely bound and can be dissolved. If the concentration of poly-β-CD **14** is lowered, 72% are bound (Table 12) meaning the bound mass of **14** is significantly lower than the bound mass of **29**. The cyclodextrin torus hinders the adsorption of **14** on Al_2O_3 compared to **29**. The desorbed mass of **14** is zero concluding that **14** is strongly bonded to the surface. There are no outer layers as in **29** that can be dissolved again.

11.7. Synthesis of Iso-cyanatofunctionalized Si_3N_4

The reaction scheme for the iso-cyanatofunctionalization (-NCO, -N=C=O) is as follows:

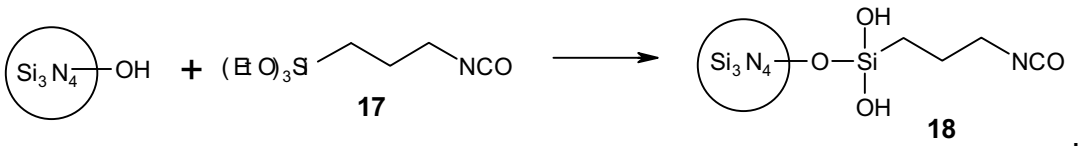

The silicon nitride is used without further purification because there is no DRIFT-detectable contamination (Figure 38) and the elemental analysis does not show noticeable amounts of other elements. n-Hexane is used as a solvent. The non-aqueous solvent has the advantage to decrease the hydrolysis of the isocyanato group compared to water as solvent. It is undried since the small water content of n-hexane works as a catalyst for the silanisation reaction[189]. The ethoxy group of **17** is converted by water to a hydroxyl group reacting with the silanol groups of the Si_3N_4–surface[190].

The synthesis is carried out as follows: 2 ml 1-tri-ethoxy-silyl-3-isocyanato-propane **17** (density 1.002 g/ml; Fluka, Switzerland) are added to 50 ml n-hexane in a screwable beaker, yielding a turbid, slightly brown suspension. 3.00 g Si_3N_4 are suspended in this mixture and stirred in the closed beaker for 20 h at room temperature. The product covers the inner surfaces of the beaker as a loose sediment. It is isolated by centrifugation with a table centrifuge at 3800 min^{-1} for 15 min. The transparent and colorless supernatant solution is decanted and the remaining residue is washed twice with 40 ml n-hexane at a time as described above. The n-hexane is allowed to evaporate at room temperature for several hours. Then the material is ground in an agate mortar yielding 2.66 g of **18**.

A DRIFT-spectrum is collected in Figure 56 (1^{st}).

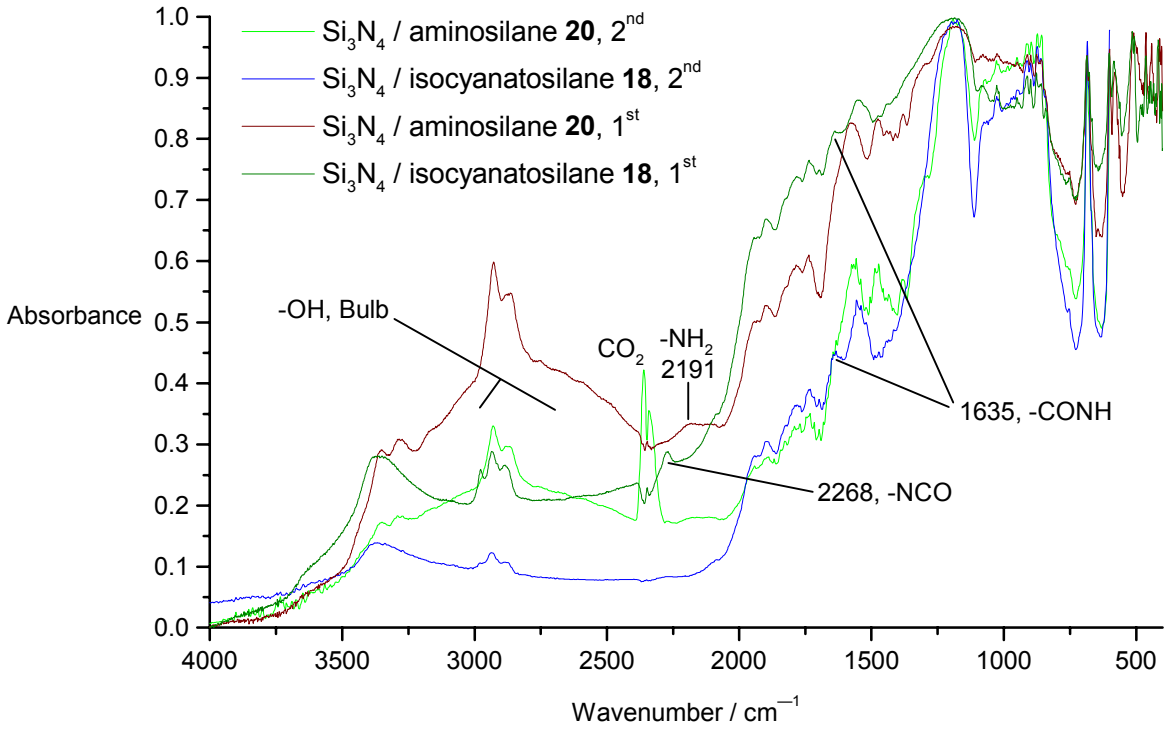

Figure 56: DRIFT-spectra of **18** and **20**.

A second reproducible spectrum is measured from **18** 22 days later (Figure 56, 2nd). As the methylene (2930 cm^{-1})- and the hydroxyl (3350 cm^{-1})-signals are decreased, there is a continual loss of isocyanatosilane by evaporation (0.15 absorbance units, $-CH_2$, 1st; 0.025 abs. u., $–CH_2$, 2nd; 0.15 abs. u., -OH, 1st; 0.05 abs. u., -OH, 2nd). Compared to the aminosilane (0.2 abs. u., $-CH_2$, 1st; 0.11 abs. u., $-CH_2$, 2nd) the adsorbed amount is significantly lower. In the first spectrum of **18** there is a small NCO-signal (0.01 abs. u.) that disappears in the second spectrum showing that the NCO-group is hydrolyzed before the first measurement and between the first and second. The CONH-signal at 1635 cm^{-1} is increasing from the first to the second measurement, a hint for carbamic acid as an intermediate product in the hydrolysis reaction of the NCO-group. No amino groups are detectable. Either the carbamic acid is not hydrolyzed to the amine or the intensity and sensitivity are too low. In summary the hydrolysis of **18** with time is depicted in the following scheme:

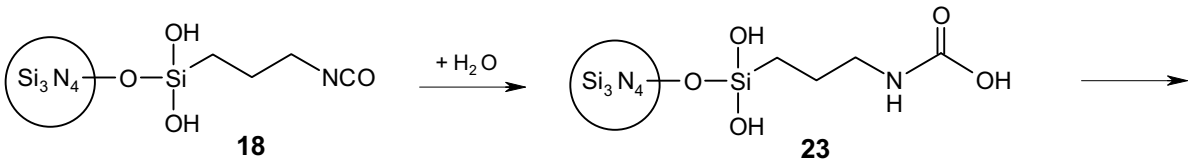

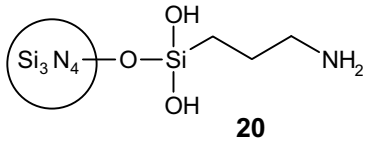

1-Tri-ethoxy-silyl-3-isocyanato-propane (= tri-ethoxy-(3-iso-cyanato-propanyl)-silane) **17** can be attached upside down, so that the iso-cyanato group is attached to the Si_3N_4–surface and the silanol groups protrude into the solution. The following scheme illustrates this:

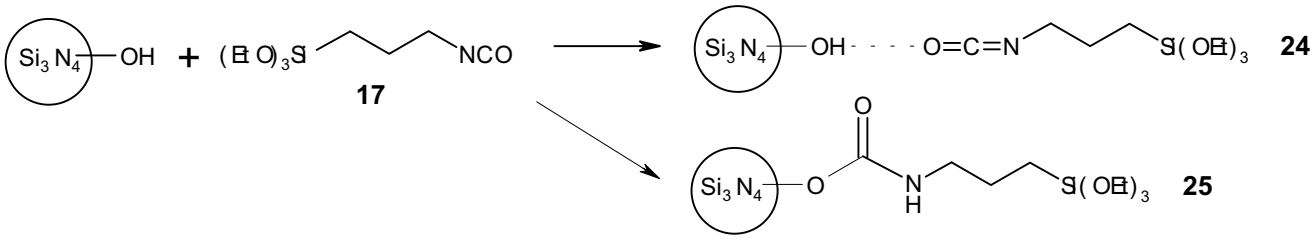

A hydrogen bridging bond between the H of the silanol of the Si_3N_4-surface and the O of the carboxy group are the binding force in **24**. An approach of the silanol-O-atom to the carboxy-C-atom leads to the silylurethane **25** in a carbonyl reaction. The tri-ethoxy groups are hydrolyzed to tri-silanol groups[189, 190] available for further reactions.

11.8. Synthesis of Aminofunctionalized Si_3N_4

The reaction for the aminofunctionalization (-NH_2) is as follows:

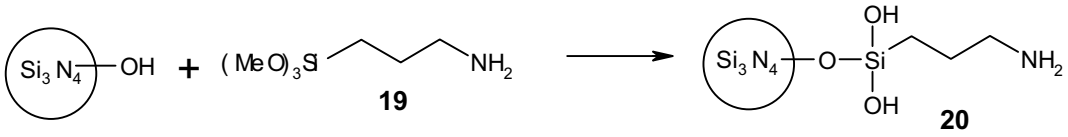

For synthesis 2 ml 1-Amino-3-(tri-methoxy-silyl)-propane (= (3-aminopropyl)-tri-methoxysilan, Fluka, density 1.016 g/ml) **19** are suspended in 50 ml n-hexane, retaining a colorless slightly turbid suspension. Undissolved **19** remains at the bottom of the vessel as a bubble. Other parts of **19** stick to the glass wall of the pipette. Then 3.00 g Si_3N_4 are added. The reaction is stirred in a sealed beaker at room temperature for 19 h 30 min and centrifuged at 3800 min^{-1} for 15 min. The supernatant solution is decanted and the precipitate is washed twice with 40 ml n-hexane. After the second washing the supernatant solution is clear and colorless meaning every undissolved parts of **19** are removed. The yield is 3.11 g of **20**.

During the preparation some Si_3N_4 is lost (≈300 mg per 3.00 g Si_3N_4). The yield of coated Si_3N_4 is higher than its educt amount meaning a large amount of **19** is fixed on Si_3N_4. The DRIFT-spectrum reveals the same result (Figure 56). A second reproducible DRIFT-spectrum is taken 22 days later. During this time the intensity of the methylene signal is decreased as well as the adsorbed amount concluding that **19** is partly evaporated. The molecules that are directly attached to the Si_3N_4-surface have a stronger interaction (covalently bonded or ionically) than the molecules in the outer sphere which are loosely attached to the others. The adsorbed amount of **19** (0.11 abs. u., -CH_2, 2nd) is higher than that of the iso-cyanatosilane **17** (0.025 abs. u., -CH_2, 2nd). There is a big bulb in the spectrum due to OH-groups of water, the surface layers trap a lot of water that evaporates. The amino groups are clearly detectable (3350, 3287, 2191, 1480, 1384 cm^{-1} in spectrum of **20** in Figure 56). As an additional view of Figure 56 the signals are labeled in Figure 57. The amino groups do not appear in the spectra of Si_3N_4 (Figure 38) or the other compounds, so they derive from the amino group of the aminosilane. The amino groups are partly protonated by protons of H_2O or of silanol groups. The signals for the amino groups are shifted to

lower energies (frequencies, wave numbers). The amino groups are bridged either by the solid surface, water or other amino groups.

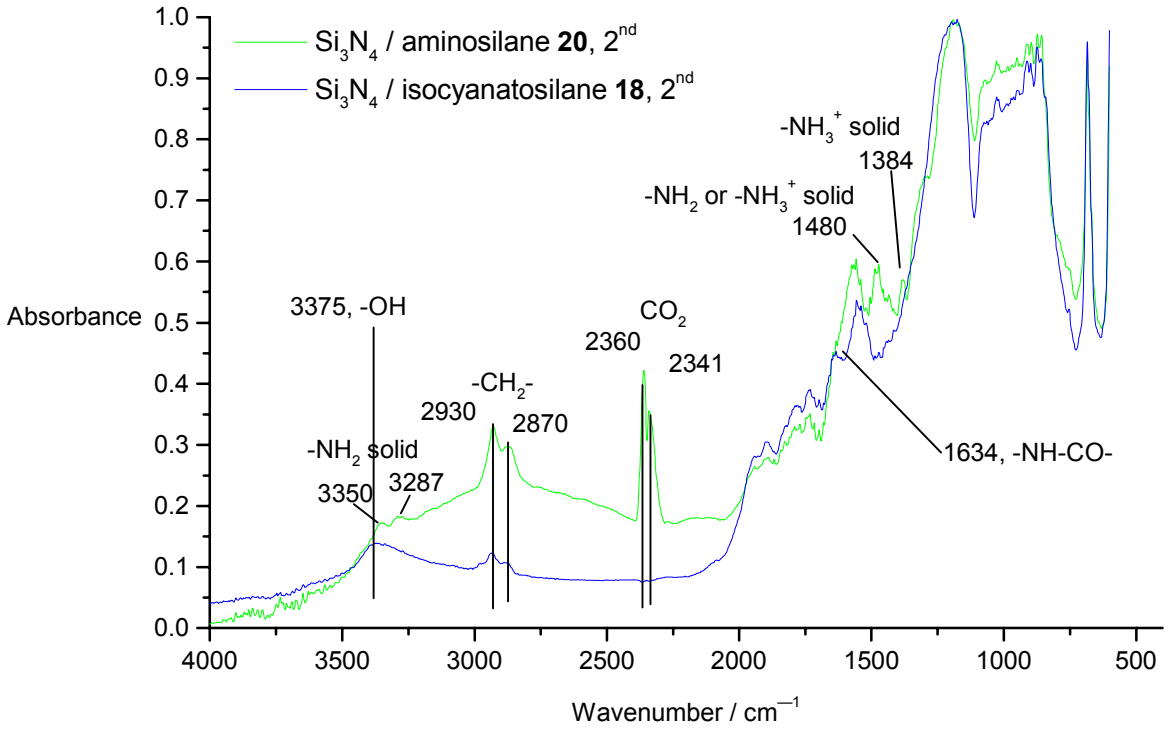

Figure 57: DRIFT-spectra of **20** and **18**, same as Figure 56, but with labeled signals.

Additionally another way of attachment must be considered: The amino silane could also be attached upside down to the Si_3N_4–surface[191]. After hydrolysis a silanol group is protruding into the solution. The scheme illustrates this:

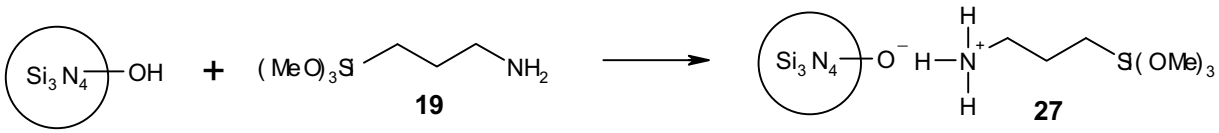

12. Interaction of Ceramic Particles

12.1. Covalent Interaction of Si_3N_4-Powder-Particles

The crosslinkage of the iso-cyanatofunctionalized Si_3N_4 **18** with the amino-functionalized Si_3N_4 **20** will be investigated. The crosslinking reaction of **18** with **20** yield a gel. Due to the crosslinking the rheological parameters like the storage modulus G', the loss modulus G'' and the viscosity are changed. These changes prove that the crosslinking reaction took place. First the reactants **18** and **20** are characterized by ζ-potential measurements in water to retain ζ(pH). The changes of G', G'' and the viscosity should clearly be ascribed to the crosslinkage and not to flocculation of oppositely or uncharged particles. To exclude this a pH value (pH=9) is selected for the suspensions of **18**, **20** and the gels, where the ζ-potentials are slightly negative (-12 mV) and have a similar value. So the interparticle potential of **18** and **20** is repulsive.

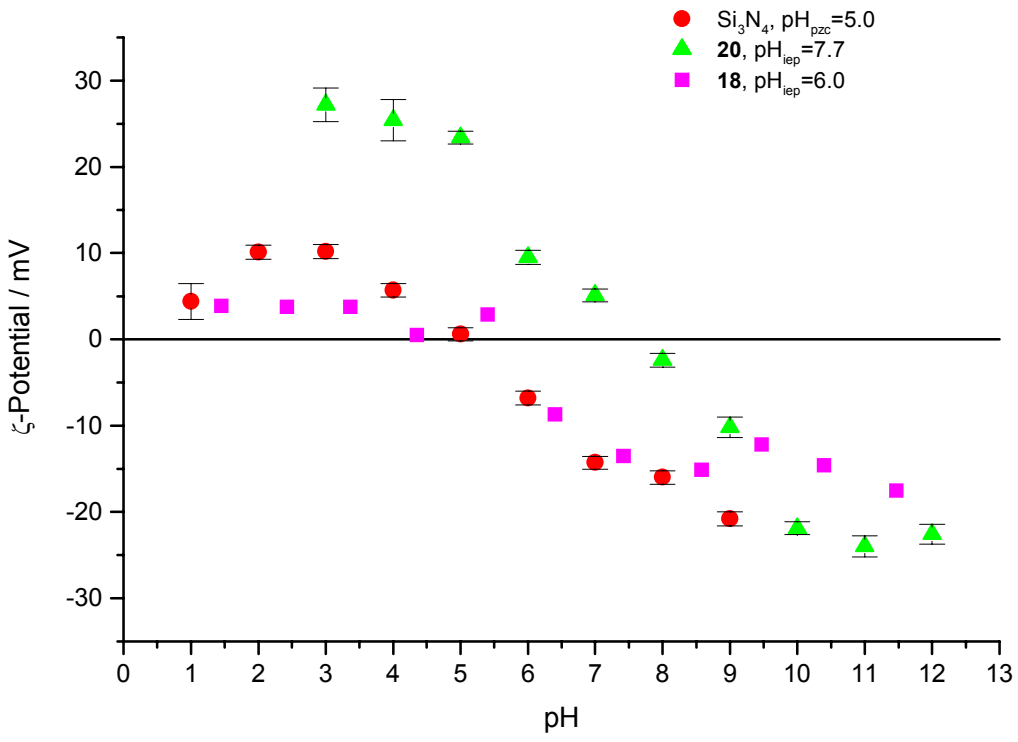

Figure 58: ζ-Potential of **18**, **20** and Si_3N_4 in water.

The sample preparation for 5 ml of a 20 vol% gel is described as follows, the total volume (5 ml) is kept constant for every volume fraction: 1.72 g **18** (10 vol%) and 1.72 g **20** (10 vol%) are weighed in a small beaker corresponding to 3.44 g ceramic powder of 1 ml volume. 3.5 ml bidistilled water with a pH of 10 is filled into a small screwable beaker. Both powders are alternately added in portions by stirring with a spatula. Before the addition of the last portions, the pH is drawn to 10 again by the addition of 250 μl NaOH solution. This lowers the viscosity because of the increased surface charge and supports the mixing and homogenisation of the components. The sample is ultrasonicated for 15 min while cooling with an ice bath to suppress heating of the sample. The pH is adjusted to 9 with 250 μl NaOH solution so that 4 ml water (80 vol%) are added in total. The pH has to be checked several times and is adjusted to 11 during the preparation of samples with a higher volume fraction. Dependent on the viscosity the suspensions are injected into the rheometer by a syringe or a spatula.

The rheological investigations were performed with a dynamic stress rheometer from Rheometrics using cone plate geometry. The cone diameter was 40 mm, the cone angle was 0.039 rad and the gap between cone and plate was 53 μm. The temperature was kept constant at 20.0 °C and evaporation of water was suppressed by housing the cone. The oscillation frequency was 1 rad/s=0.15 Hz in the dynamic measurements. The steady measurements of viscosity versus shear rate were directly carried out after the oscillatory ones.

The functions of the storage modulus G’ and of the loss modulus G’’ versus the stress τ are plotted in Figure 59. G'(τ) and G''(τ) are not time dependent (Figure 59) meaning no reaction occurs during this time period. The time of the beginning of the first measurement of the first sample is set as zero.

The storage modulus G’ expresses the solid state properties of the sample, the loss modulus G’’ represents the liquid properties. The point in the plot of G’(τ) and G’’(τ) where G’ crossed G’’ is called cross-over or transition. As expected the stress values of the first transition, G' and G'' at the viscoelastic plateau (left, horizontal part of the curves) increase with the volume fraction (Figure 60). This is congruent to the increasing viscosity with increased volume fraction. **18** and **20** as reference systems

have a viscoelastic plateau at 10^5 Pa, that is more or less independent from the volume fraction. Contrarily the viscoelastic plateau of the gel ranges from 10^1 to nearly 10^6 Pa, which is higher than that of **18** and **20** (Figure 61 and 62). The reference systems **18** and **20** exhibit a transition stress of 10^2 Pa. The transition of the gels varies from 10^{-1} to 10^3 Pa.

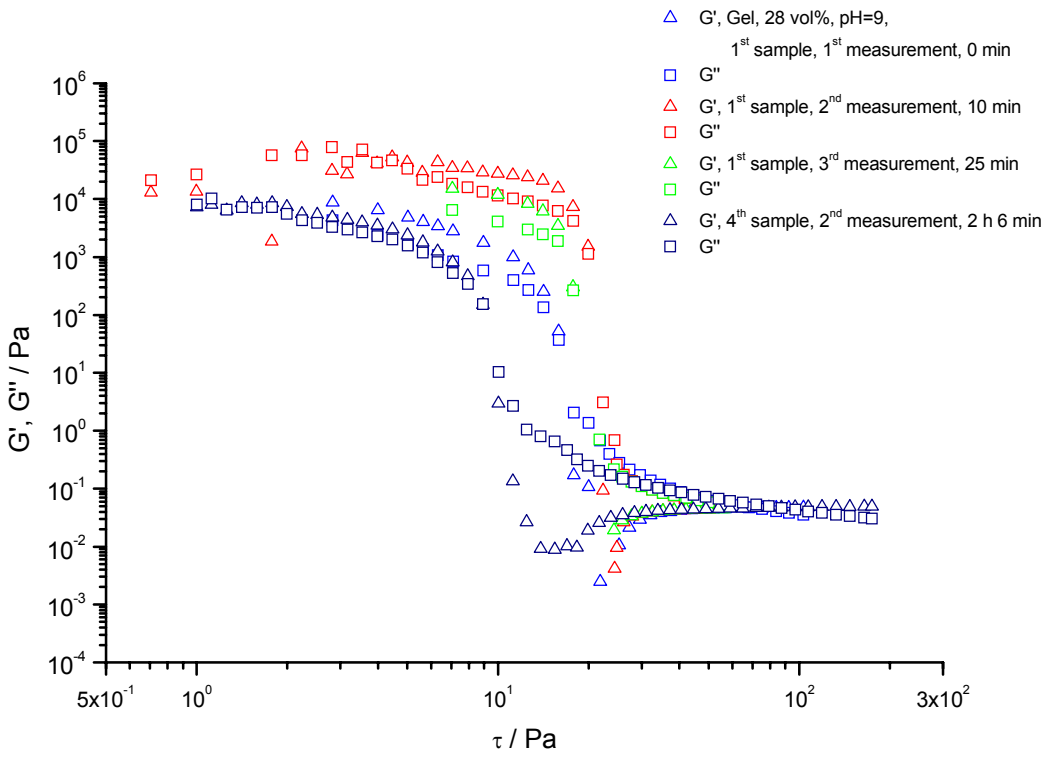

Figure 59: G'(τ) and G''(τ) in dependence of time for a 28 vol% gel of **18** + **20**.

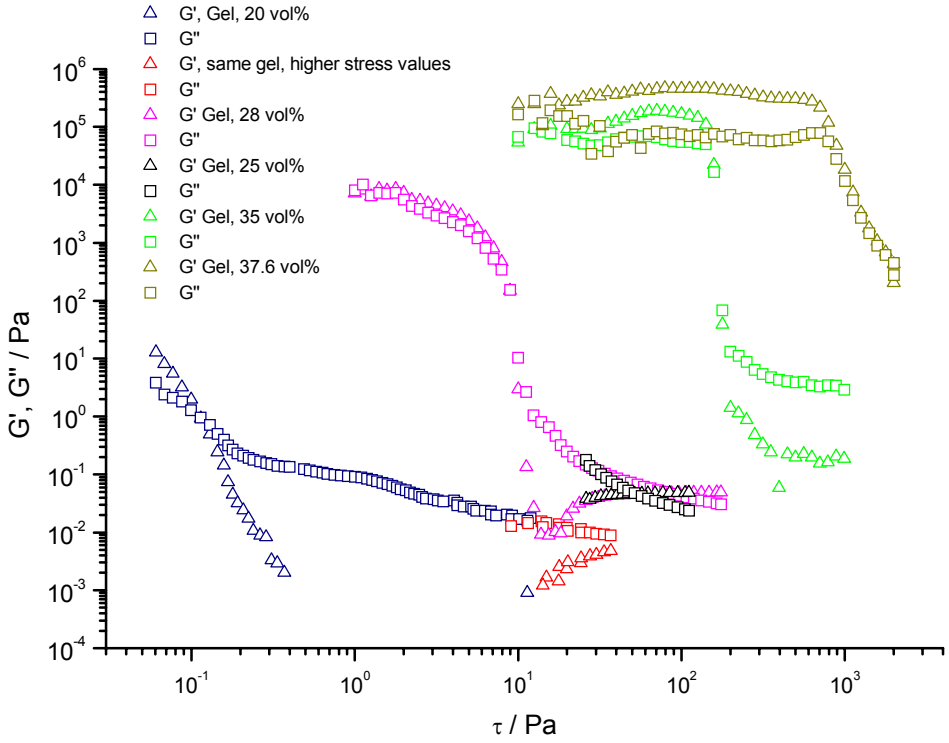

Figure 60: G'(τ) and G"(τ) in dependence of the volume fraction for gels of **18** + **20**.

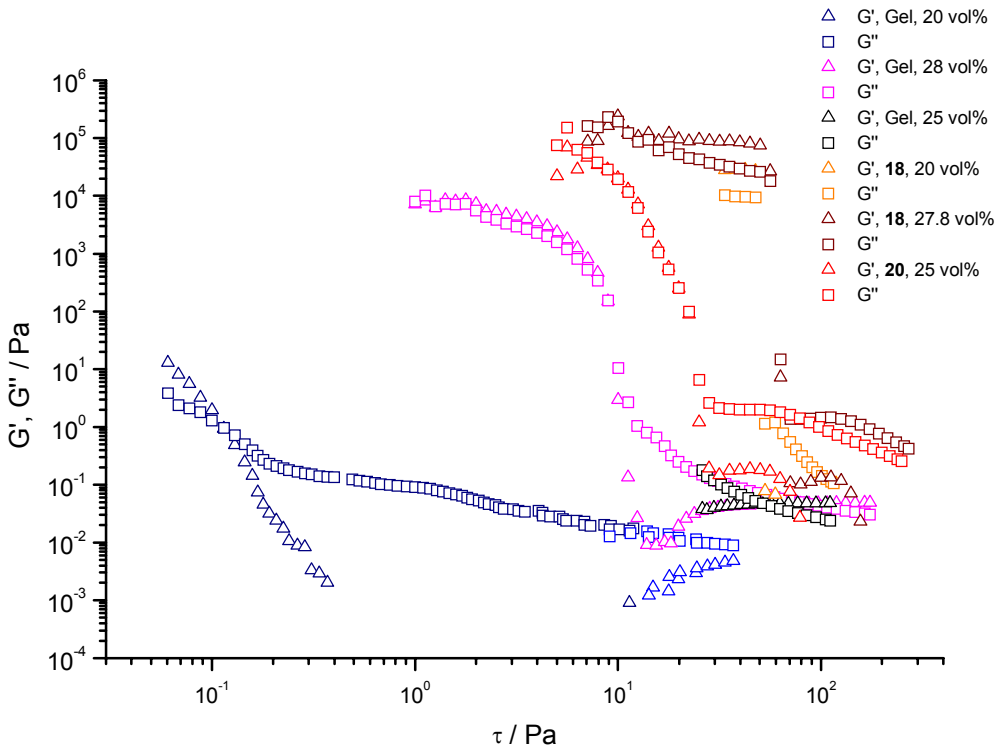

Figure 61: G'(τ) and G"(τ) for suspensions of **18**, of **20** and for gels of **18** + **20** from 20 to 28 vol%.

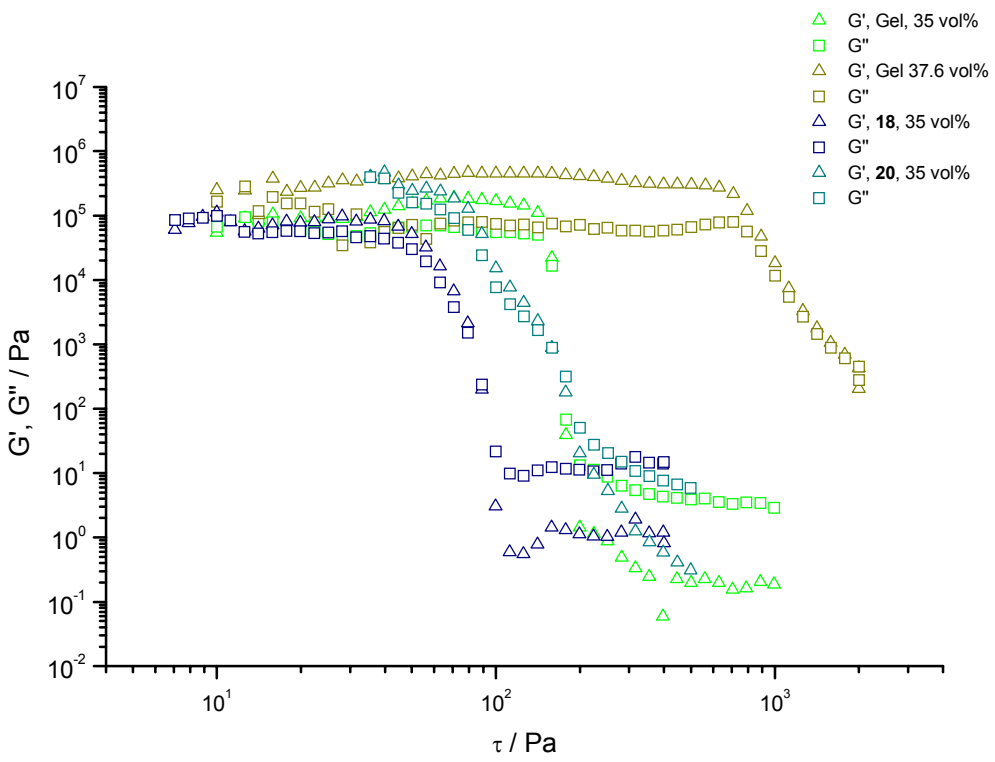

Figure 62: G'(τ) and G"(τ) for suspensions of **18**, of **20** and for gels of **18** + **20** from 35 to 37.6 vol%.

G' of the 28 vol% gel has a minimum at a shear stress τ of 12 Pa. This minimum is not present in the curves of the reference systems (Figure 61). At τ=40 Pa the 25 and 28 vol% gel exhibits a second cross over missing in the reference systems. Right to the transition of **18** and **20** in Figure 61 G" and especially G' decrease whereas both moduli of the gel sustain on the same level. Summarizing, the curves of the gels are different from the reference ones, while **18** is similar to **20**. The gels do not behave like a mixture of their components. This shows a chemical reaction took place to that the changes in the rheological behavior are attributed.

Figure 63-65 reveal that the viscosity of the gels with lower volume fractions from 20 to 28 vol% is lower compared to the corresponding reference systems. This can be explained by the presence of clusters formed by the reaction products of **18** and **20** in the gels. The cluster formation decreases the total surface of the particles exposed to the water and decreases the total interaction energy of the particles leading to a reduced viscosity. This is in agreement with the low values of G', G" and the transition compared to the reference systems (Figure 61).

The behavior of G’ and G’’ of the gels can be understood in the following way. At stresses in the range of the viscoelastic plateau G' is higher than G". This means that the gels have solid-like properties. The particles are vibrating against each other maintaining the microstructure of the gel.

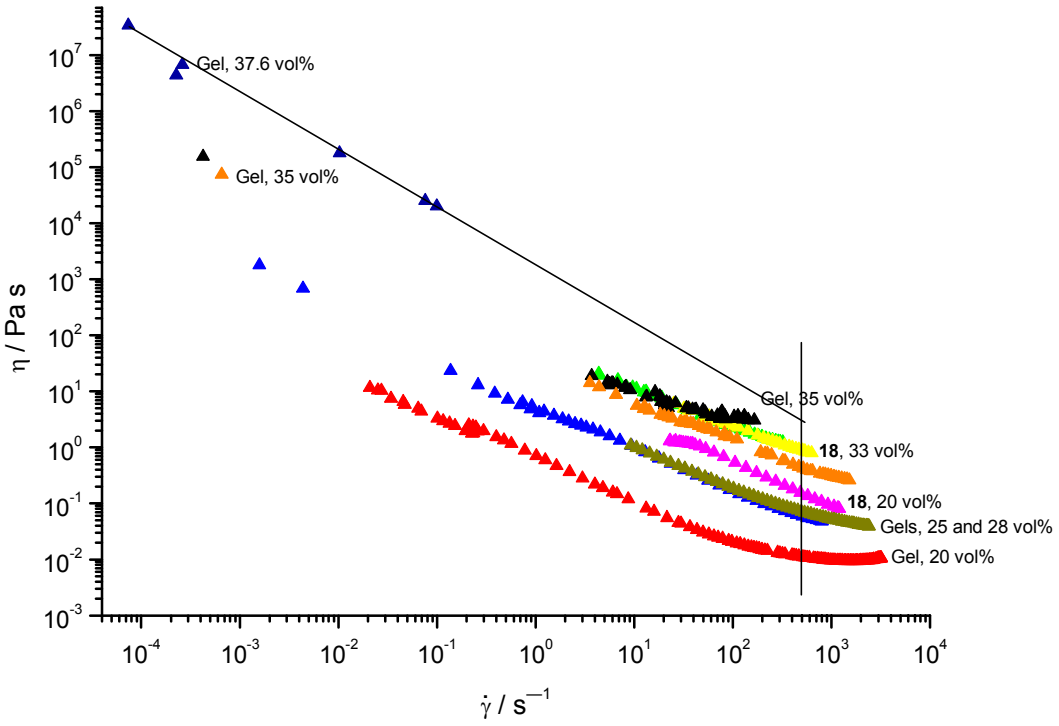

Figure 63: η versus $\dot{\gamma}$ of gels and **18**.

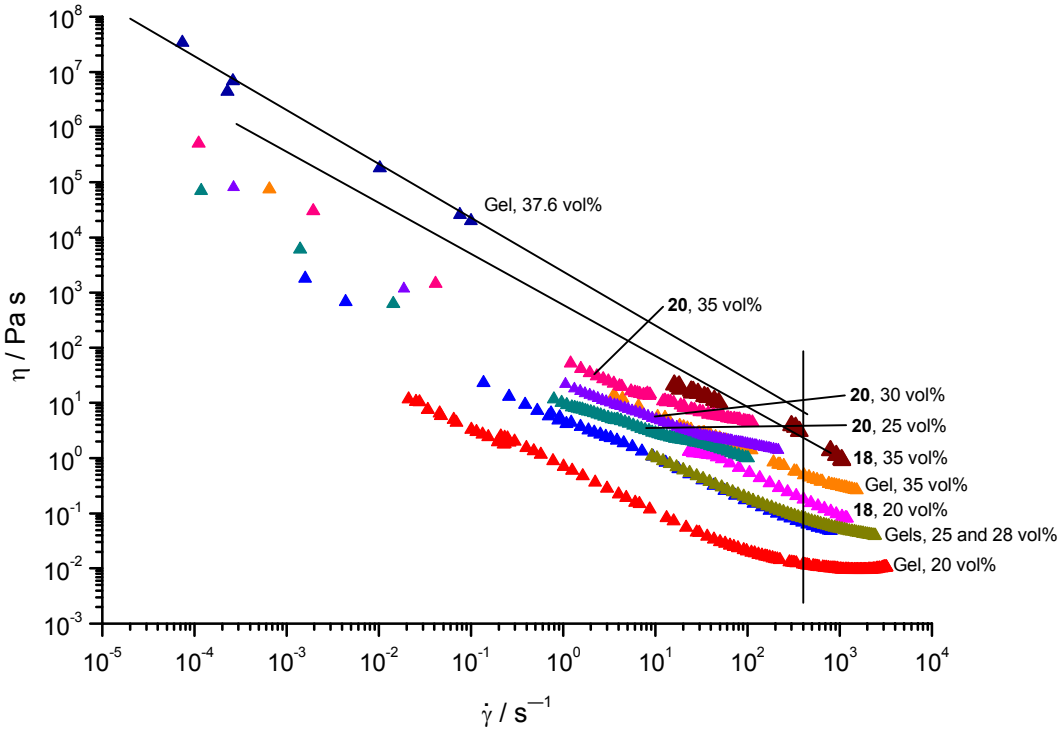

Figure 64: η versus $\dot{\gamma}$ of gels and **20**.

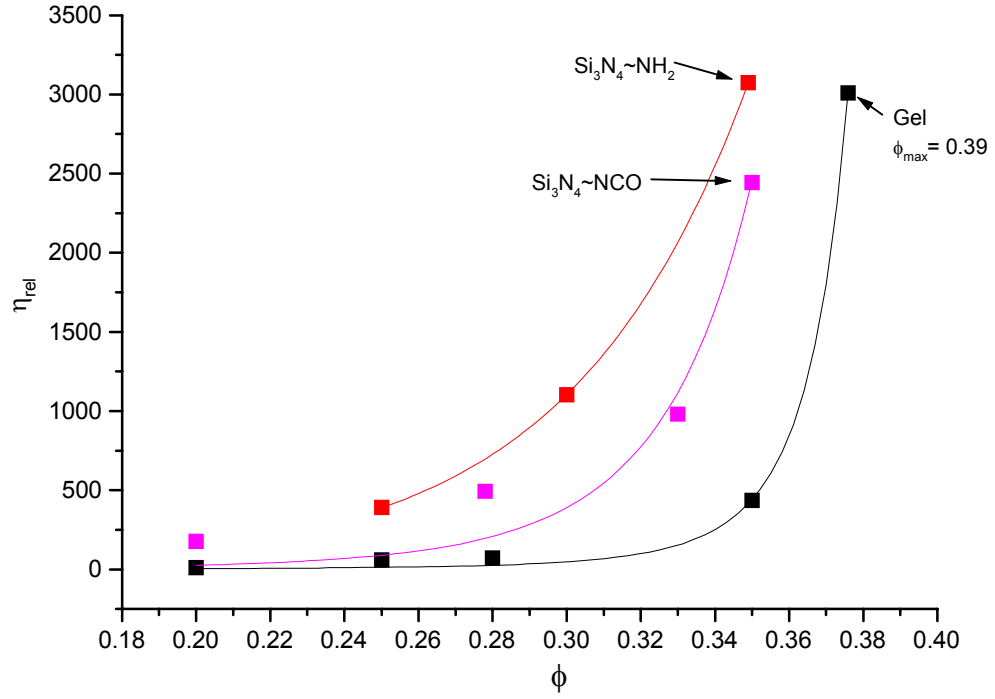

Figure 65: Relative viscosity η_{rel} versus volume fraction ϕ for the gel formed by mixing, **18** and **20**.

After the cross-over the particles slip beside each other. The suspensions start to flow and have a liquid-like behavior exhibited by G'' values higher than the G' values. The clusters have the capability to absorb energy and to set energy free. This results in the second transition at τ=40 Pa where the clusters elastically take up energy from particle-cluster and cluster-cluster collisions by deformation and relaxation of the cluster. The reference systems do not have this elastic energy absorption mechanism. G' and G'' of the reference systems decrease to very low values. The curve of G' is bent in a 90° angle and G' is too low to be measured.

From 20 to 28 vol% the viscosity of the gel is lower than that of the reference systems (Figure 63). A 20 vol% suspension of **18** has a higher viscosity than a 28 vol% gel. At 35 vol% the viscosity of the gel starts to increase drastically because a lump begins to be formed spanning the entire beaker (percolation cluster). At 37.6 vol% the viscosity of the gel overshoots that of the reference systems (Figure 65) caused by the gelation and the network attraction.

The data points of the gel in Figure 65 are fitted with the Mooney equation $\eta_{rel} = \exp\left(\frac{[\eta]\phi}{1-\frac{\phi}{\phi_{max}}}\right)$ obtaining ϕ_{max}=0.39, where η_{rel} is the relative viscosity, [η] the Staudinger index, ϕ the volume fraction and ϕ_{max} the maximum solid loading; neither the Mooney equation nor the Krieger-Dougherty equation $\eta_{rel} = \left(1-\frac{\phi}{\phi_{max}}\right)^{-[\eta]\phi_{max}}$ applied to **18** fits the data well. The curve for the gel is shaped like a 90° angle bent at the critical volume fraction of gelation at ϕ_{crit}=35 vol%, whereas η_{rel} for both reference systems increases more slowly than that of the gel. This is due to lack of gelation of the reference systems.

The required compounds needed for covalent interaction of the ceramic particles are commercially available, in any amount at a low price. So this method is interesting for industrial applications like plastic forming.

The reaction of **18** and **20** is carried out in dilute suspension (0.567 g **18** + **20**/l, $1.65*10^{-4}$ vol%), too. 850 µg **18** and 850 µg **20** are suspended in 3 ml H_2O in a small

screwable beaker, shaken and ultrasonically treated for 10 min. After another 5 min, a cylindrical, long tube with a small diameter (NMR-tube) is filled with the suspension with a 1 ml syringe with a long canula. The pH of the suspension is ≈6.5.

After 18 hours agglomerates with 50-500 μm diameter according to the LOM images (Figure 66-69) are formed that settle down and stick to the wall of the tube.

The agglomerates show that **18** reacts with **20** in dilute suspension, but here the reaction leads to sedimentation whereas the highly concentrated suspensions (20-37.6 vol%) do not sediment. They are gelled under formation of a percolation cluster leading to a consolidation of the slurry. So the desired effect can be controlled by the concentration of the suspension. These phenomena can be understood using the DLVO-theory. The pH_{pzc} of **18** is 6.0, the pH_{pzc} of **20** 7.7, so both are close to the pH of the suspension (≈6.5). This induces a coagulation parallel to the reaction. Under these conditions both forces – the colloidal and the chemical – are directed towards a particle attraction causing an agglomeration. Whereas in the rheological investigation the particle potential is set to a repulsive one with a pH of 9. In both cases the reaction takes place independently of the potential.

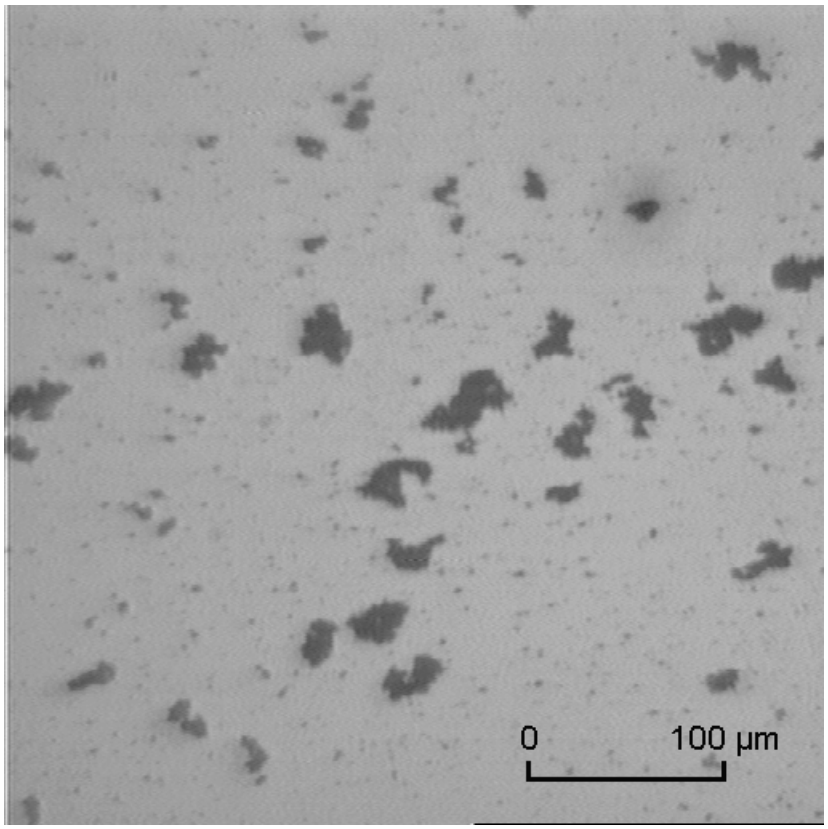

Figure 66: LOM-image of agglomerates of **18** + **20**.

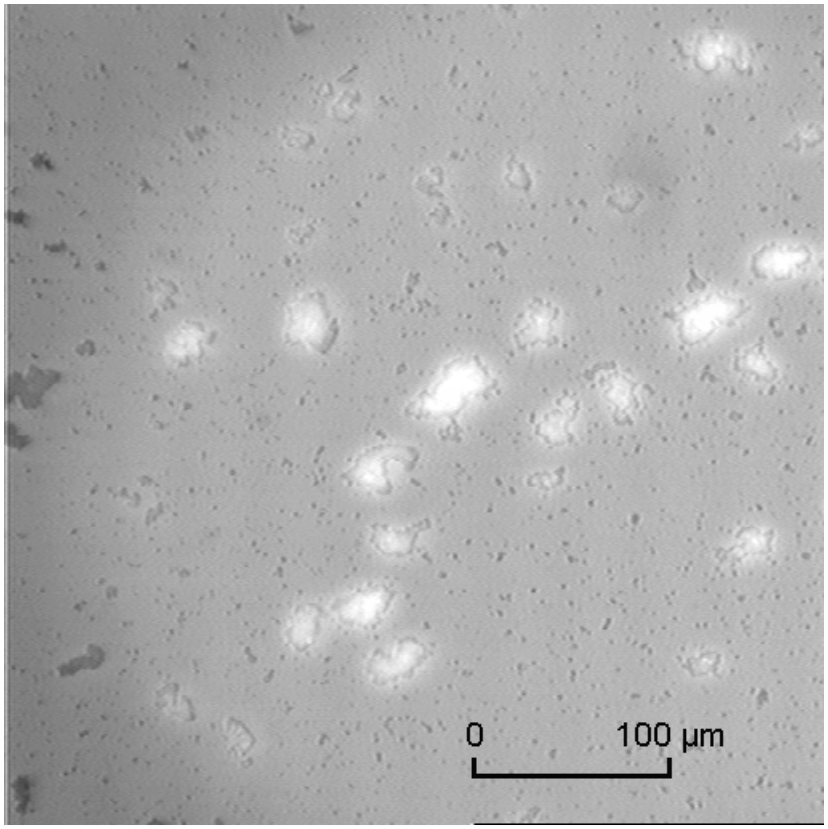

Figure 67: LOM-image of agglomerates of **18** + **20**.

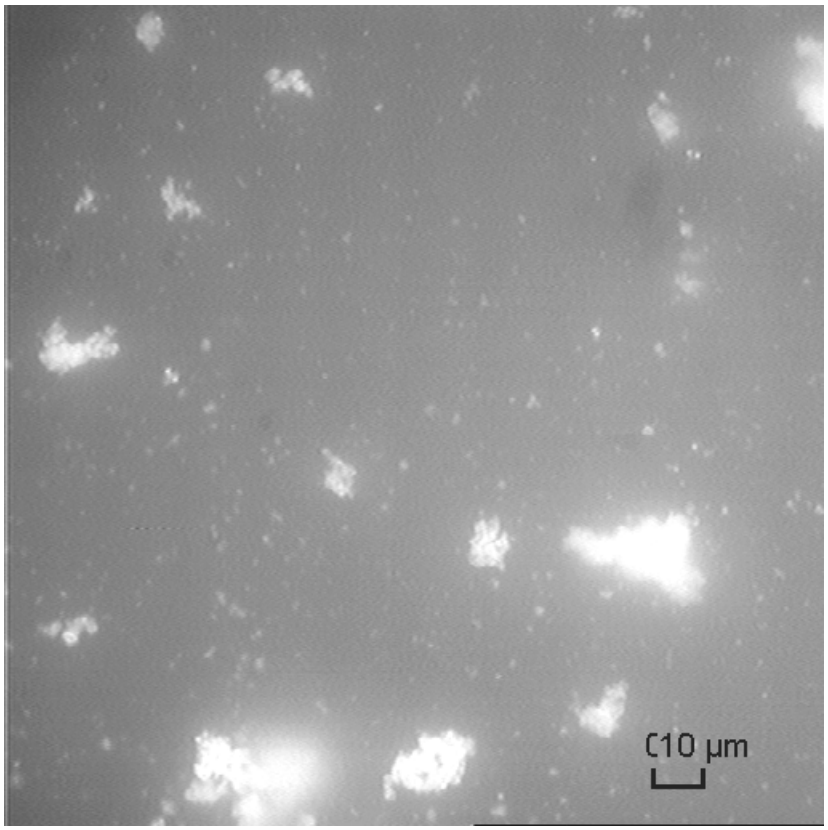

Figure 68: LOM-image of agglomerates of **18** + **20**.

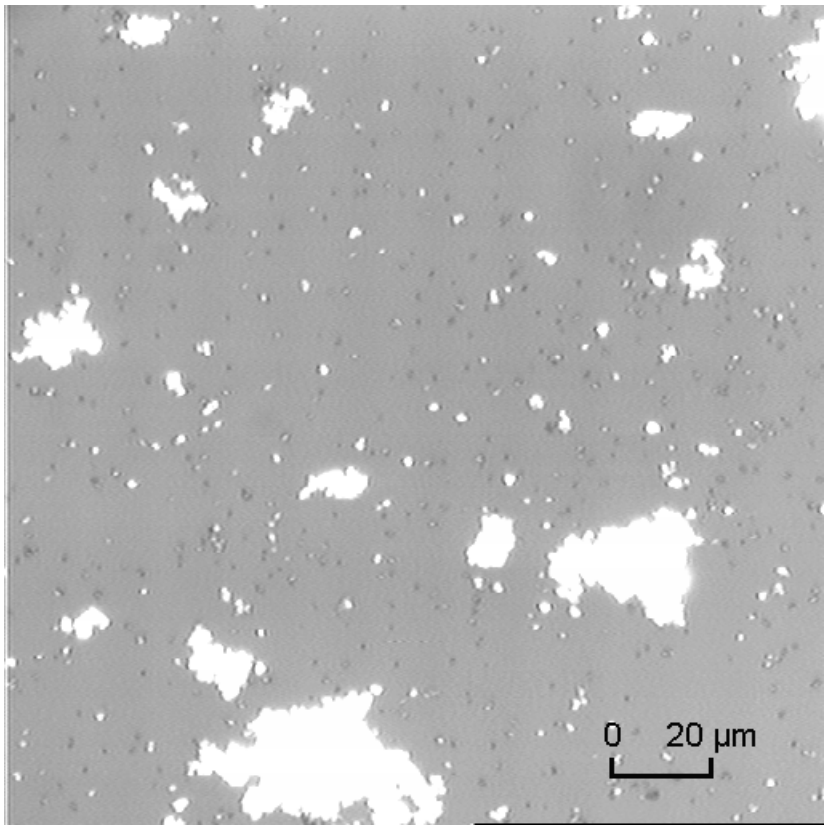

Figure 69: LOM-image of agglomerates of **18** + **20**.

12.2. Heterosupramolecular Interaction of Si_3N_4 Particles

The cyclodextrinfunctionalized Si_3N_4 particles **6** will be crosslinked with the guest polymer **16**. The particles will be bridged via the polymer guest molecule **16**. The crosslinkage leads to an enhanced sedimentation of the particles.

The synthesis of guest polymer **16** (M_W=70800 g/mol, M_W of backbone 60000 g/mol) is described in[192] (named **10a**), similar to the synthesis of **14**.

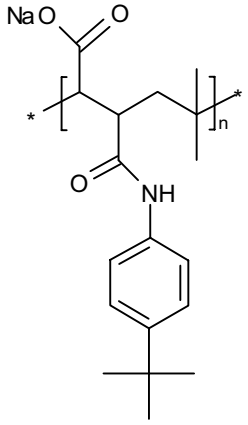

16

A scheme of the reaction is presented in Figure 10. The tert-butyl-anilide side chain of **16** is a proper guest for β-cyclodextrin. One tert-butyl-anilide of **16** is intercalated by a β-cyclodextrin that is attached to Si_3N_4. A second of the same molecule **16** is intercalated by a β-cyclodextrin fixed to the same Si_3N_4 particle or to another one. If it is fixed to the same Si_3N_4 particle, the steric barrier of the Si_3N_4 particle is enlarged providing an enhanced dispersibility. If **16** with an attached Si_3N_4 particle is fixed to another Si_3N_4 particle, the two particles are bridged and enhance sedimentation.

To receive more information, some reference systems are also investigated. The reaction and the analysis of the systems are done simultaneously by observation of the sedimentation behavior. 30 mg **16** are dissolved in 3 ml phosphate buffer (pH=7.2, 0.03 molar), 1.7 mg **6** therein suspended, shaken and ultrasonicated for 10 min. After another 5 min, the suspension is filled into a NMR-tube with a 1 ml syringe with long canula and the sedimentation observed. A second tube with 1.7 mg **6** in 3 ml phosphate buffer without the polymer guest **16** is likewise prepared, as well as a third tube with 1.7 mg epoxyfunctionalized Si_3N_4 **5** with 30 mg **16**.

The sedimentation rate after 120 h is as follows:
6 > **6**+**16** > **5**+**16**.

This can be explained using the DLVO-theory. With 0.03 mol/l the electrolyte concentration is high, so that a stabilization through electrostatic double layer forces is reduced. In system **6** is no stabilizing polymer present, so that there are no polymer induced forces, but attractive Van-der-Waals forces resulting in sedimentation of **6**. The Van-der-Waals interaction between spheres of the same material is always attractive. In **6** + **16** and **5** + **16** the polymer stabilizes the particles leading to a lowered sedimentation compared to **6**. Bridges between the particles in **6** + **16** enhance the sedimentation compared to the cyclodextrin-free system **5** + **16** where no bridges are present.

Summarizing, Si_3N_4 particles could successfully be crosslinked by using cyclo-dextrins. This is very interesting for the consolidation step in plastic forming.

12.3. Improved Dispersibility of Al_2O_3 with Cyclodextrin

Cyclodextrins can be used to stabilize Al_2O_3 suspensions. A polymeric β-cyclodextrin that is bonded to the Al_2O_3 powder surface adsorbs a guest polymer with appropriate anchor groups. The guest polymer is attached as a second layer on the cyclodextrin layer. These two layers enlarge the steric barrier and increase the dispersibility.

A scheme of the reaction is shown in Figure 12. The tert-butyl-anilide side chain of the guest polymer **16** is intercalated by the β-cyclodextrins of the poly-β-cyclodextrin attached to Al_2O_3 (system **15** with a high concentration of **14**). So **16** is bonded as a second layer to the Al_2O_3. The reaction is carried out as a sedimentation experiment.

30 mg **16** are dissolved in 3 ml phosphate buffer (pH=7.2, 0.03 molar). 2.9 mg **15** are suspended, shaken and ultrasonicated for 10 min. After 5 min waiting the suspension is filled into a NMR-tube with a 1 ml syringe with long canula and the sedimentation is observed. Reference systems are prepared in the same manner: A second tube is prepared with as-received Al_2O_3, a third tube is prepared with **15** and in a fourth tube Al_2O_3 is filled and **16** is added.

The sedimentation rate after 120 h is as follows:
Al_2O_3 > **15** > Al_2O_3 + **16** > **15** + **16**.

This can be explained using the DLVO-theory. The electrolyte concentration of 0.03 mol/l suppresses a stabilization by electrostatic double layer forces. In the Al_2O_3 system are the only remaining forces the attractive, electrodynamic Van-der-Waals forces causing sedimentation. System **15** is similar to Al_2O_3, the poly-β-CD **14** enlarges the steric barrier of the particles inducing a reduced sedimentation. Whereas in Al_2O_3 + **16** and **15** + **16** the guest polymer **16** is adsorbed on the Al_2O_3 enlarging the steric barrier and leading to a stabilization of the particles due to polymer induced forces. **15** + **16** exhibits the lowest sedimentation because it has additionally **16** as a second layer on the poly-β-cyclodextrin layer. This second layer increases the steric barrier furthermore.

In **15** + **16**, **16** adsorbs to single ceramic particles without bridging them. This causes improved dispersibility compared to the cyclodextrin free system. In **6** + **16**, **16** bridges different ceramic particles causing sedimentation, because **6** has a small amount of cyclodextrins on the surface as compared to **15**. β-Cyclodextrin works as an anchoring group for the guest polymer **16**. The probability that several tert-butyl-anilide groups intercalate into β-cyclodextrins located on the same ceramic particle is not very likely. The other tert-butyl-anilide groups are complexed by β-cyclodextrins fixed to another ceramic particle building up a heterosupramolecular interaction in-between. In **15** + **16**, **16** is fixed to a single ceramic particle because there are enough β-cyclodextrins attached to it.

In summary, a cyclodextrin layer and an additional guest polymer layer as a second layer could successfully be attached to Al_2O_3 particles. These particles show an enhanced dispersibility which could be used in plastic forming.

13. Discussion

For a heterosupramolecular or covalent interaction of particles by crosslinking or attachment to a polymer backbone a suitable surface modification is required that enables a selective reactivity between the two desired components. So cyclodextrins and silanes are attached to the surfaces. The attachment of the cyclodextrins can be done monomeric covalently or polymeric ionically.

A commercially available β-cyclodextrin derivative, 3-chlor-5-sodium-hydroxyl-trianzinyl-β-cyclodextrin, is covalently bound to the Si_3N_4 surface in one step. An effortful derivatisation of the cyclodextrin is not required. The triazinyl ring is not bound to a defined position at the cyclodextrin torus having in average 2.8 triazinyl groups. The number per glucose unit and the position are not specified. The DRIFT spectrum proves the attachment of 3-chlor-5-sodium-hydroxyl-trianzinyl-β-cyclodextrin to the surface and ζ-potential measurements pH_{iep}=7.2.

In another covalent approach mono-6-amino-β-cyclodextrin **3** is bound to epoxy-functionalized Si_3N_4 **5**. The synthesis of the cyclodextrin starts with β-cyclodextrin, that is monofunctionalized at the 6-position to the tosylat **1** and the amino-cyclodextrin is obtained via hydration of the azide **2**. The hydration is done with a hydrogen donor (ammonium formate, hydrazine hydrate). The reaction is monitored by TLC and the isolation and purification are improved. The epoxy groups are induced on the Si_3N_4 by reaction with (2,3-epoxypropyl-propyl-ether)-trimethoxysilane **4**. The mono-6-amino-β-cyclodextrin is bonded to the epoxy-functionalized Si_3N_4 **5** as the last step. This route provides a regioselectivity and a spacer between the cyclodextrin torus and the surface ensuring flexibility. The adsorbed amount is as low as approximatively 25% of the total mass. This is in contrast to 9% for the non-modified Si_3N_4 revealing that mono-6-amino-β-cyclodextrin binds to the epoxy group. Washing desorbs the loosely bound parts, 17% are still remaining.

Because of the seven amino groups of heptakis-6-amino-β-cyclodextrin **9** this molecule binds more easily to **5** than mono-6-amino-β-cyclodextrin **3** with one amino group. This is exhibited by the intensive DRIFT-signals (0.1 absorbance units,

methylene). The seven amino groups lower the complex binding constant of the cyclodextrin to a guest. A disadvantage of **9** is its low solubility in solvents. The amino groups cause a strong basic shift of the pH_{iep} to 9.8.

Poly-β-cyclodextrin **14** has a side chain with a carboxylic acid terminus that can be attached to α-Al_2O_3 ceramic powders and a β-cyclodextrin containing side chain. This is an interesting way to the covalent monomeric route described above and Al_2O_3 is as well functionalized with cyclodextrin in a one step reaction. DRIFT shows that poly-β-CD **14** is immobilized on the Al_2O_3 surface. The adsorbed amount can be varied. The maximum amount is higher than for the other systems. The ad- and desorption investigations carried out under the same conditions as for the Si_3N_4 systems allow a comparison: 57 mass% are adsorbed in a 0.1 % solution and 72% in a 0.042% solution, while 25% of mono-6-amino-β-cyclodextrin **3** are adsorbed on **5**. After redispersing the Al_2O_3 / cyclodextrin in water no poly-β-CD **14** is detected in the supernatant solution in contrast to mono-6-amino-β-cyclodextrin on epoxy-functionalized Si_3N_4 where 30% of the adsorbed mass are redissolved.

The influence of the cyclodextrin torus on the adsorption is proven by the adsorption of copoly-maleic-acid-alt-isobutene **29** (the backbone of poly-β-CD **14**) on Al_2O_3. **29** has a high affinity to Al_2O_3 (100%), whereas adsorption is reduced to 57% by the cyclodextrin torus which hinders the adsorption of poly-β-CD **14**. If Al_2O_3 / **29** is washed with water, approximatively 20% of the bound amount are redissolved. Only the inner molecules are tightly bonded to the surface, the outer ones are physisorbed and are easily redispersed. In the case of **14** every molecule is tightly fixed to the surface, so that the desorbed amount is 0%.

As already shown some ceramic / cyclodextrin systems were prepared, requisites for the heterosupramolecular interaction of particles using host guest chemistry. Two or more cyclodextrins bearing on Si_3N_4 particles are attached to the guest polymer **16**. The β-cyclodextrin on the Si_3N_4 **6** works as an anchor for the tert-butyl-anilide units of the guest polymer **16**. So several particles are crosslinked via a long chain polymeric molecule. The heterosupramolecular binding is caused by the intercalation chemistry of the β-cyclodextrin, its reaction monitored by the sedimentation behavior. The sedimentation rate after 120 h is as follows:

6 > **6**+**16** > **5**+**16**. According to the DLVO-theory the 0.03 mol/l electrolyte concentration reduces the stabilization by electrostatic double layer forces. So the only remaining forces are polymer induced forces and Van-der-Waals forces. In system **6** is no stabilizing polymer present, so that there are no polymer induced forces, but attractive Van-der-Waals forces resulting in sedimentation of **6**. In **6** + **16** and **5** + **16** the polymer stabilizes the particles leading to a lowered sedimentation compared to **6**. Bridges between the particles in **6** + **16** enhance the sedimentation compared to the cyclodextrin-free system **5** + **16** where no bridges are present.

16 reacts with single particles of **15** (Al_2O_3 with a high coverage of poly-β-CD **14**) because the intraparticular reaction being preferred compared to the interparticular reaction. This means no bridges are formed between the particles. The two layers on the particles increase the steric barrier and improve the dispersibility strongly, the same molecules achieving opposite effects – improved dispersibility and sedimentation. The critical factor is the adsorbed amount.

A covalent interaction between two ceramic particles is achieved by formation of a molecular bridge, crosslinking both particles. Si_3N_4 is functionalized with two different commercially available silanes which can react with each other with their non silyl termini. 1-triethoxysilyl-3-isocyanato-propane **17** is bonded to Si_3N_4 obtaining **18** and 1-trimethoxysilyl-3-amino-propane **19** to Si_3N_4 resulting in **20**. The reaction is indicated in diluted suspension by the formation of agglomerates (50-500 µm) and sedimentation. Stable highly filled suspensions (20-37.6 vol%) could be prepared with a maximum solid loading of ϕ_{max}=0.39, too, gelling at the critical volume fraction ϕ_{crit}=0.35. The data of the relative viscosity η_{rel} in dependence of the volume fraction ϕ can be fitted with the Mooney equation. The viscosity of the 20-28 vol% gels is lower and G' and G'' have an additional cross over compared to suspensions of **18** and **20**.

With cyclodextrins attached covalently and ionically to Al_2O_3 and Si_3N_4 powders and differently functionalized silanes bonded to Si_3N_4 particles a heterosupramolecular, long chain and a covalent, short chain linkage of particles is achieved, respectively. A reaction between two fixed components and a dissolved one is successfully performed as an interesting extension to the inclusion chemistry of solved and

immobilized hosts with solved guests. By control of the coverage of the particles with cyclodextrin the reaction can be carried out as an intraparticular or as an interparticular reaction inducing improved dispersibility or enhanced sedimentation.

The covalent crosslinkage of Si_3N_4 powder particles presented here uses silanes that are commercially available, in any amount at a low price. So this method could be interesting for industrial applications of plastic forming. The heterosupramolecular crosslinkage of cyclodextrin-functionalized Al_2O_3 powders is also an interesting alternative for consolidation with plastic forming.

14. Future Prospectus

The dispersion of ceramic powders has a remarkable potential scientifically and technically. Cyclodextrin polymers on particles improve their dispersibility by their enlarged steric barrier. The cyclodextrins provide a supramolecular chemistry which induces a manifold flexibility and immense opportunities for ceramic processing. With these possibilities the dispersion behavior can be changed and fitted to the required demands such as the adsorption of a guest polymer as a second layer on the cyclodextrin polymer layer on a particle enhancing the dispersibility furthermore.

Most solid-liquid-transitions, applied in ceramic processing, are irreversible. Therefore, a reversible transition is interesting when shear thinning is asked. The cyclodextrin-functionalized Si_3N_4 system crosslinked by the guest polymer (Figure 10) should be shear sensitive: Without shearing the viscosity should be high due to the crosslinkage of the particles, whereas by shearing the viscosity should be lowered (shear thinning), because the guest in the side chain of the polymer, intercalated into the cyclodextrin, is pulled out of the cyclodextrin and the crosslinkage is broken. If no shear stress is applied anymore, the guest is again complexed by the cyclodextrin and the viscosity increases. Another possibility to lower the viscosity can be the addition of a low molecular mass guest that has a higher complex formation constant for the cyclodextrin than the polymer. The low molecular mass guest ejects the side chain of the polymer out of the cyclodextrin.

Systems with a temperature dependent viscosity are very attractive for plastic forming applications. It is true that the temperature dependence of the complex constant for the host guest binding is low, however, for enhancement the strongly temperature dependent complex formation constant of the tri-amino-pyrimidine-barbituric-acid-complex[193-195] can be used (Figure 70). Tri-amino-pyrimidine is included in one part of the cyclodextrins that is immobilized on the particles, and the barbituric-acid is complexed by the other part of the cyclodextrins. Around room temperature both molecules should form a complex, that dissociates at higher temperatures (≈ 50 °C). By this association and dissociation behavior the particles should be reversibly crosslinked and resolvable inducing the desired transition.

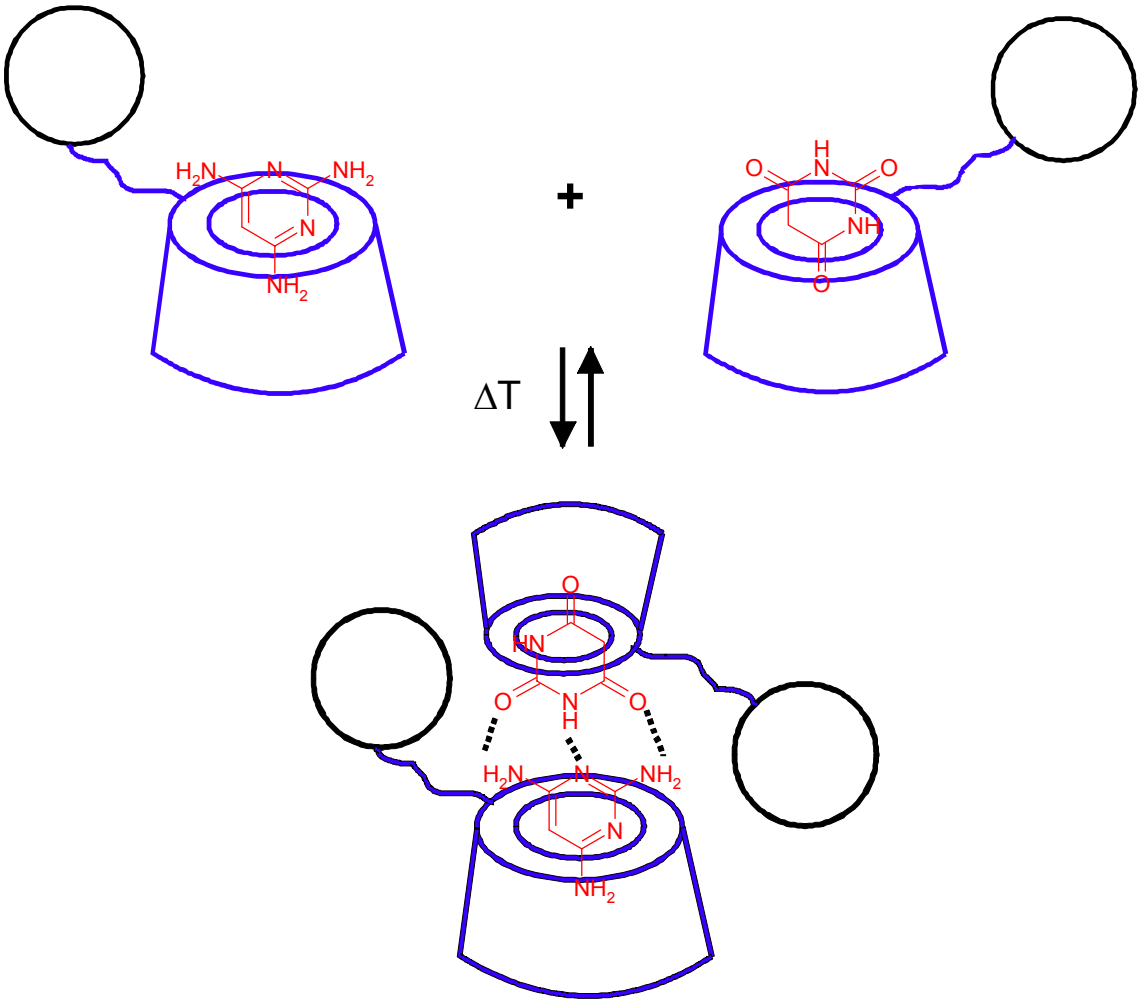

Figure 70: Temperature dependent reversible crosslinking of particles.

For many ceramic applications also the homogeneous mixing of powders is an important step in the manufacturing process. To achieve a complete dispersion the surface of different powder components could be chemically modified with reactants thus mixing creates a distribution in which each particle of one component is neighored by a particle of the other component. This can be done successfully by crosslinking as described in this work in two ways: firstly the ceramic powders are functionalized with two different groups reacting with each other so that a covalent bond is formed. Secondly the cyclodextrin-functionalized particles are attached to the side chain of a polymer molecule via heterosupramolecular host guest inclusion chemistry to be bridged by a polymer molecule. Like that two different kinds of ceramic powders can be mixed homogeneously also a phase separation (demixing) is suppressed by the molecular connection of the particles. This is especially valid for ceramic substances having marked differences in mass densities and particle sizes

which can be mixed that way without risking separation by sedimentation of the substance with the higher density.

The deposition of ceramic layers[196-201] is of interest for the production of coated materials. The ceramic layer may protect the substrate material against atmospheric influences such as oxidation and may improve the wear behavior and tribological properties. For these demands a lateral homogeneous depostion onto the substrate is required which can be achieved by the depostion of ceramic powder particles on a substrate similar to the liquid phase deposition method (LPD). A main methodical difference is that with the LPD method the ceramic substance is synthesized in situ and immediately deposited on the substrate whereas here an already available powder is modified and deposited.

Another interesting possibility of the application of the technology described here are multilayer systems consisting of different ceramic compounds in which desired material properties can be combined (Figure 71). The system in Figure 71 could be built up by an alternative deposition of tert-butyl-anilide-functionalized PZT (lead zirconate titanate) and cyclodextrinfunctionalized Al_2O_3 onto a cyclodextrin-functionalized substrate via the tert-butyl-anilide-cyclodextrin-complex.

Furtheron for mixed-oxide ferroelectric and piezoelectric compounds[197, 202-205] like barium titanate and PZT the technology described here can be applied for lateral heterogeneous deposition of substrates which opens new fields for the production of electrical and electronic devices (Figure 72)[206-210]. Gold dots on a substrate (Figure 72) are of interest for the induction of the lateral heterogeneity and for the bonding of bifunctional thiols or disulfides. After modification of gold with thiols or disulfides that have e.g. a tert-butyl-anilide terminus as an anchor group, cyclodextrin-functionalized PZT could be bonded to the thiol or disulfide.

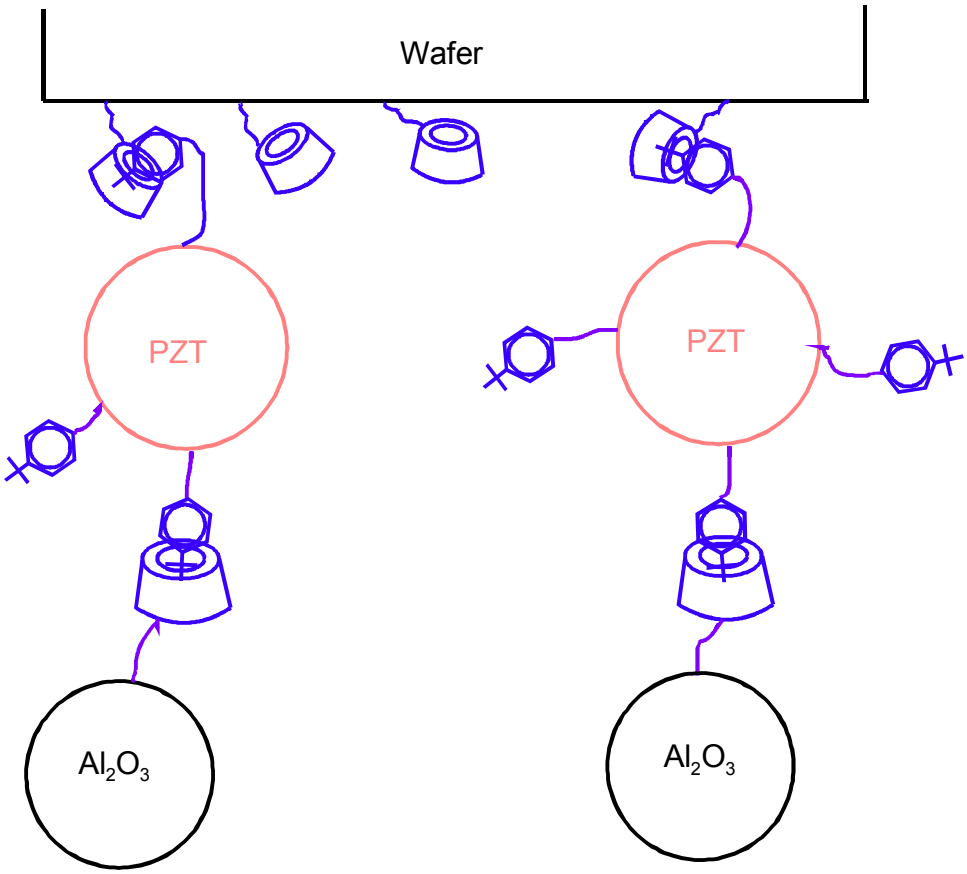

Figure 71: Construction of ceramic mulitlayer systems.

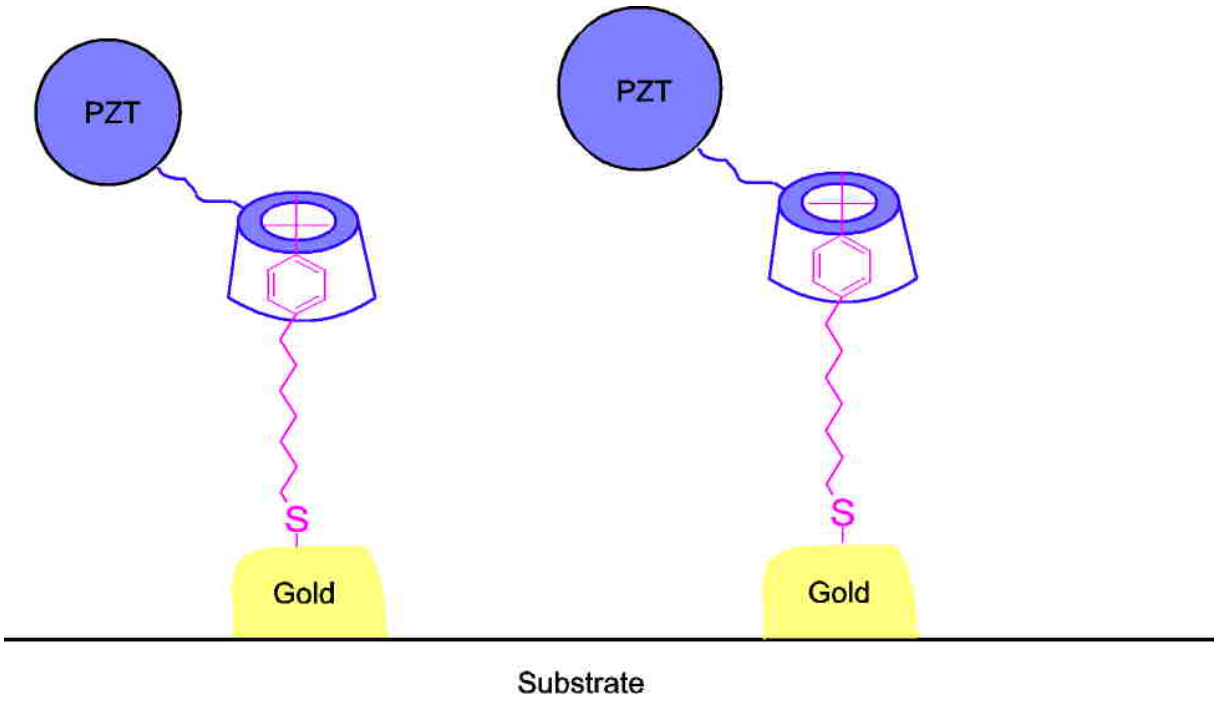

Figure 72: Nanostructured deposition of ceramics.

The host guest chemistry of the cyclodextrinfunctionalized powders prepared here could also be useful for the storage of substances. Sensitive compounds (e. g. especially such of light sensitivity) can be protected by the cyclodextrin torus, or radioactive compounds are immobilized and attached to a solid substrate. This decreases the outgoing radiation and makes their handling easier.

Another usage for cyclodextrin-coated ceramic powders could be the separation and purification of multi-component systems. When a suspension containing several compounds flows over cyclodextrin-functionalized powders, the desired molecules being intercalated into cyclodextrin. The powder with the bonded substance can be stored after centrifugation. To be set free, the powder is suspended in a solution containing molecules with a higher binding constant to the cyclodextrin than the intercalated compound. The desired substance is ejected into the solution.

15. Abstract

New concepts of particle interaction for the processing of ceramic powders are developed. They are based on chemical reactions either by heterosupramolecular or covalent interaction of proper reactants. For this the particles are functionalized so that they are able to undergo defined reactions with each other. A commercially available β-cyclodextrin derivative, 3-chlor-5-sodium-hydroxyl-trianzinyl-β-cyclodextrin, is covalently bound to the Si_3N_4 surface in an one step reaction. An effortful derivatisation of the cyclodextrin is not required. The triazinyl ring is not bound to a defined position at the cyclodextrin torus (in average 2.8 triazinyl groups per cyclodextrin).

In the next covalent approach mono-6-amino-β-cyclodextrin is bound to epoxy-functionalized Si_3N_4. This route provides a regioselectivity and a spacer between the cyclodextrin torus and the surface ensuring flexibility. The ad- and desorption behavior is investigated by rotation angle measurements, the adsorbed amount is low: approximatively 25% of the total mass is adsorbed. This is in contrast to 9% for the non-modified Si_3N_4 revealing that mono-6-amino-β-cyclodextrin binds to the epoxy group. Washing desorbs the loosely bound parts, 17% are still remaining.

Because of the seven amino groups of heptakis-6-amino-β-cyclodextrin this molecule binds more easily to epoxy-functionalized Si_3N_4 than mono-6-amino-β-cyclodextrin with one amino group. This is exhibited by the intensive DRIFT-signals.

The cyclodextrinfunctionalized Si_3N_4 could heterosupramolecularly be crosslinked by a guest polymer bearing tert-butyl-anilide as an anchor for the cyclodextrin in the side chain. This is interesting for the consolidation step in plastic forming.

Al_2O_3 powder could be cyclodextrin-functionalized in one step by the deposition of a polymeric β-cyclodextrin derivative.

A two layer system consisting of a cyclodextrin polymer and a guest polymer was built up on Al_2O_3 powder particles. Due to the enlarged steric barrier the dispersibility of the Al_2O_3 is improved which is interesting for ceramic powder processing.

A covalent interaction between two ceramic particles is also achieved by functionalizing Si_3N_4 with two different commercially available silanes which can react with each other with their non silyl termini thus forming a molecular bridge between particles. 1-triethoxysilyl-3-isocyanato-propane is bonded to Si_3N_4 and 1-trimethoxysilyl-3-amino-propane reacts with Si_3N_4. The reaction is indicated in diluted suspension by the formation of agglomerates (50-500 µm) and sedimentation. Stable highly concentrated suspensions (20-37.6 vol%) could be prepared with a maximum solid loading of ϕ_{max}=0.39, too, gelling at the critical volume fraction ϕ_{crit}=0.35. The data of the relative viscosity η_{rel} in dependence of the volume fraction ϕ can be fitted with the Mooney equation and the moduli G'(τ) and G''(τ) were measured. The viscosity of the 20-28 vol% gels is lower and G' and G'' have an additional cross over compared to suspensions of the iso-cyanatofunctionalized Si_3N_4 and the aminofunctionalized Si_3N_4. Concluding, Si_3N_4 powder could successfully be crosslinked by using low cost silanes. This technique is a promising possibility for the consolidation step in plastic forming.

16. Zusammenfassung

In der keramischen Formgebung ist der Flüssig-Fest-Übergang von Pulversuspensionen von großer Bedeutung. Er wird entweder physikalisch durch einen Entzug des Lösungsmittels oder durch thermoplastische Zweitphasen bewirkt oder chemisch durch Gelieren, Flokkulieren oder anderen durch eine Modifikation der Pulveroberfläche induzierten Reaktion. Bei den in dieser Arbeit vorgestellten Methoden werden einzelne Partikel direkt und selektiv über Molekülbrücken miteinander verknüpft. Dazu wurden einerseits Cyclodextrine verwendet und andererseits Silane, die gezielt auf die Oberflächen von suspendierten Pulverteilchen aufgebracht wurden.

Cyclodextrine sind zyclische Oligosaccharide der α-D-Glucose (cyclo-[(1$\rightarrow$4')-α-D-glucopyranose]). Die wichtigen α-, β- und γ-Cyclodextrine enthalten 6, 7 und 8 Glucoseeinheiten. Sie sind über den enzymatischen Abbau der Stärke zugänglich (Cyclodextrin-Glycosyltransferasen) und haben die Form eines hohlen Torus, in dessen Cavität vorzugsweise hydrophobe Gäste eingelagert werden können.

Als keramische Modellsubstanzen wurden α-Al_2O_3- und Si_3N_4-Pulver hoher Reinheit und mit Teilchendurchmessern im Submikrometerbereich verwendet. Die Partikelform und Topologie dieser Pulver sind mittels Rasterkraftmikroskopie (AFM) und Rasterelektronenmikroskopie (SEM) untersucht worden. Die Untersuchungen zeigen, dass die Pulver unregelmäßig geformte Plättchen mit einer fraktalen Topologie aufweisen. Die chemische Zusammensetzung ist durch Elementaranalyse bestimmt worden, die Partikelgröße und deren Verteilung mittels Laserbeugung und dynamischer Lichtstreuung. Infrarot-Spektroskopie in diffuser Reflexion und ζ-Potentialmessungen liefern Aufschluss über die Oberfläche. Al_2O_3 hat eine BET-Oberfläche von 12,3 m^2/g, einen Ladungsnullpunkt von pH_{pzc}=8-9 und einen mittleren Teilchendurchmesser (d_{50}) von 290 nm. Das kommerziell erhältliche Al_2O_3 enthält eine Substanz, die über Methylen- und Carboxylgruppen verfügt, was sich aus der Elementaranalyse und der Infrarot-Spektroskopie in diffuser Reflexion ergibt. Wahrscheinlich handelt es sich um einen Mahlhilfsstoff, der durch Waschen mit Wasser (pH=5) leicht entfernt werden kann. Das Si_3N_4 hat eine BET-Oberfläche von 12,7 m^2/g, einen Ladungsnullpunkt pH_{pzc} von 4-5 und einen mittleren

Teilchendurchmesser von d_{50}=680 nm. Auf den einzelnen Si_3N_4-Partikeln befindet sich eine durch Hydrolyse mit Luftfeuchtigkeit gebildete SiO_2-Schicht (3,76 Masse%). Sie hat an ihrer Oberfläche Silanolgruppen, die für die Anbindung der Silane wichtig sind.

Damit die einzelnen Teilchen kovalent miteinander verknüpft oder an ein langkettiges Molekül angehängt werden können, müssen sie geeignet funktionalisiert werden. Dies geschieht, indem die beiden gewünschten Partner selektiv miteinander reagieren. Zu diesem Zweck werden Cyclodextrine und Silane auf den Keramikpulvern angebracht. Die Cyclodextrine können kovalent monomer und polymer ionisch an die Keramik gebunden werden.

Ein kommerziell verfügbares β-Cyclodextrinderivat, 3-Chlor-5-Natriumhydroxyl-Triazinyl-β-Cyclodextrin (MCT-β-Cyclodextrin **31**), ist in einer einstufigen Reaktion kovalent an die Si_3N_4–Oberfläche gebunden worden. Eine aufwendige Derivatisierung entfällt. Der Triazinring ist nicht regioselektiv an das Cyclodextrin gebunden (im Mittel 2,8 Triazinylgruppen pro Cyclodextrin). Weder die Anzahl pro Glucoseeinheit, pro Cyclodextrinring noch die Stelle sind definiert. Das Infrarot-Spektrum in diffuser Reflexion belegt die Anbindung von **31** an Si_3N_4. Das ζ-Potential (isoelektrischer Punkt pH_{iep}=7,2) ist aufgrund der Hydroxylatgruppe zum Alkalischen verschoben (pH_{pzc} von Si_3N_4 ist 5,0) und liegt im Bereich von aminofunktionalisiertem Si_3N_4 **20** mit pH_{iep}=7,7. Die sieben Aminogruppen in **10** verursachen eine wesentlich stärkere Verschiebung des isoelektrischen Punktes zu pH_{iep} 9,8.

Eine andere Möglichkeit, Cyclodextrin auf Si_3N_4 zu immobilisieren, stellt die Anbindung von Mono-6-Amino-β-Cyclodextrin **3** an epoxyfunktionalisiertes Si_3N_4 **5** dar. Die Synthese von **3** geht vom nativen β-Cyclodextrin aus, das über das Mono-6-Tosylat **1** in das Azid **2** überführt wird. Die Hydrierung des Azids wird mit Hilfe eines Wasserstoffdonors (Ammoniumformiat und Hydrazinhydrat) durchgeführt. Die Reaktion, deren Fortgang dünnschichtchromatographisch (DC) verfolgt wird, die Isolierung sowie die Reinigung sind verbessert worden. Die Epoxygruppen werden durch Reaktion mit (2,3-Epoxypropyl-Propyl-Ether)-Trimethoxysilane **4** auf dem Si_3N_4 eingeführt, an die dann **3** leicht angebunden werden kann. Dieses Verfahren stellt eine regioselektive Fixierung dar, bei der der Abstandshalter für eine ausreichende

Flexibilität sorgt. Die geringe adsorbierte Menge, das Ad- und Desorptionsverhalten können durch Messung des Drehwertes untersucht werden. Ungefähr 25% der Gesamtmasse werden von **5** adsorbiert, von Si_3N_4 dagegen nur 9%. Die locker gebundenen Fraktionen werden beim Waschen wieder gelöst, sodass noch 17% auf der Keramik verbleiben.

Die sieben Aminogruppen des Heptakis-6-Amino-β-Cyclodextrins **9** erleichtern die Anbindung an **5** was sich aus den intensiven Banden im Infrarot-Spektrum in diffuser Reflexion ergibt (0.1 Absorptions Einheiten für Methylen). Gleichzeitig erniedrigen sie die Komplexbildungskonstante für Gastmoleküle. **9** hat den Nachteil, dass es sich sehr schlecht in organischen Lösungsmitteln und Wasser löst.

Eine weitere Möglichkeit der Fixierung von Cyclodextrinen auf Keramikpulvern stellt der polymer ionogene Weg dar. Poly-β-Cyclodextrin **14** enthält β-Cyclodextrin als eine Seitenkette und Carboxylatgruppen als Ankergruppen für Al_2O_3 in der anderen. Dies eröffnet die Möglichkeit, auch Al_2O_3 mit Cyclodextrinen in einem Schritt zu funktionalisieren. Infrarot-Spektroskopie in diffuser Reflexion bestätigt, dass **14** auf Al_2O_3 fixiert wird. Es kann gezielt die adsorbierte Menge eingestellt werden, wobei die maximal adorbierte Menge größer ist als die der anderen Systeme. Untersuchungen der ad- und desorbierten Menge mittels Drehwertmessungen unter denselben Bedingungen wie für das Si_3N_4-System erlauben einen Vergleich: 57 Masse% werden in einer 0,1 %-igen Lösung adsorbiert, 72 % in einer 0,042 %-igen Lösung; zum Vergleich werden 25 % von **3** an **5** gebunden. **14** ist fest an Al_2O_3 gebunden, nach Redispergierung findet man kein gelöstes **14** im Überstand, im Gegensatz zu **6**, bei dem 30 % der adsorbierten Masse wieder gelöst werden.

Von Bedeutung ist die Frage, ob der Cyclodextrintorus die Adsorption des Poly-β-Cyclodextrins **14** behindert. Zu diesem Zweck wird das Ad- und Desorptionsverhalten von Copoly-maleinsäure-alt-isobuten **29** auf Al_2O_3 untersucht. **29** ist das polymere Rückgrat von Poly-β-Cyclodextrin **14** ohne Cyclodextrinringe. **29** hat eine hohe Affinität zur Al_2O_3-Oberfläche, was sich in einer adsorbierten Menge von 100 % äußert. **14** wird zu 57 % adsorbiert, was darauf schließen lässt, dass der Cyclodextrintorus die Adsorption beeinträchtigt. Wird Al_2O_3 / **29** gewaschen, so werden ca. 20 % der gebundenen Menge wieder gelöst. Ein Teil der Moleküle ist

nicht fest an die Oberfläche gebunden, sodass diese sich wieder leicht ablösen lassen. **14** dagegen ist fest an die Oberfläche gebunden, es lassen sich keine äußeren Schichten ablösen, was aus einer desorbierten Menge von 0 % hervorgeht.

Eine kovalente Verbrückung zweier keramischer Partikel wird durch Silanisierung mit zwei Silanen erreicht, die unterschiedliche miteinander reaktionsfähige Nicht-Silyl-Termini haben. Käufliches 1-Triethoxysilyl-3-Isocyanato-Propan **17** wird an Si_3N_4 gebunden, sodass **18** entsteht. Ebenfalls kommerziell erhältliches 1-Trimethoxysilyl-3-Amino-Propan **19** wird auf Si_3N_4 fixiert, sodass man **20** erhält. **18** reagiert mit **20** in verdünnter Suspension unter Bildung von 50-500 µm großen Agglomeraten, außerdem sedimentiert **18** + **20**. Es konnten auch stabile, hoch-konzentriete Suspensionen (20-37,6 vol%) mit einer maximalen Feststoffbeladung von ϕ_{max}=0.39 präpariert werden, die bei einem kritischen Volumenbruch von ϕ_{crit}=0.35 gelieren. Die Messdaten der relativen Viskosität η_{rel} gegen den Volumenbruch ϕ können durch die Mooney-Gleichung beschrieben werden. Die Viskosität der 20-28 vol% Gele ist niedriger als die der Systeme **18** und **20**. Die 20-28 vol% Gele haben einen zusätzlichen Übergang des Speichermodules G'(τ) mit dem Verlustmodul G''(τ) (τ=Schubspannung), der den Referenzsystemen **18** und **20** fehlt.

Es werden einige Keramik / Cyclodextrin Systeme beschrieben. Sie sind die Voraussetzung für eine heterosupramolekulare Verbindung von keramischen Partikeln auf der Basis von Wirt-Gast-Wechselwirkungen. Ein oder mehrere Partikel der cyclodextrinmodifizierten Si_3N_4-Keramik **6** werden an das Gastpolymer **16** gebunden; dadurch werden mehrere Teilchen über eine langkettige Brücke miteinander verknüpft. Das β-Cyclodextrin interkaliert das tert-Butyl-Anilid des Gastpolymeren **16**. Hinweise auf die Verknüpfung der Partikel erhält man kolloid-chemisch durch eine verstärkte Sedimentation, die sich folgendermaßen anordnen lässt: **6** > **6**+**16** > **5**+**16**. Eine elektrostatische Doppelschichtstabilisierung wird gemäß DLVO-Theorie durch die Elektrolytkonzentration von 0,03 mol/l vermieden. Als weitere Kräfte können noch die sterisch induzierten und die Van-der-Waals-Kräfte vorliegen. Im System **6** ist kein stabilisierendes Polymer vorhanden, sodass nur noch die attraktiven Van-der-Waals-Kräfte wirken, die die Sedimentation verursachen. In **6** + **16** und **5** + **16** stabilisiert das Polymer **16** die Partikel was zu einer erniedrigten Sedimentation im Vergleich zu **6** führt. Brücken zwischen den Partikeln in **6** + **16**

verstärken die Sedimentation im Vergleich zum cyclodextrin-freien System **5** + **16**, in dem keine vorhanden sind.

Das Gastpolymer **16** reagiert intrapartikulär mit **15** (Al_2O_3 mit einer großen adsorbierten Menge an Poly-β-Cyclodextrin **14**) d. h., es wird auf einzelnen Partikeln abgeschieden ohne verbrückend zu wirken. Dies liegt an der hohen Belegung mit Cyclodextrin, die die Wahrscheinlichkeit für eine intrapartikuläre Reaktion gegenüber der einer interpartikulären erhöht. Durch die zwei adsorbierten Polymerschichten ist die sterische Barriere vergrößert, was eine gute Dispergierbarkeit bedingt. So lassen sich über die Belegung gegenteilige Effekte einstellen – Dispergierung und Sedimentation.

Mit den Cyclodextrinen und den geeignet funktionalisierten Silanen werden eine heterosupramolekulare, langkettige Verknüpfung bzw. eine kovalente, kurzkettige mit keramischen Partikeln durchgeführt. Damit wird eine Reaktion zwischen zwei auf einem Festkörper gebundenen Komponenten und einer gelösten erzielt, was eine interessante Erweiterung der Interkalationschemie zwischen einem gelösten oder immobilisierten Wirt und einem gelösten Gast darstellt. Es kann über die Belegung mit Cyclodextrin jeweils eine intrapartikuläre oder eine interpartikuläre Reaktion ausgelöst werden womit ein dispergierender oder ein sedimentierender Effekt der Keramik erzielt werden kann.

Beide Konzepte sind industriell für das Direktgießen in der keramischen Formgebung interessant. Die kovalente Vernetzung von Si_3N_4-Partikeln mit Hilfe von Silanen, die käuflich erhältlich sind, ist sehr einfach durchzuführen und daher sehr erfolgversprechend. Die heterosupramolekulare Vernetzung von cyclodextrin-funktionalisierten Pulverpartikeln mit Hilfe von Gastpolymeren erscheint insbesondere für die Konsolidierung von Al_2O_3-Pulversuspensionen von Bedeutung.

17. References

[1] J. S. Reed, Principles of Ceramics Processing, 2 ed., John Wiley & Sons, Inc., **1995**, 277.

[2] M. N. Rahaman, Ceramic Processing and Sintering, Marcel Dekker, Inc., **1995**.

[3] R. A. Terpstra, P. P. A. C. Pex, A. H. d. Vries, Ceramic Processing, Chapman & Hall, **1995**.

[4] F. Aldinger, H.-J. Kalz, Die Bedeutung der Chemie für die Entwicklung von Hochleistungskeramiken, *Angew. Chem.* **1987**, *99*, 381.

[5] J. Böhnlein-Mauß, W. Sigmund, G. Wegner, W. H. Meyer, F. Heßel, K. Seitz, A. Roosen, The Function of Polymers in the Tape Casting of Alumina, *Adv. Mater.* **1992**, *4*, 73.

[6] W. M. Sigmund, G. Wegner, F. Aldinger, Interaction of Organic Additives with Alumina Surfaces in a Ceramic Slurry in M. R. Society, *Mat. Res. Soc. Symp. Proc.*, *Vol. 407*, **1996**, 313.

[7] W. M. Sigmund, L. Wang, J. Sindel, M. Rotov, F. Aldinger, Interaction of Organic Additives with Ceramic Surfaces in Colloidal Slurries in M. R. Society, *Mat. Res. Soc. Symp. Proc.*, *Vol. 432*, **1997**, 339.

[8] R. M. German, Powder Injection Molding, Metal Powder Industries Federation, Princeton, **1990**, 147.

[9] O. Lyckfeldt, E. Liden, M. Persson, R. Carlsson, P. Apell, Progress in the Fabrication of Si_3N_4 Turbine Rotors by Pressure Slip Casting, *J. Europ. Ceram. Soc.* **1994**, *14*, 383.

[10] E. G. Blanchard, Pressure Casting Improves Productivity, *Am. Ceram. Soc. Bull.* **1988**, *67*, 1680.

[11] P. C. Hidber, T. J. Graule, L. J. Gauckler, Citric Acid - A Dispersant for Aqueous Alumina Suspensions, *J. Am. Ceram. Soc.* **1996**, *79*, 1857.

[12] P. C. Hidber, T. J. Graule, L. J. Gauckler, Influence of the Dispersant Structure on Properties of Electrostatically Stabilized Aqueous Alumina Suspensions, *J. Europ. Ceram. Soc.* **1997**, *17*, 239.

[13] J. Cesarano, I. A. Aksay, Processing of Highly Concentrated Aqueous α-Alumina Suspensions Stabilized with Polyelectrolytes, *J. Am. Ceram. Soc.* **1988**, *71*, 1062.

[14] J. Cesarano, I. A. Aksay, Stability of Aqueous α-Al_2O_3 Suspensions with Poly(methacrylic acid) Polyelectrolyte, *J. Am. Ceram. Soc.* **1988**, *71*, 250.

[15] K.-S. Chou, L.-J. Lee, Effect of Dispersants on the Rheological Properties and Slip Casting of Concentrated Alumina Slurry, *J. Am. Ceram. Soc.* **1989**, *72*, 1622.

[16] R. Moreno, A. Salomoni, I. Stamenkovic, S. M. Castanho, Colloidal Filtration of Silicon Nitride Aqueous Slips, Part II: Slip Casting and Pressure Casting Performance, *J. Europ. Ceram. Soc.* **1999**, *19*, 49.

[17] F. F. Lange, K. T. Miller, Pressure Filtration: Consolidation Kinetics and Mechanics, *Am. Ceram. Soc. Bull.* **1987**, *66/10*, 1498.

[18] F. M. Tiller, C. D. Tsai, Theory of Filtration of Ceramics: I. Slip Casting, *J. Am. Ceram. Soc.* **1986**, *69*, 882.

[19] L. Bergström, E. Sjöström, Temperature Induced Gelation of Concentrated Ceramic Suspensions: Rheological Properties, *J. Europ. Ceram. Soc.* **1999**, *19*, 2117.

[20] N. S. Bell, L. Wang, W. M. Sigmund, F. Aldinger, Temperature Induced Forming: Application of Bridging Flocculation to Near-Net Shape Production of Ceramic Parts, *Z. Metallk.* **1999**, *90*, 388.

[21] T. J. Graule, L. J. Gauckler, F. H. Baader, *Indust. Ceram.* **1996**, *16*, 31.

[22] M. L. Griffith, J. W. Halloran, Ultraviolet Curing of Highly Loaded Ceramic Suspensions for Stereolithography of Ceramics, *Solid Freeform Fabr. Symp. Proc.*, **1994**, 396.

[23] H. D. Lee, R. L. Pober, P. D. Calvert, Photopolymerizable Binders for Ceramics, *J. Mater. Sci. Lett.* **1986**, *5*, 81.

[24] K. Maes, M. R. Silsbee, D. M. Roy, J. H. Adair, B. E. Scheetz, Gel-Cast Organic-Inorganic Systems, *Mater. Res. Soc. Symp. Proc.*, *Vol. 245*, **1992**, 217.

[25] S. Masuda, A. Inubushi, M. Okubo, A. Matsumoto, H. Sadamura, K. Suzuki, Painting-Type Thin Films of Hybrid Organo-Ceramics for Optical Memory Discs, Mater. Sci. Monogr., *Vol. 38C (High Tech Ceram., Pt. C)*, **1987**, 2093.

[26] S. D. Nunn, G. H. Kirby, Green Machining of Gelcast Ceramic Materials, *Ceram. Eng. Sci. Proc.* **1996**, *17*, 209.

[27] R. T. Smith, J. G. P. Binner, R. M. Sambrook, Processing of High Porosity Engineering Ceramics, *Ceram. Energy Appl. Proc.*, 2 ed., *Vol. 381*, Inst. Energy´s Int. Conf., Inst. Energy, London, **1994**.

[28] X. Tang, S. A. Ibbitson, A. T. Donato, H. J. Byrd, Acrylic Emulsion Binder for Tape Casting, *Ceram. Trans.* **1996**, *62*, 157.

[29] K. Venkataswamy, R. Waack, Rapid Cure Monitoring by Dielectrometry, *Plast. Eng.* **1988**, *44*, 43.

[30] P. R. Chu, J. K. Cochran, Kinetics Optimization of UV Curable Aqueous Slurries for Applications in Ceramic Processing, *Ceram. Eng. Sci. Proc.* **1994**, *15*, 499.

[31] B.-H. Kim, P.-W. Shin, U. Paik, Y.-G. Jung, S.-C. Choi, C.-W. Park, Dispersion and Forming of Alumina Powders via Crosslinkable Organic Molecules, *Yoop Hakhoechi* **1995**, *32*, 217.

[32] A. Kulak, Y.-J. Lee, Y. S. Park, K. B. Yoon, Orientation-Controlled Monolayer Assembly of Zeolite Crystals on Glass and Mica by Covalent Linkage of Surface-Bound Epoxide and Amine Groups, *Angew. Chem.* **2000**, *112*, 980.

[33] F.-S. Xiao, S. Qiu, W. Pang, R. Xu, New Developments in Microporous Materials, *Adv. Mater.* **1999**, *11*, 1091.

[34] G. Ihlein, F. Schüth, O. Krauß, U. Vietze, F. Laeri, Alignment of a Laser Dye in the Channels of the $AlPO_4$-5 Molecular Sieve, *Adv. Mater.* **1998**, *10*, 1117.

[35] G. A. Ozin, Nanochemistry: Synthesis in Diminishing Dimensions, *Adv. Mater.* **1992**, *4*, 612.

[36] J. L. Atwood, Inclusion Compounds, Ullmann´s Encyclopedia of Industrial Chemistry on CD-ROM, 5 ed., Wiley-VCH, Weinheim, **1997**.

[37] G. Gattuso, S. Menzer, S. A. Nepogodiev, J. F. Stoddart, D. J. Williams, Carbohydrate Nanotubes, *Angew. Chem. Int. Ed. Engl.* **1997**, *36*, 1451; *Angew. Chem.* **1997**, *109*, 1615.

[38] B. König, Well-Rounded Research: Nanotubes through Self-Assembly, *Angew. Chem. Int. Ed. Engl.* **1997**, *36*, 1833; *Angew. Chem.* **1997**, 1919.

[39] M. Ma, D. Li, New Organic Nanoporous Polymers and Their Inclusion Complexes, *Chem. Mater.* **1999**, *11*, 872.

[40] W. Saenger, Cyclodextrin-Einschlußverbindungen in Forschung und Industrie, *Angew. Chem.* **1980**, *92*, 343-361; *Angew. Chem. Int. Ed. Engl.* **1980**, *19*, 344-362.

[41] G. Wenz, Cyclodextrins as Building Blocks for Supramolecular Structures and Functional Units, *Angew. Chem.* **1994**, *106*, 851-870; *Angew. Chem. Int. Ed. Engl.* **1994**, *33*, 803-822.

[42] V. T. D'Souza, K. B. Lipkowitz, Cyclodextrins, *Chem. Rev.* **1998**, *98*.

[43] J. K. M. Sanders, Supramolecular Catalysis in Transition, *Chem. Eur. J.* **1998**, *4*, 1378.

[44] J.-C. Chambron, J.-P. Sauvage, Functional Rotaxanes: From Controlled Molecular Motions to Electron Transfer Between Chemically Nonconnected Chromophores, *Chem. Eur. J.* **1998**, *4*, 1362.

[45] S. Li, W. C. Purdy, Cyclodextrins and Their Applications in Analytical Chemistry, *Chem. Rev.* **1992**, *92*, 1457.

[46] M. J. Han, K. S. Yoo, J. Y. Chang, T.-K. Ha, 5-(β-Cyclodextrinylamino)-5-Deoxy-α-D-Riboses as Models for Nuclease, Ligase, Phosphatase, and Phosphorylase, *Angew. Chem.* **2000**, *112*, 355.

[47] S. Anderson, T. D. W. Claridge, H. L. Anderson, Azo-Dye Rotaxanes, *Angew. Chem. Int. Ed. Engl.* **1997**, *36*, 1310; *Angew. Chem.* **1997**, *109*, 1367.

[48] M. A. Mortellaro, W. K. Hartmann, D. G. Nocera, Regioisomeric Effects on the Excited State Processes of a Cyclodextrin Modified with a Lumophore, *Angew. Chem. Int. Ed. Engl.* **1996**, *35*, 1945; *Angew. Chem.* **1996**, *108*, 2073.

[49] E. Monflier, G. Fremy, Y. Castanet, A. Mortreux, Molecular Recognition between Chemically Modified β-Cyclodextrin and Dec-1-ene: New Prospects for Biphasic Hydroformylation of Water-Insoluble Olefins, *Angew. Chem. Int. Ed. Engl.* **1995**, *34*, 2269; *Angew. Chem.* **1995**, *107*, 2450.

[50] F. Venema, H. F. M. Nelissen, P. Berthault, N. Birlirakis, A. E. Rowan, M. C. Feiters, R. J. M. Nolte, Synthesis, Conformation, and Binding Properties of Cyclodextrin Homo- and Heterodimers Connected through Their Secondary Sides, *Chem. Eur. J.* **1998**, *4*, 2237.

[51] P. Colson, H. J. Jennings, I. C. P. Smith, Composition, Sequence, and Conformation of Polymers and Oligomers of Glucose as Revealed by Carbon-13 Nuclear Magnetic Resonance, *J. Am. Chem. Soc.* **1974**, *96*, 8081.

[52] A. O. Pulley, D. French, *Biochem. Biophys. Res. Commun.* **1961**, *5*, 11.

[53] M. Mori, Y. Ito, J. Uzawa, T. Ogawa, Stereoselectivity of Cycloglycosylation in Mannooligose Series Depends on Carbohydrate Chain Lenght: Synthesis of Manno Isomers of β- and γ-Cyclodextrins, *Tetrahedron Lett.* **1990**, *31*, 3191.

[54] R. Bürli, A. Vasella, Cyclic "Acetylenosaccharides" - Novel Cyclodextrin Analogues, *Angew. Chem. Int. Ed. Engl.* **1997**, *36*, 1852; *Angew. Chem.* **1997**, *109*, 1945.

[55] P. R. Ashton, C. L. Brown, S. Menzer, S. A. Nepogodiev, J. F. Stoddart, D. J. Williams, Synthetic Cyclic Oligosaccharides - Synthesis and Structural Properties of a Cyclo[(1→4)-α-L-Rhamnopyranosyl-(1→4)-α-D-Mannopyranosyl]-Trioside and -Tetraoside, *Chem. Eur. J.* **1996**, *2*, 580.

[56] P. R. Ashton, S. J. Cantrill, G. Gattuso, S. Menzer, S. A. Nepogodiev, A. N. Shipway, J. F. Stoddart, D. J. Williams, Achiral Cyclodextrin Analogues, *Chem. Eur. J.* **1997**, *3*, 1299.

[57] S. Immel, Computer Simulation of Chemical and Biological Properties of Saccharides: Sucrose, Fructose, Cyclodextrins, and Starch, PhD Thesis, Technische Universität Darmstadt, **1995**, 203, http://caramel.oc.chemie.tu-darmstadt.de/~lemmi/PhDThesis_right.html.

[58] F. Schardinger, *Wien. Klin. Wochenschr.* **1904**, *17*, 207.

[59] F. Schardinger, *Zentralbl. Bakteriol. Parasitenkd. Infektionskr. Hyg. II* **1911**, *29*, 188.

[60] K. Freudenberg, M. Meyer-Delius, *Ber. Dtsch. Chem. Ges.* **1938**, *71*, 1596.

[61] K. Freudenberg, E. Plankenhorn, H. Knauber, *Chem. Ind. (London)* **1947**, 731.

[62] K. Freudenberg, E. Plankenhorn, H. Knauber, *Liebigs Ann. Chem.* **1947**, *558*, 1.

[63] D. French, M. L. Levine, J. H. Pazur, E. Norberg, *J. Am. Chem. Soc.* **1949**, *71*, 353.

[64] D. French, *Adv. Carbohydr. Chem.* **1957**, *12*, 189.

[65] S. Kitahata, S. Okada, *J. Biochem.* **1976**, *79*, 641.

[66] S. Kitahata, N. Tsuyama, S. Okada, *Agric. Biol. Chem.* **1974**, *39*, 387.

[67] H. Bender, *Arch. Microbiol.* **1977**, *111*, 271, *113*, 49.

[68] M. Shirosaka, H. Fumiya, *Amylase Symp. Proc.*, *Vol. 8*, **1973**, 43.

[69] M. Weickenmeier, Gelbildner durch Selbstorganisation von wasserlöslichen Polymeren mit Cyclodextrinpolymeren, PhD Thesis, Universität (TH) Karlsruhe, **1998**, 5.

[70] W. F. v. Gunsteren, H. J. C. Berendsen, Moleküldynamik-Computersimulationen; Methodik, Anwendungen und Perspektiven in der Chemie, *Angew. Chem.* **1990**, *102*, 1020.

[71] H. Dodziuk, K. Nowinski, Structure of Cyclodextrins and Their Complexes. Part 2. Do Cyclodextrins have a Rigid Truncated-Cone Structure ?, *J. Mol. Struct. (Theochem)* **1994**, *304*, 61.

[72] S. Immel, Computer Simulation of Chemical and Biological Properties of Saccharides: Sucrose, Fructose, Cyclodextrins, and Starch, PhD Thesis, Technische Universität Darmstadt, **1995**, http://caramel.oc.chemie.tu-darmstadt.de/~lemmi/PhDThesis_right.html.

[73] A. K. Rappé, C. J. Casewit, Molecular Mechanics across Chemistry, University Science Books, Sausalito, CA, USA, **1997**.

[74] S. Reiling, J. Brickmann, Theoretical Investigations on the Structure and Physical Properties of Cellulose, *Macromol. Theory Simul.* **1995**, *4*, 725.

[75] S. Reiling, M. Schlenkrich, J. Brickmann, Force Field Parameters for Carbohydrates, *J. Comput. Chem.* **1996**, *17*, 450.

[76] S. Reiling, J. Brickmann, M. Schlenkrich, P. A. Bopp, Theoretical Investigations on 1,2-Ethanediol: The Problem of Intramolecular Hydrogen Bonds, *J. Comput. Chem.* **1996**, *17*, 133.

[77] B. R. Brooks, R. E. Bruccoleri, B. D. Olafson, D. J. States, S. Swaminathan, M. Karplus, CHARMM: A Program for Macromolecular Energy, Minimization, and Dynamics Calculations, *J. Comput. Chem.* **1983**, *4*, 187.

[78] A. T. Brünger, Simulated Annealing in Crystallography, *Ann. Rev. Phys. Chem.* **1991**, *42*, 197.

[79] A. E. Smith, H. J. Lindner, π-SCF-Molecular Mechanics PIMM: Formulation, Parameters, Applications, *J. Comput.-Aided Mol. Design* **1991**, *5*, 235.

[80] L. Nilsson, M. Karplus, Empirical Energy Functions for Energy Minimization and Dynamics of Nucleic Acids, *J. Comput. Chem.* **1986**, *7*, 591.

[81] K. B. Lipkowitz, Symmetry Breaking in Cyclodextrins: A Molecular Mechanics Investigation, *J. Org. Chem.* **1991**, *56*, 6357.

[82] J. E. H. Koehler, W. Saenger, W. F. v. Gunsteren, A Molecular Dynamics Simulation of Crystalline α-Cyclodextrin Hexahydrate, *Eur. Biophys. J.* **1987**, *15*, 197.

[83] J. E. H. Koehler, W. Saenger, W. F. v. Gunsteren, Molecular Dynamics Simulation of Crystalline β-Cyclodextrin Dodecahydrate at 293 K and 120 K, *Eur. Biophys. J.* **1987**, *15*, 211.

[84] A. E. Mark, S. P. v. Helden, P. E. Smith, L. H. M. Janssen, W. F. v. Gunsteren, Convergence Properties of Free Energy Calculations: α-Cyclodextrin Complexes as a Case Study, *J. Am. Chem. Soc.* **1994**, *116*, 6293.

[85] S. M. Kast, K. Nicklas, H.-J. Bär, J. Brickmann, Constant Temperature Molecular Dynamics Simulations by Means of a Stochastic Collision Model. I. Noninteracting Particles, *J. Chem. Phys.* **1994**, *100*, 566.

[86] S. M. Kast, J. Brickmann, Constant Temperature Molecular Dynamics Simulations by Means of a Stochastic Collision Model. II. The Harmonic Oscillator, *J. Chem. Phys.* **1996**, *104*, 3732.

[87] L. Verlet, Computer "Experiments" on Classical Fluids. I. Thermodynamical Properties of Lennard-Jones Molecules, *Phys. Rev.* **1967**, *159*, 98.

[88] K. Lindner, W. Saenger, β-Cyclodextrin-Dodecahydrat: Häufung von Wassermolekülen in einer hydrophoben Höhlung, *Angew. Chem.* **1978**, *90*, 738.

[89] K. Lindner, W. Saenger, Topography of Cyclodextrin Inclusion Complexes. XVI. Cyclic System of Hydrogen Bonds: Structure of α-Cyclodextrin Hexahydrate, (Form II): Comparison with Form (I), *Acta Cryst.* **1982**, *B38*, 203.

[90] P. C. Manor, W. Saenger, Topography of Cyclodextrin Inclusion Complexes. III. Crystal and Molecular Structure of Cyclohexaamylose Hexahydrate, the $(H_2O)_2$ Inclusion Complex, *J. Am. Chem. Soc.* **1974**, *96*, 3630.

[91] K. K. Chacko, W. Saenger, Topography of Cyclodextrin Inclusion Complexes. 15. Crystal and Molecular Structure of the Cyclohexaamylose-7.57 Water Complex, Form III. Four-and Six-Membered Circular Hydrogen Bonds, *J. Am. Chem. Soc.* **1981**, *103*, 1708.

[92] B. Klar, B. Hingerty, W. Saenger, Topography of Cyclodextrin Inclusion Complexes. XII. Hydrogen Bonding in the Crystal Structure of α-Cyclodextrin Hexahydrate: The Use of a Multicounter Detector in Neutron Diffraction, *Acta Cryst.* **1980**, *B36*, 1154.

[93] J. F. Flier, E. Maratos-Flier, J. A. Pallotta, D. McIsaac, Circular Hydrogen Bonds, *Nature* **1979**, *279*, 343.

[94] J. E. H. Koehler, W. Saenger, W. F. v. Gunsteren, On the Occurrence of Three-Center Hydrogen Bonds in Cyclodextrins in Crystalline Form and in Aqueous Solution: Comparison of Neutron Diffraction and Molecular Dynamic Results, *J. Biomol. Struct. Dynam.* **1988**, *6*, 181.

[95] J. E. H. Koehler, W. Saenger, W. F. v. Gunsteren, Conformational Differences Between α-Cyclodextrin in Aqueous Solution and in Crystalline Form - A Molecular Dynamics Study, *J. Mol. Biol.* **1988**, *203*, 241.

[96] J. E. H. Koehler, W. Saenger, W. F. v. Gunsteren, The Flip-Flop Hydrogen Bonding Phenomenon - Molecular Dynamics Simulation of Crystalline β-Cyclodextrin, *Eur. Biophys. J.* **1988**, *16*, 153.

[97] S. Immel **1999**, http://caramel.oc.chemie.tu-darmstadt.de/~lemmi/3Dstructures.html.

[98] CD Römpp Chemie Lexikon, 1 ed., Georg Thieme Verlag, Stuttgart/ New York, **1995**.

[99] M. L. Bender, M. Komiyama, Cyclodextrin Chemistry, Springer, Berlin, **1978**.

[100] M. V. Rekharsky, Y. Inoue, Complexation Thermodynamics of Cyclodextrins, *Chem. Rev.* **1998**, *98*, 1875.

[101] J. Szejtli, Cyclodextrins and their Inclusion Complexes, Akademia Kiado, Budapest, **1982**.

[102] M. Weickenmeier, G. Wenz, Threading of Cyclodextrins onto a Polyester of Octanedicarboxylic Acid and Polyethylene Glycol, *Macromol. Rapid Commun.* **1997**, *18*, 1109.

[103] W. Herrmann, G. Wenz, Kinetics and Thermodynamics of the Inclusion of Ionene-6,10 in α-Cyclodextrin in an Aqueous Solution, *Macromolecules* **1997**, *30*, 4966.

[104] G. Wenz, B. Keller, Synthesis of Polyrotaxanes or how to Thread many Cyclodextrin Rings on a Polymer Chain, *Polym. Prep. (Am. Chem. Soc., Div. Polym. Chem.)* **1993**, *34*, 62.

[105] G. Wenz, B. Keller, Speed Control for Cyclodextrin Rings on Polymer Chains, *Macromol. Symp.* **1994**, *87*, 11.

[106] G. Wenz, P. Mischnick, R. Krebber, M. Richters, W. A. König, Preparation and Characterization of Per-O-Pentylated Cyclodextrins, *J. High Resol. Chromatogr. Commun.* **1990**, *13*, 724.

[107] E. v. d. Bey, K. Wenke, G. Wenz, Synthesis and Characterization of Immobilized Lipophilic Cyclodextrins in D. Duchêne, *Minutes of the 5th International Symposium on Cyclodextrins*, Editions de Santé, Paris, **1990**, 643.

[108] H. Dittmann, K. Scharwächter, W. A. König, Synthesis and Silica-Based Immobilization of Monofunctionalized Cyclomaltoheptaose Derivatives for Enantioselective HPLC, *Carbohydr. Res.* **2000**, *324*, 75.

[109] A. Ueno, R. Breslow, Selective Sulfonation of a Secondary Hydroxyl Groups of β-Cyclodextrin, *Tetrahedron Lett.* **1982**, *23*, 3451.

[110] G. Wenz, Synthesis and Characterisation of some Lipophilic Per-(2,6-Di-O-Alkyl-)-Cyclomalto-Oligosaccharides, *Carbohydr. Res.* **1991**, *214*, 257.

[111] W. M. Sigmund, N. S. Bell, L. Bergström, Novel Powder-Processing Methods for Advanced Ceramics, *J. Am. Ceram. Soc.* **2000**, *83*, 1557.

[112] P. G. d. Gennes, Conformations of Polymers Attached to an Interface, *Macromolecules* **1980**, *13*, 1069.

[113] P. G. d. Gennes, Polymer Solutions Near an Interface. 1. Adsorption and Depletion Layers, *Macormolecules* **1981**, *14*, 1637.

[114] P. G. d. Gennes, Polymers at an Interface. 2. Interaction between Two Plates Carrying Adsorbed Polymer Layers, *Macromolecules* **1982**, *15*, 492.

[115] P. G. d. Gennes, Polymers at an Interface; A Simplified View, *Adv. Colloid Interface Sci.* **1987**, *27*, 189.

[116] H. G. Barth, Modern Methods of Particle Size Analysis, John Wiley, New York, **1984**.

[117] R. J. Hunter, Zeta Potential in Colloid Science, **1981**.

[118] J. Lyklema, Fundamentals of Colloid and Interface Science, *Vol. I: Fundamentals*, Academic Press, **1993**; *Vol. II: Solid-Liquid Interfaces*.

[119] A. Rawle, PCS in 30 Minuten, Malvern Instruments GmbH, Herrenberg.

[120] R. Nitzsche, Malvern Short Course - Zetapotential, Malvern Instruments GmbH, Herrenberg.

[121] G. Lagaly, O. Schulz, R. Zimehl, Dispersionen und Emulsionen, Steinkopff, Darmstadt, **1997**, 361.

[122] W. Burchard, Neue Möglichkeiten der Charakterisierung von Polymersystemen durch kombinierte statische und dynamische Lichtstreuung, *Plaste Kautschuk* **1985**, *32*, 241.

[123] H. Wiese, Lichtstreuung und Teilchengrößenmessung, 1. Grundlagen und Streuung am Elektron, *GIT Fachz. Lab.* **1992**, *36*, 385.

[124] H. Wiese, Lichtstreuung und Teilchengrößenmessung, 2. Statische Lichtstreuung, *GIT Fachz. Lab.* **1992**, *36*, 762.

[125] H. Wiese, Lichtstreuung und Teilchengrößenmessung, 3. Dynamische Lichtstreuung und Fraunhoferbeugung, *GIT Fachz. Lab.* **1992**, *36*, 1029.

[126] B. E. Dahneke, Measurement of Suspended Particles by Quasi-Elastic Light Scattering, John Wiley, New York, **1983**.

[127] A. Ishimaru, Wave Propagation and Scattering in Random Media, *Vol. 1*, Academic Press, New York, **1978**; *Vol. 2*.

[128] H. R. Haller, C. Destor, D. S. Cannell, *Rev. Sci. Instrum.* **1983**, *54*, 973.

[129] W. B. Russel, D. A. Saville, W. R. Schowalter, Colloidal Dispersions, Cambridge University Press, Princeton, **1989**, 456.

[130] H. G. O. Becker, G. Domschke, E. Fanghänel, M. Fischer, K. Gewald, R. Mayer, D. Pavel, H. Schmidt, K. Schwetlick, W. Berger, J. Faust, F. Gentz, R. Gluch, K. Müller, K. Schollberg, E. Seiler, G. Zeppenfeld, Organikum, 18 ed., Deutscher Verlag der Wissenschaften, Berlin, **1990**.

[131] D. H. Williams, I. Fleming, Spektroskopische Methoden zur Strukturaufklärung, Georg Thieme Verlag, Stuttgart, **1979**, 43.

[132] H.-U. Gremlich, Infrared and Raman Spectroscopy, Ullmann´s Encyclopedia of Industrial Chemistry on CD-ROM, 5 ed., Wiley-VCH, Weinheim, **1997**.

[133] H. Günzler, H. M. Heise, IR-Spektroskopie, 3 ed., VCH, Weinheim, **1996**.

[134] S. N. Magonov, M.-H. Whangbo, Surface Analysis with STM and AFM, VCH, Weinheim, New York, **1996**.

[135] T. Höfler, G. Wenz, Determination of Binding Energies between Cyclodextrins and Aromatic Guest Molecules by Microcalorimetry, *J. Inclusion Phenom. Mol. Recognit. Chem.* **1996**, *25*, 81.

[136] T. Höfler, G. Wenz, Einschluß von Aromaten in β-Cyclodextrin und β-Cyclodextrinsulfonaten in H. Eierdanz, Perspektiven nachwachsender Rohstoffe in der Chemie, VCH, Weinheim, **1995**, 276.

[137] M. Weickenmeier, G. Wenz, J. Huff, Association Thickener by Host Guest Interaction of a β-Cyclodextrin Polymer and a Polymer with Hydrophobic Side-Groups, *Macromol. Rapid Commun.* **1997**, *18*, 1117-1123.

[138] C. Amiel, B. Sebille, New Associating Polymer Systems Involving Water Soluble β-Cyclodextrin Polymers in J. Szejtli, L. Szente, *Proceedings of the Eighth International Symposium on Cyclodextrins*, Kluwer Academic Publishers, **1996**, 107.

[139] M. Ootani (Sekusui Plastics, Japan), JP 07069382 A2, **1995**.

[140] M. Ootani (Sekusui Plastics, Japan), JP 07033173 A2, **1995**.
[141] R. P. Rohrbach (UOP Inc., USA), US 4917956 A, **1990**.
[142] R. P. Rohrbach, H. Zemel, M. B. Koch (UOP Inc., USA), US 5098793 A, **1992**.
[143] R. P. Rohrbach (UOP Inc., USA), EP 454910 A1, **1992**.
[144] K. Sarui, T. Katsura (Filton International K. K., Japan), JP 62084766 A2, **1987**.
[145] M. Weisser, G. Nelles, P. Wohlfart, G. Wenz, S. Mittler-Neher, Immobilization Kinetics of Cyclodextrins at Gold Surfaces, *J. Phys. Chem.* **1996**, *100*, 17893.
[146] M. Weisser, G. Nelles, G. Wenz, S. Mittler-Neher, Guest-Host Interactions with Immobilized Cyclodextrins, *Sens. Actuators* **1997**, *B38*, 58.
[147] G. Nelles, M. Weisser, R. Back, P. Wohlfart, G. Wenz, S. Mittler-Neher, Controlled Orientation of Cyclodextrin Derivatives Immobilized on Gold Surfaces, *J. Am. Chem. Soc.* **1996**, *118*, 5039.
[148] L. P. Meier, M. Heule, W. R. Caseri, R. A. Shelden, U. W. Suter, G. Wenz, B. Keller, Adsorption of Polymeric Inclusion Compounds on Muskovite Mica, *Macromolecules* **1996**, *29*, 718.
[149] W. A. König, R. Krebber, G. Wenz, Enantioselective Capillary Gas Chromatography on the Basis of Host-Guest Interactions with Modified Cyclodextrins, *J. High Resol. Chromatogr.* **1989**, *12*, 641.
[150] L. Wang, personal communication, **1998**.
[151] H. C. Starck, personal communication, **1995**.
[152] G. Schwier, G. Niefeld, G. Franz, Production and Characterization of Silicon Nitride Powders, *Mater. Sci. Forum* **1989**, *47*, 1.
[153] M. N. Rahaman, Y. Boiteux, L. C. D. Jonghe, Surface Characterization of Silicon Nitride and Silicon Carbide Powders, *Am. Ceram. Soc. Bull.* **1986**, *65*, 1171.
[154] G. Ramis, G. Busca, V. Lorenzelli, M. I. Baraton, T. Merle-Mejean, P. Quintard, FT-IR Characterization of High Surface Area Silicon Nitride and Carbide in L.-C. Dufour, Surfaces and Interfaces of Ceramic Materials, Kluwer Academic Publishers, **1989**, 173.
[155] T. Nakamatsu, N. Saito, C. Ishizaki, K. Ishizaki, Silicon Nitride and Oxide Powder Surface Characterization by TPD, *J. Europ. Ceram. Soc.* **1998**, *18*, 1273.
[156] L. Bergström, R. J. Pugh, Interfacial Characterization of Silicon Nitride Powders, *J. Am. Ceram. Soc.* **1989**, *72*, 103.

[157] P. K. Whitman, D. L. Feke, Colloidal Characterization of Ultrafine Silicon Carbide and Silicon Nitride Powders, *Adv. Ceram. Mater.* **1986**, *1*, 366.

[158] C. Galassi, E. Rastelli, E. Roncari, S. Ardizzone, M. G. Cattania, Characterization and Stabilization of Si_3N_4 Suspensions, *J. Mater. Res.* **1995**, *10*, 339.

[159] S. M. Castanho, J. L. G. Fierro, R. Moreno, Surface Oxidation of Si_3N_4 Green Compacts: Effect of Sintering Aids, *J. Europ. Ceram. Soc.* **1997**, *17*, 383.

[160] L. Bergström, E. Bostedt, Surface Chemistry of Silicon Nitride Powders: Electrokinetic Behaviour and ESCA Studies, *Colloids Surf.* **1990**, *49*, 183.

[161] X.-M. Yue, G.-J. Zhang, T. Watanabe, W.-P. Tai, Corrosion Behavior of Single-Crystal Alumina in Argon, Air, and Water Vapor Atmospheres at 1700-2000°C, *J. Am. Ceram. Soc.* **1999**, *82*, 2560-2562.

[162] D. F. Shriver, P. W. Atkins, C. H. Langford, Anorganische Chemie, VCH, Weinheim, **1992**, 206.

[163] A. Roosen, K. Seitz, Powder Surface Chemistry in Ceramics Powder Processing, *Ceram. Forum Int./ Ber. DKG* **1997**, *74*, 230.

[164] B. Chu, Laser Light Scattering, Academic Press, New York, **1974**.

[165] M. Born, E. Wolf, Principles of Optics, Pergamon Press, **1964**.

[166] H. C. v. d. Hulst, Multiple Light Scattering, *Vol. 1*, Academic Press, New York, **1980**; *Vol. 2*.

[167] M. Kerker, The Scattering of Light and other Electromagnetic Radiation, Academic Press, New York, **1969**.

[168] J. T. Thurston, Cyanuric Chloride Derivatives. I-VIII., *J. Am. Chem. Soc.* **1951**, *73*, 2981.

[169] J. R. Dudley, Cyanuric Choride Derivatives. IX., *J. Am. Chem. Soc.* **1951**, *73*, 3007.

[170] K. Huthmacher, F. Hübner, 1,3,5-Triazines in Houben-Weyl, Methoden der Organischen Chemie, 4 ed., *Vol. E9*, Thieme, Stuttgart, **1997**, 667.

[171] M. D. Paoli, Supramolekulare Systeme aus Cyclodextrinen und Dendrimeren, PhD Thesis, Universität (TH) Karlsruhe, **2000**, 102.

[172] J. Defaye, S. Crouzy, N. Evrard, H. Law, France), FR(98)06, 605, **1997**.

[173] M. D. Paoli, Supramolekulare Systeme aus Cyclodextrinen und Dendrimeren, PhD Thesis, Universität (TH) Karlsruhe, **2000**, 103.

[174] R. C. Petter, J. S. Salek, C. T. Sikorski, G. Kumaravel, F. T. Lin, *J. Am. Chem. Soc.* **1990**, *112*, 3860.

[175] K. Takahashi, K. Hattori, F. Toda, *Tetrahedron Lett.* **1984**, *25*, 3331.

[176] I. Kräuter, Diploma Thesis, Universität (TH) Karlsruhe, **1995**, 76.

[177] G. Nelles, PhD Thesis, Universität Mainz, **1995**.

[178] L. Jicsinszky, Catalytic Transfer Hydrogenation of Cyclodextrin Azides and Benzylated Glucose Derivatives, *J. Inclusion Phenom. Mol. Recognit. Chem.* **1994**, *18*, 247.

[179] I. Kräuter, Synthese, Strukturnachweis und Abbildung wasserlöslicher, fluoreszenzmarkierter Polyrotaxane, PhD Thesis, Universität (TH) Karlsruhe, **1999**, 121.

[180] I. Kräuter, Synthese, Strukturnachweis und Abbildung wasserlöslicher, fluoreszenzmarkierter Polyrotaxane, PhD Thesis, Universität (TH) Karlsruhe, **1999**, 150.

[181] M. D. Paoli, Supramolekulare Systeme aus Cyclodextrinen und Dendrimeren, PhD Thesis, Universität (TH) Karlsruhe, **2000**, 109.

[182] A. Gadelle, J. Defaye, *Angew. Chem.* **1991**, *103*, 94.

[183] J. L. J. Blanco, J. M. G. Fernández, A. Gadelle, J. Defaye, *Carbohydr. Res.* **1997**, *303*, 367.

[184] J. F. Stoddart, P. R. Ashton, R. Königer, D. Alker, V. D. Harding, *J. Org. Chem.* **1996**, *61*, 903.

[185] M. D. Paoli, personal communication, **1999**.

[186] V. A. Hackley, Colloidal Processing of Silicon Nitride with Poly(acrylic acid): II, Rheological Properties, *J. Am. Ceram. Soc.* **1998**, *81*, 2421.

[187] E. Lidén, L. Bergström, M. Persson, R. Carlsson, Surface Modification and Dispersion of Silicon Nitride and Silicon Carbide Powders, *J. Europ. Ceram. Soc.* **1991**, *7*, 361.

[188] M. Weickenmeier, Gelbildner durch Selbstorganisation von wasserlöslichen Polymeren mit Cyclodextrinpolymeren, PhD Thesis, Universität (TH) Karlsruhe, **1998**, 20.

[189] E. P. Plueddemann, Silane Coupling Agents, Plenum Press, New York, London, **1982**, 49, 98.

[190] E. P. Plueddemann, Silane Coupling Agents, Plenum Press, New York, London, **1982**, 32.

[191] E. P. Plueddemann, Silane Coupling Agents, Plenum Press, New York, London, **1982**, 81, 93.

[192] M. Weickenmeier, Gelbildner durch Selbstorganisation von wasserlöslichen Polymeren mit Cyclodextrinpolymeren, PhD Thesis, Universität (TH) Karlsruhe, **1998**, 47.

[193] J. A. Zerkowski, C. T. Seto, D. A. Wierda, G. M. Whitesides, Design of Organic Structures in the Solid State: Hydrogen Bonded Molecular "Tapes", *J. Am. Chem. Soc.* **1990**, *112*, 9025.

[194] J. A. Zerkowski, J. C. MacDonald, G. M. Whitesides, Investigations into the Robustness of Secondary and Tertiary Architecture of Hydrogen-Bonded Crystalline Tapes, *Chem. Mater.* **1994**, *6*, 1250.

[195] J. A. Zerkowski, J. P. Mathias, G. M. Whitesides, New Varities of Crystalline Architecture Produced by Small Changes in Molecular Structure in Tape Complexes of Melamines and Barbiturates, *J. Am. Chem. Soc.* **1994**, *116*, 4305.

[196] M. Li, K. K. W. Wong, S. Mann, Organization of Inorganic Nanoparticles Using Biotin-Streptavidin Connectors, *Chem. Mater.* **1999**, *11*, 23.

[197] R. W. Schwartz, P. G. Clem, J. A. Voigt, E. R. Byhoff, M. V. Stry, T. J. Headley, N. A. Missert, Control of Microstructure and Orientation in Solution-Deposited $BaTiO_3$ and $SrTiO_3$ Thin Films, *J. Am. Ceram. Soc.* **1999**, *82*, 2359-2367.

[198] T. Yonezawa, H. Matsune, T. Kunitake, Layered Nanocomposite of Close-Packed Gold Nanoparticles and TiO_2 Gel Layers, *Chem. Mater.* **1999**, *11*, 33.

[199] X. Zhang, J. Shen, Self-Assembled Ultrathin Films: From Layered Nanoarchitectures to Functional Assemblies, *Adv. Mater.* **1999**, *11*, 1139.

[200] E. Coronado, C. Mingotaud, Hybrid Organic/Inorganic Langmuir-Blodgett Films. A Supramolecular Approach to Ultrathin Magnetic Films, *Adv. Mater.* **1999**, *11*, 869.

[201] M. Clemente-León, H. Soyer, E. Coronado, C. Mingotaud, C. J. Gómez-García, P. Delhaès, Langmuir-Blodgett-Filme von Einzelmolekül-Nanomagneten, *Angew. Chem.* **1998**, *110*, 3053.

[202] A. R. West, Grundlagen der Festkörperchemie, VCH, Weinheim, **1992**, 57, 362.

[203] M. V. Gelfuso, D. Thomazini, J. A. Eiras, Synthesis and Structural, Ferroelectric, and Piezoelectric Properties of $SrBi_4Ti_4O_{15}$ Ceramics, *J. Am. Ceram. Soc.* **1999**, *82*, 2368-2372.

[204] M. Villegas, A. C. Caballero, C. Moure, P. Durán, J. F. Fernández, Factors Affecting Electrical Conductivity of Donor-Doped $Bi_4Ti_3O_{12}$ Piezoelectric Ceramics, *J. Am. Ceram. Soc.* **1999**, *82*, 2411-2416.

[205] R. E. Newnham, G. R. Ruschau, Smart Electroceramics, *J. Am. Ceram. Soc.* **1991**, *74*, 463.

[206] U. P. Schönholzer, L. J. Gauckler, Ceramic Parts Patterned in the Micrometer Range, *Adv. Mater.* **1999**, *11*, 630.

[207] S. Wang, J.-F. Li, K. Wakabayashi, M. Esashi, R. Watanabe, Lost Silicon Mold Process for PZT Microstructures, *Adv. Mater.* **1999**, *11*, 873.

[208] H. Fudouzi, M. Egashira, N. Shinya, Drawing and Observation of Electrified Images on Ceramic Substrates Using Electron Beam, *J. Ceram. Soc. Jap. Int. Ed.* **1996**, *104*, 532.

[209] A. Reiser, H.-Y. Shih, T.-F. Yeh, J.-P. Huang, Novolak-Diazochinon-Photoresiste: abbildende Systeme für den Computerchip, *Angew. Chem.* **1996**, *108*, 2610.

[210] D. Widmann, H. Mader, H. Friedrich, Technologie hochintegrierter Schaltungen, 2 ed., Springer, Berlin, **1996**.

18. Acknowledgment

The author wants to thank the following persons for their support and advice, the order is arbitrary and does not represent the magnitude of support:

Prof. Dr. Aldinger
Prof. Dr. Sigmund
Prof. Dr. Wenz
Prof. Dr. Roduner
Prof. Dr. Schleid
Prof. Dr. Richterring
Mr. H. Labitzke
Mr. G. Kaiser
Mr. Breitschwert
Mr. König
Mr. A. Rosinus
Mrs C. Gruber
Mr. P. Wimmer
Dr. M. Weickenmeier
Dr. M. De Paoli
Mrs P. Liebknecht
Mrs A. Hochgesandt
Mrs M. Schneider
Mr. G. Maier
Mr. T. Seeger
Mrs M. Raible
Mr. B. Biedlingmeier
Prof. Dr. K. Müller
Mr. J. Schumacher
Dr. J. Pleiss
Mrs S. Rosenfeldt
Dr. S. Immel
Dr. J. Sindel
Dr. G. Rixecker

Dr. R. Hoffmann

Mrs S. Wildhack

Mr. S.-H. Lee

Mrs U. Heinrichs

Mr. P. Gerstel

Dr. T. Niessen

Mr. T. Fuchs

Dr. M. Weinmann

Mr. M. Schweizer

Mrs S. Nast

Mr. A. Bauer

Mr. M. Christ

Mrs S. Wagner

Mr. J. Peng

Mrs S. Paulsen

Mrs N. Overbaugh

Mrs J. Weber-Bock

Mrs H. Klooz

Mrs Schwarz

Dr. E. Grallert

Dr. Moldenhauer

Mrs K. Nothelfer